Department of Civil and Mechanical Engineering

The Development of an Amorphous Approach to Ambient Cured Blended Geopolymer Mortar Mixture Design

Julian Spano

0000-0001-9477-934X

This thesis is presented for the Degree of
Master of Philosophy (Civil Engineering)
of
Curtin University

February 2021

Declaration

To the best of my knowledge and belief this thesis contains no material previously published by any other person except where due acknowledgment has been made.

This thesis contains no material which has been accepted for the award of any other degree or diploma in any university.

This thesis required no Human or Animal ethics approvals.

Signature: ……

Date: 6/2/2020

Author: Julian M. Spano
Date: 6h February 2021
Supervisor: Dr. Amin Chegenizadeh
Co-Supervisors: Dr. Trevor Htut
Dr. Matthew Rowles

Abstract

With increased focus on sustainable practices and reduced global emissions, the construction industry is faced pressure to reduce dependence on OPC concrete. Geopolymers have been highlighted as a potential substitute for OPC binders, due to their utilisation of industrial waste products to produce cementitious binders. Geopolymer adoption is hindered due to inconstancy associated with strength outcomes and production, as well as the requirement for heat curing. Formulation of ambient cured geopolymers requires the utilisation of multiple aluminosilicate source materials to develop binders for sufficient strength for industrial application, whilst cured under ambient temperatures. These binary and ternary geopolymers are typically formulated through prescription specific elemental ratio utilising the bulk composition of the feeder stocks. This method fails to consider the crystalline component which is inert in the activation and geopolymerisation process. This research aims to further develop the amorphous approach to geopolymer formulation, where by the amorphous content is assessed via XRF and Q-XRD analysis and mixture proportions prescribed with reference to the reactive elements of the feeder stocks. The scope of this research was to investigate the role specific amorphous ratios relating to Si, Al and H, had on compressive strength values, and develop the amorphous framework associated with binary, ternary and blended geopolymers.

The amorphous composition of Gladstone and Eraring Fly Ash were determined via XRF and QXRD within chapter 4. It was found that the SI/Al of Gladstone and Earing were 3.8 and 2.9 , with Gladstone's higher value attributed to the unavailability of aluminium locked within crystalline mullite. Compared to Eraring, Gladstone contained a significantly larger portion of ferric oxide compounds, deemed to be inert fillers. Silica fume and Sodium aluminate were found to be viable supplementary constituents from a mixture design perspective in reducing or increasing SI/Al value to target specific amorphous ratio value whilst adopting differing fly ashes.

Investigation of H/Si demonstrated that increased levels yielding increased flow values, with respect to Gladstone binary geopolymers, similarly when compared to previous works regard Eraring binary geopolymers. However comparable flow values for specific H/Si value were not observed. In terms of compressive strength, as observed in previous literature, higher H/Si lead to reduced compressive

strengths, deemed to be reflective of alkaline activator dilution. SEM imaging identified reduced dilution and less complete geopolymer binder for those samples with increased H/Si values. The instance of dosing (pre or post activation) did play a role in strength and flow outcomes, with further support that targeting amorphous H/Si in an effort to control flow values, it should be directed towards pre-activation dosing levels.

Investigation of amorphous Na/Al and Si/Al found that optimum compressive strengths at 28 days were achieved when targeting Na/Al = 0.54-0.74 and Si/Al = 3.1-3.5, with respect to Gladstone ternary geopolymers. These values correlated with previous Eraring based works. Some disparity between optimum compressive strength outcome of geopolymers utilising differing fly ash stocks was observed. It was observed that the inclusion of SA when targeting Si/Al, lead to increased water demand and accelerated/flash setting, supporting the notion of alkaline acceleration due to the increased presence of the alumina species within the system.

When investigating the robustness of the amorphous framework whilst adopting and maintaining amorphous ratios of Si/Al = 3.1, Na/Al = 0.6, H/Si = 8.5; and utilising various blend combinations of Eraring and Gladstone fly ash, statically similar compressive strengths were observed across all blend configurations at 7 days (32.1Mpa). At 28 days minor variation (8%) in compressive strength outcomes were limited to TG4 (51.2Mpa) compared to the other statically similar mixtures. Although the blended mixtures essential achieved the same compressive strength results, SEM imaging identified disparities between mixtures containing high levels of ether fly ash. These disparity related to the completeness and formation of the geopolymer binder and the macrostructure and densification of the ITZ.

Indexing Terms: Geopolymers, Fly Ash, Ground Granulated Blast Furnace Slag, Silica Fume, Sodium Aluminate, Admixtures, Compressive Strength, Activator Composition, Molar Concentration, XRF, QXRD, Amorphous, Mixture Design, Geopolymer Composites Mortars

ACKNOWLEDGEMENTS

During the course of this research project various individuals guided, supported and assisted me throughout the process, as such I would like to acknowledge and thank the following people.

I would firstly like to thank my supervisors, Dr Matthew Rowles and Dr Trevor Htut for their support and guidance during the entire process. I am truly grateful for their assistance and the opportunity to work alongside them on this project.

Additionally, I would like to thank the staff of the John de Later Centre and Concrete Material Laboratory at the Curtin University of Technology. I would specifically like to thank the team in relation to the quantification of the chemical composition of the aluminosilicate materials utilised within this research. The professionalism and specialist knowledge they brought to this project was invaluable and extremely appreciated.

Finally, I would like to extended my sincerest appreciation and gratitude to Mr Chee Keong Lau, a research fellow conducting research in the field of geopolymer production, quantification and reactivity. Mr Lau was an invaluable asset to this project, both physically and mentally.

TABLE OF CONTENTS

TABLE OF CONTENTS ..... **IV**

LIST OF FIGURES ..... **VII**

LIST OF TABLES ..... **IX**

LIST OF ABBREVIATIONS/ACRONYMS **1**

1. INTRODUCTION **2**
1.1 Geopolymer Concrete **3**
1.2 Research Aim and Objectives **5**
1.3 Research Scope **6**

2. LITERATURE REVIEW **8**
2.1 The Environmental Impact of Concrete **8**
2.2 Geopolymer Binders **10**
2.2.1 History and Progressive Developments 10
2.2.2 Characteristics and Applications 12
2.2.3 Limitations 13
2.3 Chemistry and Structure of Geopolymers **16**
2.3.1 Visualisation of the Geopolymer Structure 19
2.3.2 Determination of the Chemical Composition 20
2.4 Binary, Ternary and Blended Geopolymer Mortars **24**
2.4.1 Aluminosilicate Source Materials 26
2.4.2 Alkaline Activators 31
2.5 Mixture Design of Geopolymers **34**
2.5.1 Bulk Composition Mix Design 34
2.5.2 Amorphous Composition Mixture Design 36

3. METHODOLOGY **41**
3.1 Design of Experiments **42**
3.1.1 Preparatory Phase 42
3.1.2 Preliminary Phase 45
3.1.3 Secondary Phase 47
3.1.4 Tertiary Phase 49
3.2 Preparation of Experimental Components **51**
3.2.1 Preparation of Fine Aggregates 51
3.2.2 Preparation of Aluminosilicate Source Materials 52
3.2.3 Preparation of Alkaline Activators 56
3.3 Production & Testing of Geopolymer Mortar Specimens **57**
3.3.1 Geopolymer Mortar Mixing Process 58
3.3.2 Flow Testing 59
3.3.3 Casting and Curing 60
3.3.4 Compressive Strength Testing 61
3.4 Data Analysis **62**
3.4.1 Interquartile Rule 62

3.5 Specimen Analysis 63
3.5.1 Scanning Electron Microscopy 63

4. PREPARTORY PHASE 64
4.1 Particle Laser Sizing and SEM of Aluminosilicate Materials 65
4.2 Aluminosilicate Composition via X-Ray Techniques 68
4.2.1 Bulk Composition and X-Ray Fluorescence Results 68
4.2.2 Crystalline Composition and Quantitative X-Ray Diffraction Results 69
4.3 Determination of the Amorphous Phase 74
4.4 The Application of the Amorphous Mathematical Framework 76
4.4.1 Determination of the Elemental Proportion of the F-Matrix 77
4.4.2 Prescription of the W-matrix 79
4.4.3 The R-Matrix and Amorphous Ratios 80
4.5 Discussion 81
4.5.1 Particle size and Fineness 81
4.5.2 Difference in Gladstone and Eraring Fly Ash Amorphous and Crystalline Content 83
4.5.3 Supplementation of Amorphous Content through Additional Aluminosilicate Material and Alternative Activators. 85
4.6 Phase Conclusions 87

5. PRELIMINARY PHASE 88
5.1 Mixture Proportions 89
5.2 Observations 90
5.2.1 Mixing 90
5.2.2 Flow and Casting 91
5.3 Flow and Compression Results 92
5.4 Analysis 93
5.5 Discussion 95
5.5.1 The Influence of H/Si on Flow 95
5.5.2 The Influence of H/Si on Compressive Strength 97
5.6 Phase Conclusions 100

6. SECONDARY PHASE 101
6.1 Mixture Proportions 102
6.2 Observations 103
6.2.1 Mixing, Flow & Casting 103
6.3 Flow and Compression Results 104
6.4 Analysis 105
6.5 Discussion 108
6.5.1 Influence of Na/Al on Ternary Geopolymers 108
6.5.2 Influence of Si/Al on Ternary Geopolymers 111
6.6 Phase Conclusions 118

7. TERTIARY PHASE 119
7.1 Mixture Proportions 120
7.2 Observations 121
7.3 Flow and Compression Results 121
7.4 Analysis 122
7.5 Discussion 124

7.6 Phase Conclusions 130

8. CONCLUDING REMARKS 131

8.1 Conclusions 131

8.2 Future Work 134

9. REFERENCES 135

APPENDIX A – Particle Laser Sizing Results 143

APPENDIX B - Complete XRF Analysis Results 147

APPENDIX C – QXRD Results and Crystalline Composition Calculations 148

APPENDIX D – Amorphous Composition Calculations 149

APPENDIX E – Sample Calculation of Partial F-Matrix 150

APPENDIX F - F-Matrix of Individual Mixture Constituents and Calculations 152

APPENDIX G – Preliminary Phase Mixture Designs 157

APPENDIX H – Preliminary Phase Raw Data 159

APPENDIX I – Secondary Phase Mixture Designs 160

APPENDIX J – Secondary Phase Raw Data 163

APPENDIX K – Tertiary Phase Mixture Designs 164

APPENDIX L – Tertiary Phase Raw Data 166

APPENDIX M – Third Pary Copyright Permissions 167

LIST OF FIGURES

Figure 2-1 - Global cement and fossil energy production to 2016 8
Figure 2-2 - Three Groups of Tetrahedral Oligomers as Defined by Davidovits (1989) 16
Figure 2-3 - Three-dimensional Framework Structure of Na-Polysilate Polymer 17
Figure 2-4 – Representative Facture Morphology of Geopolymers Using 19
Figure 2-5- Typical Schematic of Bragg-Brentano Design XRD diffractometer 22
Figure 2-6 - SEM of Eraring Fly Ash 26
Figure 2-7 – Geopolymer Compressive Strengths With Respect to Sodium Hydroxide Molarity 32
Figure 2-8 – Compressive strength outcomes of metakaolin geopolymers. 35
Figure 2-9 - Mathematical Framework Originally Proposed by Williams and van Riessen (2010) 37
Figure 2-10 – Mathematical Mixture Design Framework 38
Figure 2-11 - Process of Determining Amorphous Atomic Ratios Using Mathematical Framework 38
Figure 3-1 - Overview of Research Experimental Processes 41
Figure 3-2 – Experimental Mixture Framework (Spano 2018) 43
Figure 3-3 – Determination of R-Matrix (Spano 2018) 44
Figure 3-4 – Calculation Method of the Amorphous Composition of the Aluminosilicate Materials 53
Figure 3-5 - Flow Testing Apparatus 59
Figure 4-1 – Particle Size Distribution from PLS of Aluminosilicate Binder Materials 66
Figure 4-2 - SEM Imaging of Eraring Fly Ash, Gladstone Fly Ash & Westbuild GGBFS 67
Figure 4-3 - Crystalline Peaks of Gladstone Fly Ash 69
Figure 4-4 - Crystalline Peaks of Eraring Fly Ash 70
Figure 4-5 - Crystalline Peaks of Westbuild GGBFS 71
Figure 4-6 - Crystalline Peaks of Ecotec Silica Fume 72
Figure 4-7 – F-Matrix : Feeder Stock Matrix 77
Figure 4-8 – W-Matrix : Weight Proportion Matrix 79
Figure 5-1: Contrasting Mortar Consistencies 90
Figure 5-2: Mortar Flows Observed Immediately after Mixing 91
Figure 5-3 - Flow (%) vs Amorphous H/Si 93
Figure 5-4 – Primary Phase Average 7 & 28 Days Compressive Strength and Strength Gain (%) 94
Figure 5-5 - Flow (%) vs H/Si Comparison 95
Figure 5-6 - Primary Phase Average 7 & 28 Days Compressive Strength and Graphical Trends 98
Figure 5-7 – SEM micrographs of PG1 (Left) and PG4 (Right) at 2000x Magnification. 99
Figure 6-1: Observations of SG5 and SG6 103

Figure 6-2 - Flow Results of the Secondary Phase Mixtures Prior to Casting 105
Figure 6-3 - Comparison of Compressive Strength and Amorphous Na/Al 106
Figure 6-4 - Comparison of Compressive Strength and Amorphous Si/Al 107
Figure 6-5 - SEM Micrographs of SG3 (Left) and SG4 (Right) at 2000x Magnification 109
Figure 6-6 - SEM Micrographs of SG5 (Left) and SG6 (Right) at 1000x Magnification 112
Figure 6-7 - SEM Micrographs of SG7 (Left) and SG9 (Right) at 1000x Magnification 115
Figure 6-8 - SEM Micrographs of SG7 (Left) and SE1 (Right) at 1000x Magnification 117
Figure 7-1 - Tertiary Phase Average 7 & 28 Days Compressive Strength 122
Figure 7-2 - SEM Micrograph of TGE1 at 300x Magnification 125
Figure 7-3 - SEM Micrograph of TGE1 at 300x Magnification 126
Figure 7-4 - SEM Micrograph of TGE1 at 1000x Magnification 127
Figure 7-5 - SEM Micrograph of TGE5 at 1000x Magnification 128

LIST OF TABLES

Table 2-1 - Bulk Oxide Composition of Various Fly ashes 27
Table 2-2 - Amorphous and Crystalline Composition of Collie Fly Ash 28
Table 2-3 - Bulk Chemical Composition of Various GGBFS 29
Table 2-4 - Average Compressive Strengths of Geopolymer Pastes 36
Table 2-5 - Contribution of Amorphous Content to Geopolymer Formulation by Element 39
Table 3-1 - Preliminary Phase Mix Configurations 46
Table 3-2 – Secondary Phase Binder Mix Configurations 48
Table 3-3 – Tertiary Phase Binder Mix Configurations 49
Table 3-4 – Alkaline Activation Utilisation 56
Table 3-5 – Production and Testing Requirements 57
Table 3-6 – Number of Mixes and Specimens 60
Table 3-7 – Number of Specimens Tested for Each Mixture Batch 61
Table 4-1 – Summary of Particle Laser Sizing Analysis 65
Table 4-2 – XRF Bulk Oxide Composition Summary of Aluminosilicate Materials 68
Table 4-3 - Crystalline Composition Result Summary of Aluminosilicate Materials Conducted via QXRD .. 73
Table 4-4 – Amorphous Composition of Gladstone Fly Ash, Eraring Fly Ash and Westbuild GGBFS 75
Table 5-1 – Bulk Mixture Proportions - Preliminary Phase 89
Table 5-2 – Summary of Flow Results – Preliminary Phase 92
Table 6-1 – Bulk Mixture Proportions - Secondary Phase 102
Table 6-2 – Summary of Results – Secondary Phase 104
Table 6-3 - Comparison Between Mixtures Targeting Si/Al < 3.0 From This Research and Spano (2018) . 111
Table 6-4 - H/Si, 28 Day Compressive Strength (MPa) and Flow of SG7, SG8 and SG9 114
Table 7-1 – Bulk Mixture Proportions - Tertiary Phase 120
Table 7-2 – Fly Ash Bulk Percentages 120
Table 7-3 – Summary of Flow Results – Tertiary Phase 121

LIST OF ABBREVIATIONS/ACRONYMS

ANOVA	Analysis of Variance
BSE	Back Scatter Electrons
C-A-H	Calcium Aluminium Hydrate
C-A-S-H	Calcium Alumino-Silicate hydrate
CO_2e	CO_2 equivalent
C-S-H	Calcium Silicate Hydrate
FA	Fly Ash
GGBFS	Ground Granulated Blast Furnace Slag
GHG	Green House Gas
ICDD	International Centre for Diffraction Data
IQR	Inter-Quartile Rule
K/N-A-S-H	Potassium/Sodium Alumino-Silicate Hydrate
LOI	Loss on Ignition
LVSTD	Low Vacuum Secondary Tescan Detector
N-A-S-H	Sodium Alumino-Silicate Hydrate
OPC	Ordinary Portland Cement
PLS	Particle Laser Sizing
QXRF	Quantitative X-ray diffraction
SA	Sodium Aluminate
SCM	Supplementary Cementitious Material
SE	Secondary Electron
SEM	Scanning Electron Microscopy
SF	Silica Fume
SH	Sodium Hydroxide
SS	Sodium Silicate
XRF	X-ray Fluorescence

1. INTRODUCTION

With the increasing prevalence to reduce man-kinds carbon footprint bearing down on all facets of modern life, the civil and construction industry is experiencing ever growing pressure to produce environmentally responsible alternatives to Ordinary Portland Cement (OPC) concretes. OPC concretes and the production of OPC have historically been known to contribute significantly to global emissions. With increased globalisation, urbanisation and the continued growth of developing nations, demand for OPC has experienced exponential growth since the mid-1940's. OPC production is estimated to contribute to 8% of global green-house gas emissions (Favier, Scrivener and Habert, 2019). The extent of emissions produced due to OPC production and global sustainability agreements, such as the Paris Agreement, have further cemented the notion that more sustainable alternative need to be considered.

In an effort reduce the extent of OPC produced, the cement industry has continued to further utilise supplementary cementitious materials (SCM) formed as by-products from industrial processes. These SCM are used as admixtures within typical concrete production to induce favourable qualities and properties (Bouzoubaa and Lachemi 2001, Khatri, Sirivivatnanon, and Gross 1995). Various SCM include fly ash, ground blast furnace slag (GGBFS) and silica fume, by-products of coal power generation and metal/alloy production processes. The use of SCM and their beneficial properties have led to the development and utilisation of cement alternatives known as geopolymers.

Currently, geopolymer concretes are utilised within precast applications due to limitations associated with heat curing and inconsistent compressive strength outcomes. Increased adoption and industry utilisation are hindered by current and typical mixture formation processes, which are not robust enough to deliver consistent mechanical properties. Development of these processes by researchers and industry alike are further hindered by the varied composition of fly ash and GGBFS stock materials, which in part is influenced by the industrial processes and materials involved in their production. Research targeted toward developing geopolymer mixtures which consider the amorphous (reactive) composition of these stock materials aims to assist in the further development of geopolymer mixture design moving forward.

1.1 Geopolymer Concrete

Formulation of geopolymer concrete involves replacing the OPC content with an aluminosilicate rich source materials such as, fly ash, GGBFS or Metakaolin. Rather than combining source material with water, typical to OPC concrete production, the aluminosilicate material is combined with a solution of high alkalinity, known as an alkaline activator. The addition of alkaline activating solution prompts a dissolution – re-solidification process (Williams 2015), whereby the aluminosilicate material is essentially dissolved and reformed into a 3D matrix. This reformed 3D matrix exhibits increased durability and mechanical properties compared to traditional OPC concretes, specifically in relation to fire, chemical and acid resistance. In addition to these favourable properties, the utilisation of typically waste product materials such as fly ash and GGFBS contributes the sustainability of geopolymer utilisation. Prior to investigating the benefits of SCM and geopolymers large volumes of fly ash produced internationally were deemed as waste and disposed of in landfills (Hardjito and Rangan 2005).

Despite from the previously outline benefits, geopolymer adoption as an OPC substitute has seen limited traction in the civil and construction industry. Mass adoption has been limited due to notions associated with inconsistent mechanical properties and the requirement for heat treatment to develop sufficient strength. Unary geopolymer binders (those which use a single aluminosilicate material) utilising fly ash, require heat curing to develop much of their mechanical strength due to the low-reactivity of fly ash stock materials. Heat curing erodes much of the sustainability benefits associated with geopolymer production. Additionally, heat curing processes limit geopolymers adoption to precast applications. To migrate the need for heat curing, investigation of binary geopolymers which utilised a combination of GGFBS and fly ash, have shown promising results in developing ambient cured geopolymers as GGBFS inclusion promotes early age compressive strength. Researchers are highlighting GGFBS inclusion as a potential solution to produce ambient cured geopolymer for cast in-situ applications (Saha and Rajasekaran 2017, Spano 2018). The presence of an additional aluminosilicate material although found to facilitate additional geopolymerisation, also attributes to increased complexities and considerations during production and subsequent assessment of these mixtures. This is primarily due to the concurrent formulation of various geopolymer bonds (Yip et al. 2008) and the differing mechanical and rheological properties of each material.

The inconsistencies observed in geopolymer production is believed to be attributed to the differing composition of the aluminosilicate materials such as fly ash and GGBFS, which is governed by the chemical processes associated with their production. In an effort to address this current mixture design processes prescribe mixture proportions based on the bulk or total composition of the stock material. These values are associated with silicon (Si) and aluminium (Al), two elements which align with typical geopolymer bonding mechanisms. This approach does little to consider the extent of amorphous (reactive) and

crystalline (non-reactive) content within the stock materials. It was suggested by Williams and van Riessen (2010) that the amorphous content should be targeted in an effort to develop a more reliable method to the bulk mixture design processes. This formed the basis of an amorphous approach to geopolymer mixture design. The amorphous approach utilises x-ray techniques to examine and determined the bulk and crystalline phases of the aluminosilicate source materials, to then determine the amorphous composition. A mathematical framework was proposed in an effort to consider the amorphous content of the mixture constituents and aid the mixture design processes. This framework was later expanded by Parnham (2016) and Spano (2018) to align with binary geopolymer production. Both Parnham (2016) and Spano (2018), utilised the framework to produce ambient cured binary (fly ash and GGBFS) geopolymer mortars, whilst reporting optimum ranges of amorphous ratios related to calcium (Ca), sodium (Na), hydrogen(H) and aluminium (Al). Parnham's 2016 works were actualised thorough an investigation of geopolymers containing fly ash and ground-granulated blast-furnace slag blended by amorphous ratios (Lau et al. 2019).

The amorphous approach to geopolymer formulation is still under developed and determination of its robustness and ability to produce geopolymers of consistent strength is still not quantifiable. However, researchers have been able to produce mixtures of high compressive strength without the need for heat curing using binary geopolymers. One hypothesis yet to be confirmed, is whether targeting specific amorphous ratios can lead to consistent strength values, regardless of the fly ash stock material. Very little has been done to address the differing composition of the fly ash stock materials and balance out shortfalls in amorphous content via supplementation. As the composition of fly ash is known to vary, addressing this notion is another challenge facing the amorphous approach and developing consistent mixtures regardless of the fly ash source.

1.2 Research Aim and Objectives

The aim of this research was to investigate if an amorphous approach to blended geopolymer production can yield consistent compressive strength results, whilst adopting a ambient curing regime. This research aimed to use various mixture constituents to supplement shortfalls in the amorphous content of the geopolymer aluminosilicate source materials, during the mixture design and production process. Upon completing various stages of the research scope and programme, detailed analysis of the experimental results and outputs were undertaken. This was done in correlation with the following research objectives in an effort to address the aim of the research.

The objectives of this research were as follows:

- To examine the extent of difference in reactive composition of two main fly ash stocks.
- To determine if complementary constituents such as silica fume or sodium aluminate can be used to supplement short falls in the reactive composition of fly ash stock materials.
- To investigate if an amorphous approach can be utilised to produce geopolymer mortars of comparable compressive strengths.
- To report the interaction between various reactive elemental ratios, specifically those associated with calcium (Ca), sodium (Na), hydrogen(H) and aluminium (Al).

1.3 Research Scope

This research is situated within the bounds associated with binary, ternary and blended geopolymer mortars cured at ambient temperature. The utilisation of a an amorphous approach to mixture design and proportioning forms one of the main pillars of this research. This approach was supported by a mathematical framework which aided in the formulation of geopolymer mixtures with prescribed amorphous content related to Si, Al, Ca, Na and H.

The scope of this project is defined by four phases, three of which consisted of experimental testing and analysis.

The four phases were:

- Preparation phase
- Preliminary phase
- Secondary phase
- Tertiary phase

The preparation phase involved the preparation of all relevant experiment components and constituents. This phase specifically related to the characterisation and determination of the amorphous content of the mixture constituents. This stage used bulk chemical composition analysis via XRF and crystalline chemical composition analysis via QXRD, to determine the amorphous composition of the aluminosilicate source materials. Within this phase, amorphous composition analysis was undertaken to examine the extent of difference in reactive composition between two differing fly ash stocks. This was undertaken to identify and address shortfalls in various reactive elements through the utilisation of supplementary constituents within the mixture design process.

Upon the completion of the preparation phase, the subsequent three phases defined the experimental scope of the research. In conjunction with the development of mixture designs and the production of specimens, experimental testing was undertaken to obtain compressive strength and flow results.

The preliminary phase, signified the first experimental phase and as such Gladstone fly ash binary geopolymers were produced and the influence of water content was examined. This was specifically undertaken with respect to the amorphous ratio of H/Si. The mixtures produced within this phase were compared to previously produced binary geopolymer mixtures (Spano et al. 2018) which utilised Eraring fly ash as the main binder stock. This phase served two purposes; one, to determine the required amount of

free water to produce a geopolymers with sufficient workability when using Gladstone fly ash; and two, to compare the compressive strengths associated with amorphous H/Si of differing fly ash materials.

The secondary phase, involved the development, preparation and testing of ternary geopolymer mixtures whereby the amorphous Si/Al and Na/Al ratios were varied and examined. Similarly, to the preliminary phase this was undertaken utilising Gladstone fly ash ternary geopolymers, and compared to equivalent Eraring fly ash ternary geopolymer mixtures (Spano 2018). This was undertaken through varied levels of the silica fume and sodium aluminate inclusion to manipulate amorphous Si/Al, and varied concentrations of sodium hydroxide to manipulate amorphous Na/Al.

The tertiary phase, involved the production of blended geopolymer specimens which utilised a combination of both Gladstone and Eraring fly ash stocks. Within this phase the amorphous content and associated amorphous ratios were held constant for all the specimens produced. This was undertaken in conjunction with SEM imaging to investigate the morphology and macrostructure of the specimens produced.

The mixtures produced in the three experimental phases, were done through the utilisation of the amorphous mathematical framework. Results and optimised values associated with each phase assisted in the definition of the variables for the subsequent phase. This was undertaken to ensure a holistic approach to the research scope and programme.

2. LITERATURE REVIEW

2.1 The Environmental Impact of Concrete

Modern day concrete can be produced through various mixture design processes for a multitude of purposes, however the main binding element of concrete is that of cement. Ordinary Portland Cement (OPC) is known for its reliability in the formulation of concretes for construction and civil applications. The sustainability of OPC is constantly being questioned due to the high levels of embodied energy associated with the construction material. The embodied energy of a material/object is typically adapted to a unit of measure known as embodied carbon dioxide (CO_2e). CO_2e is used to compare various carbon dioxide or greenhouse emitting processes to determine their global warming potential (Turner and Collins 2013). The primary contributor to the high levels of CO_2e associated with OPC is the high levels of energy require for its production, specifically the calcination of limestone. (Turner and Collins 2013). This in conjunction with other production processes approximately result in 840kg of CO_2e being emitted/produced in the production of one tonne of OPC. This paired with the projections highlighted in Figure 2-1, demonstrate that global OPC production will continue to rise above 4,000 Mt/yr (Andrew 2018) . This notion has the global community concerned regarding continued and increased CO_2 emissions, global warming and climate change policies.

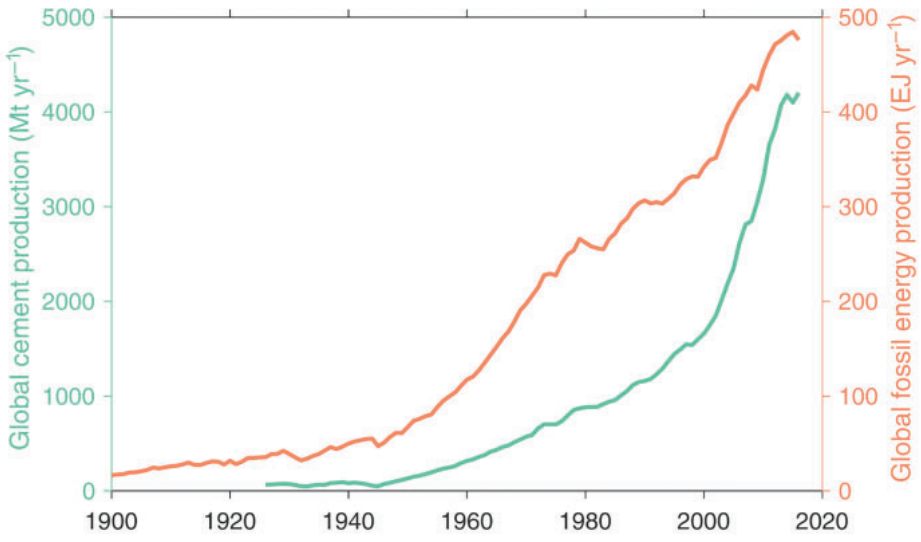

Figure 2-1 - Global cement and fossil energy production to 2016 (Andrew 2018)

Numerous environmental and climate change scientists, academics and advocates have drawn strong correlations with human industrialisation and development to increased levels of atmospheric CO_2 and global warming. Significant research has been undertaken with reference to increased global temperatures, the involvement of CO_2 and other greenhouse gases (GHG) and the greenhouse gas effect on global temperatures. Many of which state that carbon dioxide does not have to highest global warming potential, however the current rate of emissions far out way the global warming potential of CO_2 to other GHG, such as methane which has a global warming potential of 25 time that of carbon dioxide. Many believe that if current emission are not cut, global temperature will continue to rise. Increased global temperatures are believed contribute to increased storm intensity and frequency, extended droughts, increased sea levels, destruction of agricultural lands and reduced biodiversity.

In an effort to retard global temperature rises and the predicted detrimental effects, global leaders are focused on reducing global emission through prescribed limits on GHG emissions. Prescribed emission targets associated with CO_2, have been brought into effect through the ratification of international agreements such as the Kyoto Protocol (in effect until 2020) and the Paris Agreement (Grubb, Vrolijk, and Brack 1997, Rogelj et al. 2016). The Paris Agreements aims to limit the average global temperature rise to below 1.5- 2°C (Favier, Scrivener and Habert, 2019). Prescribed emission targets cause heavy emitting industries, such as the electrical generation industry and construction industry to reduce or offset their emissions through research and development of new and emerging technologies. However, the success of these international treaties and meeting such stringent targets rely on the government parties involved, their domestic initiatives and the regulatory authority they exercise.

With the implementation of emission target moving forward, the cement industry is being pressured to pursue alternatives binders and supplementary cementitious materials (SCM). Reducing the industries dependence on OPC binders is being explored through the development of alternative binders which utilised industrial by-products. A suggested alternative to replace or supplement the use of OPC, are binders known as Geopolymers. Geopolymers utilise waste products from industrial processes such as fly-ash, produced during coal power generation, to produced binders which exhibit superior properties to typical OPC binders. Large volumes of ‘waste’ fly ash are disposed of in landfill globally resulting in numerous environmental issues (Hardjito and Rangan 2005). Utilisation of such waste products has the potential to offset emissions from other non-cement producing processes, and limit the amount of emissions associate with cement production through a reduced need for OPC. Van Deventer et al. (2010) suggested that difference in CO_2e of OPC and geopolymer binders can be up to 80%, however this is dependent on the system boundaries, locations of source materials and curing requirements of the geopolymer binders.

2.2 Geopolymer Binders

2.2.1 History and Progressive Developments

Utilisation of first and second generation construction binders such as lime and OPC have been prevalent throughout history, with lime mortars being used by ancient Egyptians as early as 4000BC (Davidovits, 2020). Alternative binders such as geopolymers have been referred to as a third generation binders, due to their cementitious properties and mechanical characteristics. (Singh et al. 2015). Typical geopolymer binders are manufactured through the amalgamation of aluminosilicate materials and high alkaline solutions. In the 1940's Purdon successfully synthesised cementitious construction binders through the alkaline activation of non-cementitious solids (GGBFS) (Provis and Van Deventer 2009), however it wasn't until the late 1970's that significant research was directed towards the production of a polymer binder which utilised both aluminosilicate source materials and an alkaline activating solution. Davidovits (1979) proposed that through the alkaline activation of source materials rich in silicon (Si) and aluminium (Al), that a polymer binder could be produced. It wasn't until 1988 that Davidovits introduced the term "geopolymer" to described the cementitious binder that was produced through the dissolution and polymerisation process associated with geopolymer production (Davidovits 1988). Continued research into various types of aluminosilicate source materials and the activation process associated with each has fuelled research moving forward. Various researchers, (Palamo, Grutzeck, and Blanco 1999, van Jaarsveld and van Deventer 1999, Lee and Van Deventer 2002), have focused heavily on the polymerisation of low calcium fly ash, due to the environmental benefits associated with repurposing the large volumes of waste fly ash produced annually; and the high levels of Si and Al, found with this source material. However the varied nature of fly ash, complex bonding mechanisms and inherent difficulty of analysis still limit the adoption of geopolymers in main stream construction processes.

Apart from the environmental benefits associated with geopolymer binders, recent research has been driven by the superior properties geopolymer exhibit over OPC binders. Researchers have focused on the development of geopolymer binders which use various aluminosilicate source materials , such as fly ash, GGBFS, silica fume and rice husk ash. Modern research has focused on the effect various aluminosilicate source materials have on mechanical, rheological and service properties of geopolymer binders. Extensive research has been focused on unary geopolymers (those which use a single aluminosilicate source material), primarily fly ash or GGBFS geopolymers, as the drivers behind the geopolymerisation process and the resultant bonding mechanisms are still relatively unknown and inconsistent (Yip et al. 2008). In an effort to conduct industry relevant research, various researchers (Temuujin, van Riessen, and MacKenzie 2010, Hardjito and Fung 2010, Brough and Atkinson 2002) have explored geopolymer mortars (binder and sand). Although more relevant, geopolymer mortars are paired with additional hurdles and issues due to the

utilisation of sand filler materials leading to workability issues, increase alkaline activator demand and slow curing rates. These slow curing rates and low compressive strength have been found to be attributed to the presence of voids within the geopolymer matrix attributed to unreacted fly ash particles (Singh et al. 2015). Recent research associated with binary geopolymers (those which use two aluminosilicate source materials), has found that the short fall in compressive strength of geopolymers cured at ambient temperature can be addressed using a combination of fly ash and GGBFS (Lau et al. 2019). However, increased levels of GGBFS result in reduced workability and inhibit casting processes. Supplementary aluminosilicate source materials and alternative alkaline activators used to target specific reactive elements have been used to develop ternary geopolymers with promising results. Spano (2018) utilised silica fume in combination with fly ash and GGBFS to produce ambient cured geopolymers of up to 70MPa, whilst reducing the required amount of activating solution to be added to facilitate the dissolution and geopolymerisation.

With significant research conducted on unary geopolymers, both binary and ternary geopolymers are still relatively uncharted areas of research. Binary and ternary geopolymers enable the utilisation of a combination of aluminosilicate source materials in an effort to employ the complementary characterises of each source material. This can be seen with binary geopolymers, whereby the early age strength of GGBFS and the rheological benefits of fly ash are paired to address the low reactivity fly ash geopolymers and poor workability of GGBFS geopolymers. Currently literature has extensively developed mixture designs and geopolymer proportions upon the bulk composition of constituents. This approach has been identified as problematic in the production of geopolymers of consistent quality as it does little to identify the reactive and non-reactive composition of the mixture components. To remedy this notion, Williams and van Riessen (2010) suggested that an amorphous approach should be undertaken to identify the reactive composition of the geopolymer constituents. It was suggest that this approach would better identify and define the available elemental content required for increased geopolymerisation. This concept was paired with a mathematical framework which both Sweeney (2017) and Lau et al. (2019) used to develop fly ash and GGBFS unary geopolymers utilising an amorphous approach to mixture design. This framework was adapted and expanded by Parnham (2016) to produce binary geopolymers, in an effort to explore the influence GGBFS had on an amorphous approach to ambient cured geopolymers. Parnham's 2016 works were later published in 2019 (Lau et al. 2019). The mathematical framework was manipulated further in 2018 by Spano to assist in determining the influence silica fume and sodium aluminate had on the ambient cured geopolymers. Of the above amorphous researchers, recommendations put forward revolved around exploring the uses of differing fly ash types, determining the influence specific reactive elemental ratios have on compressive strength, investigating water/alkaline activator demand and addressing inconsistency issues during production (William 2015, Sweeney 2017, Lau et al. 2019, Lau et al. 2020, Spano et al. 2020).

2.2.2 Characteristics and Applications

One of the main driving factors of continued geopolymer research is the advanced characteristics and properties it exhibits compared to OPC. These enhanced properties include, high fire resistance, low permeability and strong chemical resistance. Such properties, paired with potential environmental benefits of reduced OPC dependence make geopolymers an attractive alternative to traditional OPC concretes.

2.2.2.1 Chemical and acid resistance

The high chemical and acid resistance of the formed geopolymer matrix allows for the utilisation of geopolymers in harsh environments (Bakharev 2005, Hardjito 2004). This is primarily due to the dense an non-porous nature of the geopolymer matrix. These properties have led to the adoption of precast geopolymer sewer pipes, whereby exposure to weak acids from bacterial actions, sulphates, water and atmospheric CO_2 (Oualit et al. 2012), typically result in accelerated degeneration of traditional OPC sewer pipes. Additionally hazardous material and chemical immobilisation has been suggested as a potential use for geopolymers and the absorptive and durability properties of the geopolymer matrix (Davidovits 2002, Davidovits 1991).

2.2.2.2 Mechanical Strength

One of the main performance measure associated with geopolymers and OPC binders, mortars and concretes is mechanical strength. The strength of geopolymers is influenced by several factors, these include mixture ratios, curing temperature and conditions, free water content and the types and extent of the bonding mechanisms involved. A specific measure of mechanical strength and measure used to prescribed concrete within design and construction is compressive strength. The compressive strength of geopolymer specimens are introspective of completeness of the formed geopolymer matrix, the morphology of the microstructure and how it was formed, as well as the macrostructure and specifically the presence of voids and microcracks (Williams 2015). Continued research has explored various parameters utilising elevated and ambient curing regimes, alkaline activator type and concentration as well as various aluminosilicate source materials, all in an effort to yield high compressive strengths. Elevated temperature curing has provided an efficient means of reaching compressive strength of up to 80MPa (Hardjito and Rangan 2005, Saha and Rajasekaran 2017). Yet this erodes the environmental benefits of using geopolymer due to the energy required to heat and cure the geopolymer components. Additionally this limits the utilisation of geopolymers to precast elements as heat curing in-situ construction components can be complex, costly and reduced the quality the cast components.

2.2.3 Limitations

Mass adoption of geopolymers within the construction industry is hinder by several limitations which make them a less practical option to consistent performing OPC alternatives.

2.2.3.1 Inconstancy

A significant issue facing the increased adoption of geopolymers is the reproduction of consentient mechanical and physical properties. Issues associated with variable setting times and the concept of flash setting are a common occurrence during geopolymer binder design and reproduction. Additionally, inconsistent strength outcomes provide little reassurance in terms of quality and design capacity. The suggested cause of such inconstancies in geopolymer production is hinted towards the varied composition of the source materials (Williams 2015). Van Jaarsveld and van Deventer (1999) established that setting times of geopolymer mortars are dependent on the tendency of fly ash particles to react the alkaline activating solution. The varied nature in which fly ash is produced through coal power generation tends to result in fly ash materials of varied composition (Malhotra et al. 1994) , this paired with the composition and concentration of alkaline activating solutions, dictates the extent of the dissolution process and geopolymerisation reaction (Kumar et al. 2007).

These inconsistent outcomes reflect back towards the chemical composition and the extent of the reactive elements available to facilitate more complete geopolymerisation. This being said, bulk mixture design does little to differentiate the chemical composition of the differing aluminosilicate source materials and the non-reactive crystalline elements.

2.2.3.2 Heat curing

As outlined previously, geopolymer production typically requires heat curing to develop compressive strength. This notion limits the extent in which geopolymer binders can be adopted. Heat curing regimes adopted by Hardjito and Rangan (2005) and Oliva, Monita and Nikraz (2009) achieved compressive strength of up to 80MPa, whilst curing specimens for 24 hours at temperatures of 60 - 90°C. Heat curing at these temperatures and durations approximately contribute 13% of the CO_2e emissions associated with geopolymer production (Turners and Collins 2013). Although the application of heat can promote geopolymerisation, extended durations of elevated heat curing can have detrimental effects to the formation of the geopolymer matrix (Perera et al. 2017). The contributing failure of samples at a later ages is believed to be due to the thermolysis of the geopolymer bonds exacerbated through long duration heat curing (Singh et al. 2015).

Ambient cured fly ash based geopolymers struggle to develop sufficient compressive strength due to the low reactivity and slow geopolymerisation process. Binary geopolymers which utilise varied levels of GGBFS have shown favourable results in producing geopolymers which mirror the compressive strength outcomes of those achieved by researchers utilising heat curing methods (Lau et al. 2019, Saha and Rajansekaran 2017, Spano 2018). Spano (2018) also demonstrated that highly amorphous aluminosilicate source materials such as silica fume have a significant contribution to the compressive strength of ambient cured ternary geopolymers and may assist in reducing the need for heat curing.

2.2.3.3 Workability

Workability in terms of cementitious mortars refers to the ability of a mixture to be mixed, placed, consolidated and finished, with ease and without loss of homogeneity (American Concrete Institute (ACI) Standard 116R-00 (ACI 2000). An acceptable level of flow (a measure of workability) for cementitious mortars has been prescribed by the ASTM C270-19a (ASTM 2019) to be approximately 110 ± 5% however, acceptable levels should be accessed based on the setting and casting requirements of specific applications. In terms of the workability of geopolymers there are several factors which aid the workable nature of the mixture and hinder it. These factors are associated with the characteristics of the constituents and the production process.

Source materials such as fly ash and GGBFS have opposing effects on workability and flow. The spherical nature of fly ash particles have been used in OPC concrete to increase workability. This premise is believed to attribute to the increased flow and rheological properties of geopolymer pastes. In retrospect, the angular nature of GGBFS particles, due to the grinding processes is believed to have determinantal effects on flow. This paired with the finer nature of GGBFS can lead to low slump and flow results (Deb, Nath, and Sarker 2014). The influence of GGBFS is also heavily dependent on water and activator dosing, concentration and composition. Activator composition is also known to influence the workable state of the geopolymer mixture due to activator viscosity and dissolution potential. Highly viscous activating solutions such as sodium silicate can reduce workability values, whilst high molarity (14M) activators with low viscosity such as sodium hydroxide, can increase the dissolution process (Lee and Van Deventer 2002), leading high flow values, but increase the presence of reactive ions causing reduced setting times, flash setting and low workability levels (Rahim et al. 2014).

During the production process of typical OPC mortars and cements, the addition of free water is undertaken to increase workability and flow. With respect to geopolymer production, the addition of excess water has shown negative effects through the dilution of the alkaline activation solutions. Increasing the water to solids ratio can reduce compressive strength by 5MPa (Rangan 2008). However insufficient free water leads

so incomplete bonding and poor compressive strength. Sufficient free water is require to facilitate mixing and ion transportation (Barbosa, MacKenzie, and Thaumaturgo 2000). Parnham (2016) found that differing fly ash stocks (Eraring and Gladstone) required varied levels of free water incorporated, demonstrating the inconsistencies associated with geopolymer production. Spano et al. (2018) also demonstrated that varied levels of free water incorporated before and after activation had varied effects. It was also highlight that initial wetting of the dry constituents (fly ash, GGBFS and sand) resulted in geopolymers with mortar like properties that facilitated sufficient compaction. However over wetting produced slurry like mortars which experience aggregate/sand segregation.

2.3 Chemistry and Structure of Geopolymers

Geopolymers are produced through the synthesis of solid aluminosilicate source materials activated by alkaline solutions, resulting in a highly cross-linked amorphous gel binder (Provis et al. 2009). The geopolymerisation process can be summarised into a dissolution-reorientation-solidification reaction (Williams 2015). Part, Ramli and Cheach (2015) more accurately described these stages as; the dissolution of the aluminosilicate source material under highly alkaline conditions; the transportation and reorientation of dissociated ions and coagulation and gelling of oxides; and the polycondensation and solidification of these oxide rich gels to produce a 3D silico-aluminate structure. In 1989, Davidovits defined these 3D networks based on the consequential chemical bonding into three groups as defined in Figure 2-2.

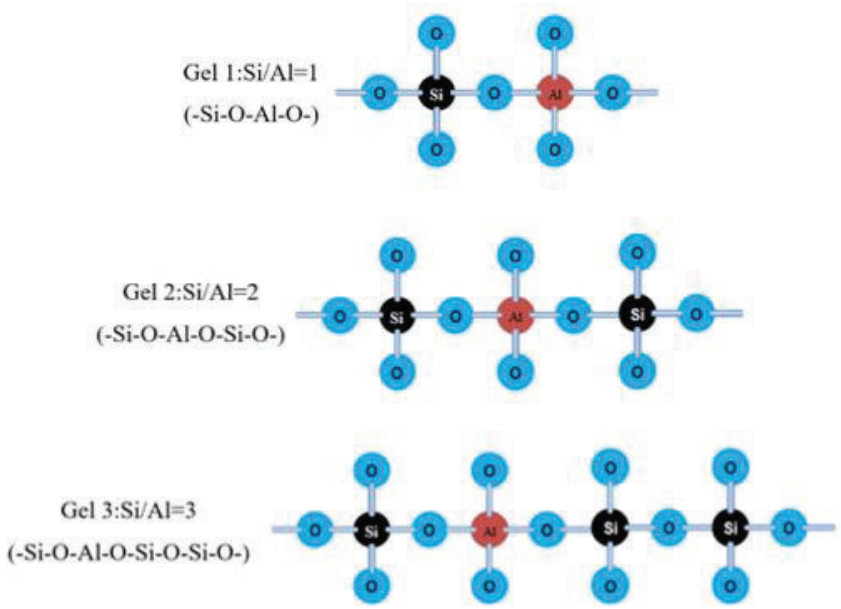

Figure 2-2 - Three Groups of Tetrahedral Oligomers as Defined by Davidovits (1989) (Zhang et al. 2020)

These groups are known as poly(sialate) (-Si-O-Al-O-), poly(sialate-siloxo) (-Si-O-Al-O-Si-O-), and poly(sialate-disiloxo) (-Si-O-Al-O-Si-O-Si-O-). Each of which are dependent on the ratio of silicone and aluminium, and are bridged together through shared oxygen ions. These tetrahedral oligmers form a three dimensional polymeric chain/ring structure allowing the binder to gel (Xu and Van Deventer 2000). The Si-O-Al networks allow geopolymers to develop their strength through the polymerisation of silicone and alumina to form a cementitious framework (Sweeney 2017). The anionic nature of these oligomers is balanced by positive ions such as Ca^{2+}, Na^{+}, K^{+} (Lau et al. 2019,). Figure 2-3 represents a 3D geopolymer framework of Si-O-Al bonds neutralised with sodium ions (Na^{+}). This neutralisation is due to the presence of Na^{+} within the alkaline activating solution.

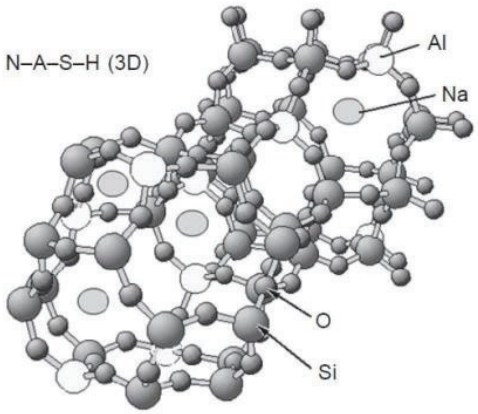

Figure 2-3 - Three-dimensional Framework Structure of Na-Polysilate Polymer (Garcia-Lodeiro et al. 2015)

Specific bonding mechanisms associated with geopolymerisation is dependent on the presence of these positive ions, as well as the availability of aluminium. Initial bonding mechanisms and those associated with early age compressive strength are typically dependant on the availability of calcium. Source materials low in calcium such as Class F fly ashes produced K/N-A-S-H gel monomers (Potassium/Sodium Aluminium Silicon Hydrate) (Singh et al. 2015). This is due to the tenancy for high pH environments with limited calcium availability to support the polymerisation of aluminate and silicate species. In retrospect, the presence of calcium leads to the formation of Calcium Silicate Hydrates (C-S-H), typical to OPC hydration reactions and C-A-S-H (Calcium Aluminium Silicon Hydrate) gels, which are associated with geopolymerisation. The extent of the networks formed and the transportation of these positive ions are dependent on the free water content available for ion transportation and the extent of ions present (Barbosa, MacKenzie, and Thaumaturgo 2000).

As outlined above, the bonding mechanisms involved in geopolymer production reflect those similarly observed during the hydration process of OPC (C-S-H) and those of aluminosilicate geopolymerisation through alkaline activation (K/N-A-S-H and C-A-S-H). Yip, Lukey and Van Deventer (2005) found that these bonding mechanisms can co-exist, however their interaction is complex. The geopolymerisation bonds of N-A-S-H and C-A-S-H have been identified as much slower forming than those of C-S-H (Hanjitsuwan et al. 2014). This reflects the early forming C-S-H phase and the subsequent early age compressive strength associated with geopolymers of high calcium content, such as binary fly and GGBFS geopolymers. The speed at which each of these bonds form are due to numerous factors, however a major component is due to the availability of the dissociated species and pH of the system (Singh et al. 2015). The slow leaching nature of Al from the aluminosilicate source material, compared to Ca and Si, which are dissociated first, result in the slower forming geopolymer bonds (N-A-S-H and C-A-S-H) contributing to later strength gain and early age

strength supplied by the formation of C-S-H. This is problematic in low calcium fly ash geopolymers as heat curing is required to accelerate and induce increased N-A-S-H bonds. Introduction of GGBFS has been used to facilitate the development of the C-S-H and promote early age compressive strength. This results in the Ca^{2+} ions to be initially favoured over Na^{+} ions, resulting in mainly calcium bonding phases (C-A-S-H and C-S-H). Excessive levels of GGBFS (>50wt%) have shown the detrimental effects of increased C-S-H bonds in conjunction with geopolymer bonds, through the development of micro-cracks within the macrostructure of geopolymer samples (Deb, Nath, and Sarker 2014).

In summary the chemical composition of the constituents play a vital role in the completeness, extent and type of bonding mechanisms of geopolymers. These bonding mechanisms although found to coexist are complex and can be influenced by the type of source materials used, the pH of the system, and dissolution process. Reactive elements such as Ca, Al, Si, Na and O are present in the newly formed bonds, which form part of the geopolymer matrix and influence mechanical properties such as compressive strength.

2.3.1 Visualisation of the Geopolymer Structure

Visualisation of the macro structure of geopolymers can be undertaken through the utilisation of Scanning Electron Microscopy (SEM). SEM can be used to reveal the surface morphology and chemical composition. SEM is preferred over modern light microscopy, due to the increased magnification and clarity it can achieve. Light microscopy is limited due to the wave length of white light used and the power of the objective lens. Conventional SEM imaging can achieve magnifications ranging from 20x to 30000x.

SEM analysis focuses high energy electrons at a solid sample to generate a variety of signals from the surface of the sample. These accelerated electrons dissipate as they decelerate into the sample to produce a number of signals which include secondary electrons, back scatter electrons and diffracted back scatter electrons. Secondary electrons are used to show the morphology/topography and macrostructure of the sample, whereas backscatter electrons are used to illustrate the contrasts in composition of multiphase samples. Back scatter electrons are less useful for geopolymer samples as the common elements, such as such as Na, Ca, Si and Al, all have similar atomic numbers. This leads to images with limited contrast in which topographic detail is lost.

Secondary electron SEM images have been used to visually examine the completeness of dissolution-reformation process associated with geopolymer production. Figure 2-4 demonstrates the application of SEM images to examine the fracture surface of geopolymer samples which utilised differing fly ash types.

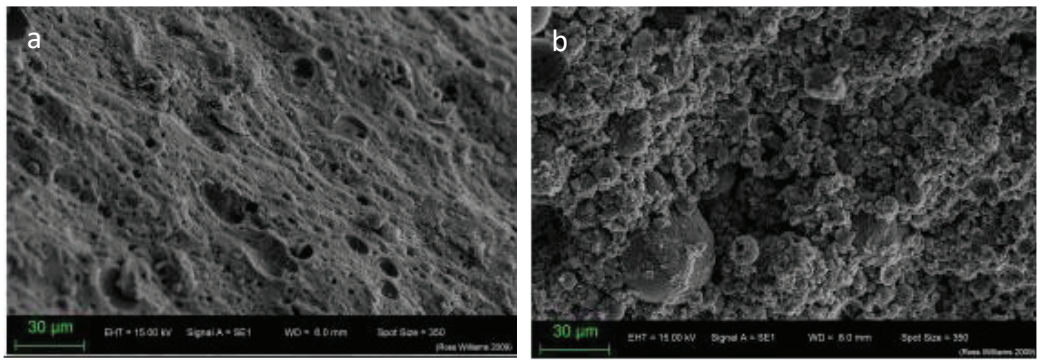

Figure 2-4 – Representative Facture Morphology of Geopolymers Using
(a) Port Augusta Fly Ash and (b) Bayswater Fly Ash (Williams and van Reissen 2010)

The SEM images above demonstrate the difference in the morphology and topography of two geopolymer samples. The smoother and complete nature of the geopolymer produced by the Port Augusta fly ash demonstrates increased geopolymerisation in contrast to the grainy and course topography of the Bayswater fly ash. This notion was supported by Williams and van Riessen (2010) with the Port Augusta sample achieving considerably higher compressive strengths (45Mpa) to that of the Bayswater sample (9.5Mpa).

2.3.2 Determination of the Chemical Composition

2.3.2.1 Amorphous and crystalline phases

Geopolymers and aluminosilicate solids consist of two phases, a non-reactive crystalline phase and a reactive amorphous phase. The presence of these phases dictate the reactivity of the aluminosilicate materials or the completeness of the geopolymerisation reaction with respect to formed geopolymers. The highly ordered lattice structure of the crystalline phase compliments the shapeless nature of the amorphous phase. As such, the fixed molecular structure of the crystalline lattice results in a phase which is highly stable and significantly less reactive compared to the amorphous phase. The unstructured nature of the amorphous phase is referred to as glassy, due to its formless and reactive nature. Amorphous solids are those involved in the dissolution process and responsible for providing the reactive ions responsible for the geopolymer bonds. In retrospect the inert nature of the crystalline phase is attributed to strength of polycrystalline bonds. This notion typically defines the crystalline content in aluminosilicate materials as a filler in geopolymer mixture design. In general, the newly formed geopolymer matrix is essentially crystalline in nature. However, unreacted amorphous contents is still present due to incomplete dissolution and the formation of secondary precipitates, which form around amorphous solids and inhibit further dissolution and therefore higher levels of geopolymerisation (Lee and Deventer 2002).

When adopting an amorphous approach to mixture design, amorphous solids in aluminosilicate materials such as silicone and aluminium are targeted to facilitate the development of the geopolymer bonds mentioned in *2.3 - Chemistry and Structure of Geopolymers*. The reactivity of the aluminosilicate source materials is heavily influenced by the silicone and aluminium glass content (William 2015, Tennakoon et al. 2015). This highlights the importance of determining the amorphous composition of the source materials as it defines the extent and completeness of geopolymerisation and newly formed geopolymer crystalline lattice.

Current mixture design processes consider the chemical composition of the aluminosilicate source materials with reference to bulk composition. Bulk composition refers to the total composition of the source material considering the inert crystalline and reactive amorphous phase. This provides an inaccurate measure of the source materials reactivity and quantity of desired elements, as a portion is typically locked away within crystalline oxides. As such, the true reactivity and amorphous composition is represented whilst being combined with the crystalline content, resulting in geopolymers of sub-par and inconsistent mechanical properties. To accurately determine both the amorphous and crystalline composition of the source materials, two x-ray analysis techniques are required; X-Ray Fluorescence (XRF) and Quantitative X-Ray Diffraction (QXRD).

2.3.2.2 X-Ray Fluorescence (XRF)

X-Ray Fluorescence (XRF) is a x-ray technique which is used to determine the total (bulk) chemical composition of sample or aluminosilicate material. This process is used to determine the total wt% of each elemental oxide within a given sample. The XRF process exposes a sample to high energy x-rays in an effort to determine the quantity and composition of elemental oxides, through a phenonium known as fluorescence. Fluorescence is instigated by emitting high energy x-rays at a sample. This excites the electrons of the inner orbitals causing electrons to be ejected from the atom due to x-ray interaction known as photoelectric absorption. The ejected electrons result in a vacancy within the inner orbital which is subsequently filled by those of a higher orbital. This transition results in energy being emitted from the atoms, as the electron moves closer to the atom nucleus. This emitted energy can be measure and is defined as the fluorescence phenomena. The fluorescence of each element is unique, as such this is measured and quantified to determine the total composition of a sample.

2.3.2.3 Quantitative X-Ray Diffraction (Q-XRD)

Quantitative X-Ray Diffraction (QXRD) uses an x-ray diffraction (XRD) process and quantitative data analysis to determine the crystalline composition of a sample. XRD data is obtained by bombarding a sample with x-rays and measuring the diffracted patterns of x-rays which interact with the crystalline structure of the sample material. The interaction between the source material and crystalline materials result in distinct peak patterns and various angles. Specific crystalline materials yield unique diffraction angle and peaks. This concept is often analogised with reference to distinguishing someone by their fingerprints. The diffracted x-rays are measured and recoded using a linear detector within the XRD apparatus. Figure 2-5, demonstrates a schematic of a common x-ray diffractometer, which is based off the Bragg-Brentano Design.

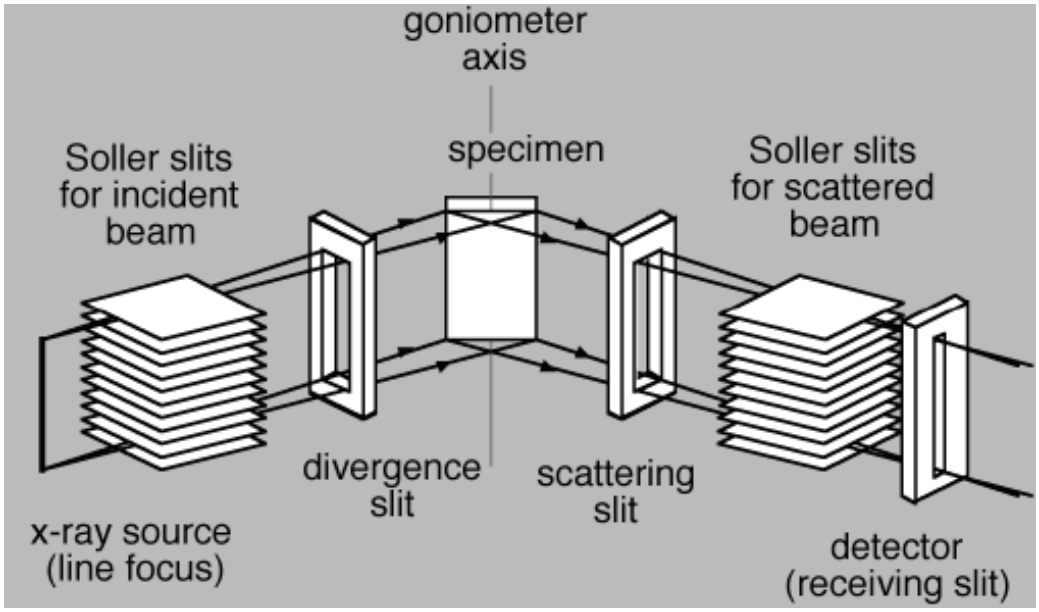

Figure 2-5- Typical Schematic of Bragg-Brentano Design XRD diffractometer

The Bragg-Brentano design x-ray diffractometer is commonly used to determine the crystalline composition of powdered materials. Diffractometers of this design have long been used for powder samples, as such instrument errors have been studies in detail. These errors are associated with the spectroscopic properties of the x-ray source (varied x-ray wavelength), axial divergence aberration (influence of incident and diffracted beam angles), flat specimen aberration (influence of sample surface shape) and sample transparency effect (influence of material absorption). The influence of these effects are modelled using various analytical geometry and resulted in the precise instrument function of the commonly used Bragg Brentano design.

The diffraction data produced by the XRD apparatus can then be used to determine and quantify the type of crystalline content within the sample. This process involves quantitative data analysis. Quantitative analysis using the whole pattern of the diffraction data is referred to as Rietveld analysis. Rietveld analysis examines the whole diffraction pattern to determine the structure, size and quantity of each crystalline oxide. Utilisation of the whole pattern, rather than a select number certain peaks produces increased accuracy and consistency of results (Rietveld 1969). Rietveld analysis examines each pattern against "standard" patterns and the crystalline structure of previously analysis and known samples.

Quantification of the crystalline phases present in fly ash and GGBFS stocks have utilised Rietveld quantitative phase analysis (Rietveld, 1969) paired with TOPAS software (Coelho, 2018). This method uses the internal standard method (Hill and Howard, 1987). The internal standard method involves adding a known amount of a stable, unreactive and pure crystalline powdered material to a sample to derive the concentration of a phase in the crystalline composition. This method allows Rietveld analysis to be undertaken on the XRD data, whereby Rietveld weight fractions are converted to values via the internal standard method to obtain the amorphous composition and crystalline composition in percentage of weight (Coelho, 2018). This analysis is undertaken within the TOPAS software and allows for the determination of multiple crystalline phases with each sample whilst limiting errors.

2.4 Binary, Ternary and Blended Geopolymer Mortars

The terms binary (two) and ternary (three) refer the number of source materials used within the geopolymer formulation. These geopolymers utilise multiple aluminosilicate source materials in an effort to exploit the complimentary characteristics of each specific source material. Through the utilisation of multiple aluminosilicate source materials many of the shortfalls associated with unary fly ash geopolymers can be overcome. The term blended geopolymer refers to geopolymers which utilise a combinations of a single source material, ie two types of fly ash.

Binary geopolymers consist of two aluminosilicate source materials, typically fly ash and GGBFS. The inclusion of GGBFS aids the setting process, overcoming the low reactivity and slow setting times of fly ash based geopolymers. As outlined in *2.3 - Chemistry and Structure of Geopolymers*, this instigates additional bonding mechanisms not present in low calcium fly ash based geopolymers. The inclusion of GGBFS and the formulation of binary geopolymers mitigate the need to heat curing of geopolymer specimens in most cases (Cheah, Part, Mahyuddin 2017). This notion is dependent on the reactivity of the fly ash stock materials, levels of GGBFS included and alkalinity of the activating solutions. Increased levels of GGBFS reduce workability, whilst increasing compressive strength to a certain extent. Levels above 50wt% have demonstrated negative effects through the introduction of micro crack within the macrostructure of the geopolymer structure (Perera et al. 2007).

Ternary geopolymers employ a thrid aluminosilciate source materials in a effort to promote geopolymer bonds and facilitate the benefitical propeties of geopolymers. An additonal source material which as shown promise is that of silica fume. High amorphous silica fume, a by product from silica and ferros alloy production, is comprised prodominatly of amorphous silicone. As such, when included into geopolymer production its fine nature and highly amorphous composition results in geopolymer of increased compressive strength. The inclusion of upto 7wt% of silica fume within a ternary geopolymer binder was found to be optimum (Spano 2018). This was further supported by Adek et al. (2014) who found that the inclusion of up to 6-8% of colloidal nano-silica increased the compressive strength of fly ash geopolymers mortars to optimum values. This was due to the increased presence of reformed crystalline SiO_2 found within the geopolymer matrix. Similarly to GGBFS, high levels of silica fume have shown negative effect associated with flow and compressive strength. This is believed to be due to the formation of agglomerates (clusters of particles), which hindered the formation of both the C-S-H and geopolymers phase (Khater 2013).

Geopolymer mortars incorporate the binder constituents (aluminosilicate source material and alkaline activators) with sand aggregates. The inclusion of fine sand increases the liquid/activator demand on the

system depending on the initial moisture content of the material and proportions incorporated. Geopolymer mortars of high compressive strengths can be achieved through optimisation of activator dosing (Temuujin, van Riessen, and MacKenzie 2010), however limited research has been conducted into specifying appropriate dosing levels. This being said researchers have reported that levels of 10-30wt% of sand aggregates within the geopolymer binder exhibited acceptable flow, were those incorporating 40-50wt% suffered poor compaction and lower compressive strengths (Chindaprasirt et al. 2007). In retrospect both, Lau et al. (2019) and Spano et al. (2020), incorporated levels of silica sand between 50-60wt%, to produce binary and ternary geopolymers of up 70Mpa, under ambient curing conditions. Both researchers utilised water dosing to ensure sufficient flow for casting and compacting. Parnham (2018) incorporated additional water into the geopolymer mortar during mixing to mitigate workability issues, whereas Spano et al. (2018) initially dosed the dry constituents with free water prior to activation. Water dosing is favourable over alkaline activator dosing as excessive levels of unreacted activator can result in serviceability issues and leaching carbonate salts such as efflorescence. Additionally increased levels of alkaline activators contribute to the embodied energy of the produced geopolymer, reducing the sustainability associate with using geopolymers as an alternative to OPC.

The following sections outline the constituents of the ternary geopolymer mortars, the varied nature of their composition, specific properties which make them favourable and how they influence the mechanical properties of formed geopolymers.

2.4.1 Aluminosilicate Source Materials

2.4.1.1 Fly ash

Fly ash is recognised as a by-product of coal power generation and typically defined as a fine powder/ash consisting of spherical shaped partials. These particles are formed form the combustion of ground or powdered coal (ACI-Committee 232. 2018). Figure 2-6, shows the spherical shape of the fly ash particles examined under scanning electron microscopy.

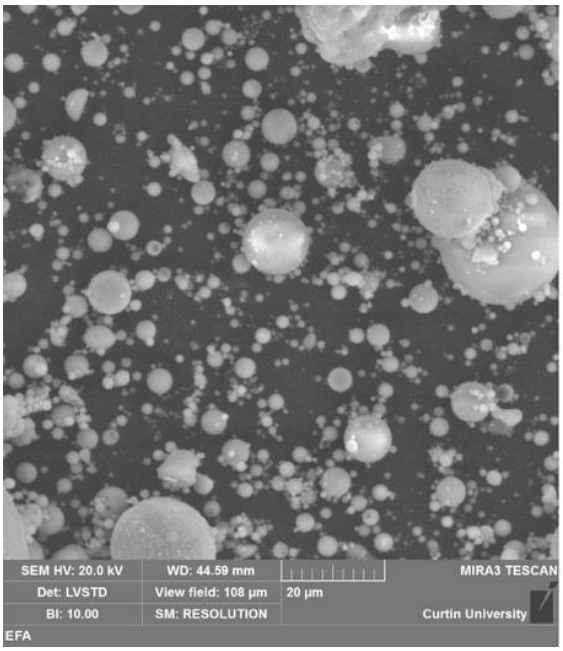

Figure 2-6 - SEM of Eraring Fly Ash

Although the shape of fly ash particles are generally are consistent, the chemical composition of fly ashes produced by various coal fire processes, typical power generation stations, are varied due to the range of coals mined and utilised globally (Malhotra et al. 1994). Additionally, the nature of the combustion process is heavily responsible for the complex morphology and rheology of fly ash production. Gardner et al. 2015, stated that the varied rate of reactivity associated with fly ash particles is reflective of the composition, mineralogy and particle size of the coal burned. The numerous combustion processes employed in regards to power generation processes and the various coals utilised result in fly ashes of varied chemical composition. This notion can be seen from the data presented in Table 2-1.

Table 2-1 - Bulk Oxide Composition of Various Fly ashes (Tennakoon et al. 2014)

	SiO_2	Al_2O_3	CaO	MgO	Fe_2O_3	Na_2O	P_2O_5	Cr_2O_3	K_2O	MnO	SO_3	TiO_2
Gladstone	51.10	25.60	4.30	1.45	12.5	0.77	0.89	–	0.70	0.15	0.24	1.32
Collie	60.0	24.60	0.15	0.99	8.56	0.36	0.22	0.04	0.36	0.04	0.18	1.53
Eraring	63.20	25.20	0.07	0.57	3.36	0.72	0.25	–	1.81	0.07	0.18	0.99
Bayswater	80.40	14.00	0.04	0.31	3.57	0.10	0.09	–	0.85	0.04	0.08	0.49

As defined in Table 2-1, it can be seen that fly ashes of various locations do consist of the same type of oxides, however the quantities associated with each can vary significantly. An example of which can be seen when comparing the bulk chemical composition associated with SiO_2 for Gladstone and Bayswater fly ash, with Bayswater containing almost 60% more bulk silicone oxide. This notion becomes increasingly important when referencing to those elements responsible for the formation of geopolymer bonds.

In terms of fly ash production there is very little governance associated with the quality of fly ashes produced unlike OPC. This being said, fly ash is defined into specific classes based primarily on calcium content. Fly ashes produced from the combustion of bituminous coal typically results in F Class fly ash due to the low CaO content. As defined by ASTM C618-9 (ASTM 2019-3), F Class fly ash must contain <10% CaO content, otherwise defining it as C Class. F Class fly ash is believed to be favourable due to the high aluminosilicate glass content and low Ca content (Hardjito and Rangan 2005). Detailed research conducted by Chen Tan (2010) and van Riessen and Chen Tan (2013) found that the entire chemical composition did not influence geopolymerisation. Compound oxides such as Fe_2O_3 were found to act as fillers as they did not react with the alkaline activators. Chen Tan (2010) also stipulated that SiO_2 and Al_2O_3 should only be considered and although Na_2O did react, its content was negligible and should be disregarded.

When referencing fly ash composition in association with geopolymer mixture design, often identification and separation of the crystalline and amorphous phases are omitted. Table 2.1, defines the total composition (crystalline and amorphous) of the fly ash samples. Consideration of the crystalline composition is paramount as it is essentially inert. Spano (2018) found that with a sample of Eraring fly ash, up to 13% of SiO_2 and Al_2O_3 were locked up in crystalline oxides such as Quartz and Mullite. Higher levels of crystalline content were reported by Chen Tan et al. (2010) when considering Collie fly ash as seen in Table 2-2.

Table 2-2 - Amorphous and Crystalline Composition of Collie Fly Ash (Chen Tan et. al 2009)

Component	Weight %
Amorphous	59.16 ± 0.70
Quartz	20.15 ± 0.16
Mullite	15.66 ± 0.65
Hematite	1.31 ± 0.05
Maghemite	3.71 ± 0.04

Additionally, much of the amorphous content is also believed to be encapsulated within the fly ash spheres. Mechanical activation (grinding) and increasing a fly ashes fineness has shown increased compressive strengths, however quantification of the mechanisms responsible (increased reactive content and bonds or densification due to increased packing) is difficult to quantify as they are believed to be concurrent (Williams 2015).

2.4.1.2 Ground granulated blast furnace slag

Similarly to fly ash, ground granulated blast furnace slag (GGBFS) is a by-product of industrial processes. GGBFS is produced through the quenching process associated with iron production. GGBFS production and the chemical composition of the produced slag is dependent on the temperature of quenching, method of steel produced and grinding process. The speed and rapidness of the quenching process results in slags with increased vitrification and reduced crystallisation (Virgalitte et al. 1995). Table 2-3 demonstrates the total composition of various GGBFS slag samples.

Table 2-3 - Bulk Chemical Composition of Various GGBFS

	SiO_2	Al_2O_3	CaO	MgO	Fe_2O_3	Na_2O	P_2O_5	Cr_2O_3	K_2O_5	MnO	SO_3	TiO_2
West Build (Spano 2018)	33.24	13.20	40.97	5.41	0.97	0.03	0.03	0.01	0.30	0.20	0.93	0.56
BGC (Lau et al. 2019)	32.00	14.10	44.24	5.32	0.43	0.24	0.01	0.01	0.31	0.37	1.97	0.62
Frontier Cement	32.19	16.07	39.43	9.14	0.32	0.30	0.02	0.01	0.36	0.23	2.31	0.68

As seen in Table 2-3, a large component of the chemical composition of GGBFS is CaO. The high calcium content associated with GGBFS results in cementitious properties when ground to cement-size particles and included within OPC concretes. GGBFS is incorporated as an SMC to typical OPC concretes to reduce heat of hydration and reduce OPC content, as it develops calcium silicate hydrate (C-S-H) bonds reflective of those developed by OPC. Virgialitte et al. (1995) acknowledged that the reactivity and cementitious properties of GGBFS are dependant of a range of factors, which include:

a) the elemental composition of the GGBFS;
b) the alkali concentration of the reacting system;
c) the amorphous content;
d) particle size;
e) temperature of the system during the hydration process

Although the above factors influence the chemical composition of the GGBFS, current literature does little to address these factors in term of geopolymer mixture design. Similarly to fly ash, little is done to identify and consider the crystalline and amorphous phases of GGBFS. However, compounds such as Bassanite and Gypsum form a large component of the crystalline composition of the GGBFS samples. These calcium sulphates, specifically Gypsum, are added to GGBFS within Australia to aid the hydration process when GGBFS is utilised as a SMC in OPC concretes (Yip et al. 2008). When incorporated to geopolymers GGBFS

promotes early age compressive strength and reduces the need to provide heat curing. Inclusion of up to 50wt% demonstrated can increase compressive strength without negative effects (Saha and Rajasekaran 2017, Lau et al. 2019). However, higher levels have been found to induce micro-cracks which reduce compressive strength. The angular shaped nature of the ground particle have also shown to increase water/activator demand on the system, reducing workability and reducing setting time (Lau et al 2019).

2.4.1.3 Silica Fume

Silica fume is a highly amorphous powder by-product of ferrosilicon alloy production. Also referred to as micro-silica, its chemical composition is dependent on the reduction of coal and high purity quartz (Khater 2013). The reduction of quartz attributes to silica fume's high silica content. This paired with its high fineness, and high pozzolanic nature has led to silica fume being used in high performance concretes. The highly reactive nature of silica fume is known to attribute to increase compressive strength, reduce permeability and increase abrasion resistance, specifically with respect to OPC concretes. This is due to mechanisms associated with increased packaging and densification as well as increased C-S-H bonds (Langan, Weng, and Ward 2002).

Geopolymer production has begun to use silica fume for the same favourable characteristics it exhibits in traditional concrete production. The inclusion of silica fume with in geopolymer mixtures has demonstrated increases in compressive strength (Dutta et al. 2010, Adek et al. 2014, Spano 2018). The inclusion of nano and micro-silica of up to 10% has been shown to led to optimum compressive strengths. This is due to the increased presence of reformed crystalline SiO_2 found within the geopolymer matrix. However, Okoye, Durgaprasad and Singh (2015) found that levels above 40% resulted in mixtures with poor workability. The observed reduction in workability is believed to be attributed to the increased demand on free water as geopolymer bonds are formed at an accelerated rates in the presence of silica fume (Khater 2013). Barbosa et al. (2000) stated that as the aluminosilicate stock dissociates water is absorbed and required to facilitate ionic transportation, free water is then released at a later stage when the polycondensation process instigates. The workability issues which arise when high levels of silica fume are incorporated into the geopolymer mixture, is due to its almost completely amorphous nature and extreme fineness. This results in silica fume being favoured in the dissolution process. High levels of dissociated Si produced additional C-S-H and C-A-S-H, N-A-S-H depending on the availability of Ca and Al, when sodium based activators are utilised (Yip, Lukey and Van Denventer 2005), and the pH of the system (García-Lodeiro et al. 2011). The high Si content within silica fume is believed to be favourable when focusing on the mixture design of geopolymers and addressing shortfalls in the Si content of main aluminosilicate fly ash stock.

2.4.2 Alkaline Activators

The primary function of the liquid activators associated with geopolymer production is the dissolution of the aluminosilicate source material. Alkaline activator with a high dissolution potential are favourable as they ensure leaching of the amorphous content from the source material is more complete, therefore resulting increased geopolymer bonds. Numerous alkaline activators have been used to synthesis construction materials from as early as 1940's. Viable options include potassium hydroxide (KOH), potassium silicate (K_2SiO_3), sodium silicate (Na_2SiO_3) and sodium hydroxide (NaOH). Initial research into alkaline activated GGBFS was undertaken by Purdon in Europe in the 1940's, and demonstrated that alkaline activation using NaOH could produce geopolymers of comparable compressive strength to OPC (Li, Sun, and Li 2010). It wasn't until much later that Duxon et al. 2007, stated that NaOH had greater aptitude to dissociate the silicate and aluminate species from the geopolymer stock material, compared to other alkaline activators, resulting increased geopolymer bonds, higher compressive strengths and increased durability properties.

2.4.2.1 Alkaline Activator Concentration

Alkaline activator concentration is a major contributor to the level of dissolution associated with the leaching of amorphous content from within the aluminosilicate source materials. Williams (2015) stated that dissolution rates is generally complex and generally unequal and partially complete. Leaching studies conducted by Lee and Deventer (2002) found that the concentration of the activating solution played a pivotal role on the extent of dissolution. During this study it was noted that the calcium and silicon species dissociated much earlier than aluminium. It was also noted that low molarity solutions resulted in lower levels of amorphous content being leached from the source material. This was due to the formation of secondary precipitates which lined the external surface of the fly particles. In contrast, high molar solutions inhibit precipitation and lead to higher dissolution rates. Many researchers have explored the influence activator concentration has on compressive strength, as increased dissolution is believed to lead to increased geopolymer bonds.

Figure 2-7 demonstrates the varied results obtained by researchers when exploring various concentration of NaOH with reference to ambient and heat cured geopolymers.

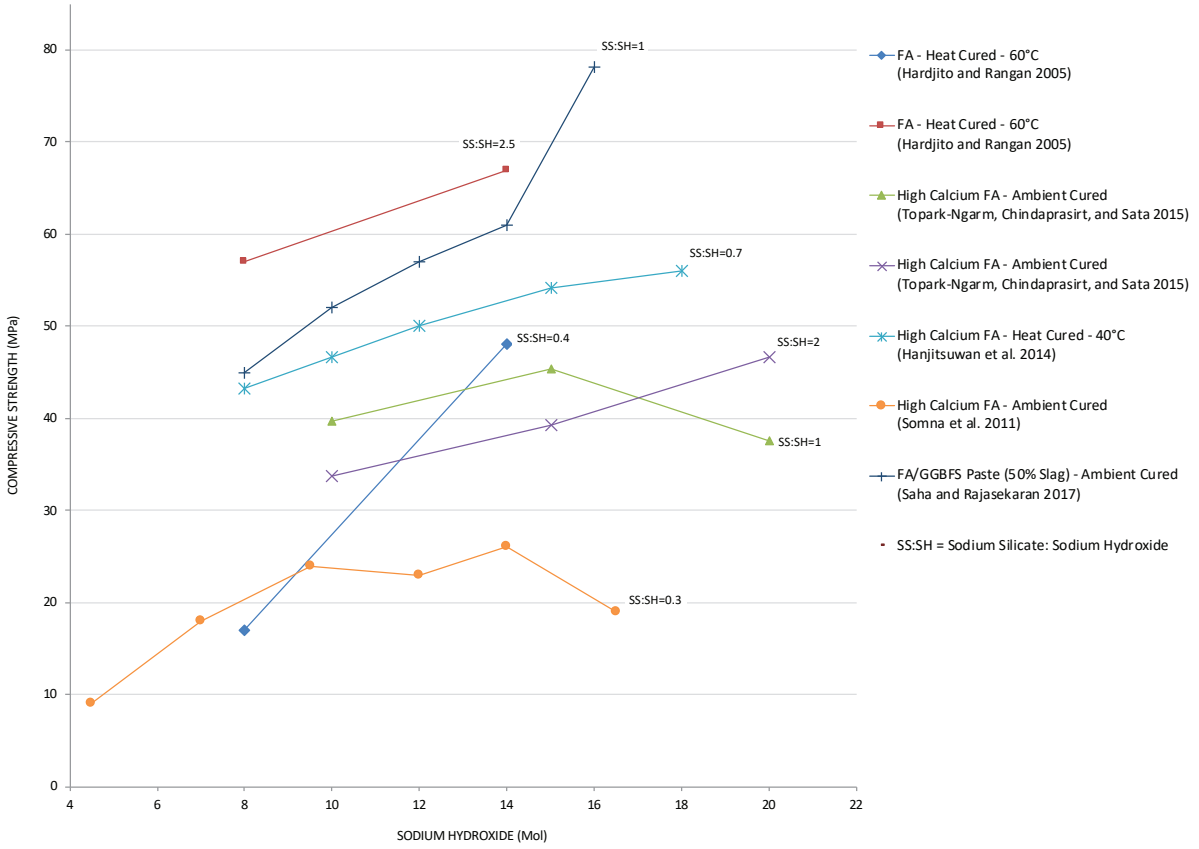

Figure 2-7 – Geopolymer Compressive Strengths With Respect to Sodium Hydroxide Molarity (Spano 2018)

As defined above, increased concentration values demonstrate high compressive strength values, in line with the notion that high molar solutions leach more amorphous content, which in turn develops a more complete geopolymer matrix. In addition to instigating and promoting the dissolution process, high concentration alkaline activators also provide increased levels of alkali metals such as sodium, with respect to sodium based activators. This is increasingly important in the formation of N-A-S-H geopolymer bonds as amorphous Na content within fly ash is negligible (Chen Tan 2009). High molar concentrations, although found to increase dissolution and promote increased geopolymerisation, have demonstrated negative effects in terms of setting times. Spano (2018) noted that NaOH molar concentrations of 14M, did initially increase workability, however resulted in geopolymer mixtures which experience increased setting time and a limited workable state. This was specifically apparent when examining with ternary fly ash, GGBFS and silica fume geopolymers.

2.4.2.2 Alkaline Activator Composition

Similarly to the utilisation of multiple aluminosilicate source materials, researchers favour a combination of alkaline activators to exploit the various characteristics associated with each chosen. A typical combination of activating solutions is sodium silicate and sodium hydroxide. Sodium hydroxide is favoured due to its strong dissolution potential, whereas sodium silicate due to the role it plays in providing soluble silica to the system. Sodium Silicate to Sodium Hydroxide (SS:SH) is typical portioned from 0.4 to 2.5. Low levels (0.4-1) have been found to produce geopolymers with lower compressive strengths. This is believe to be due to the role soluble silica plays on the formation of geopolymer bonds and the lower levels of sodium silicate present (Hardjito and Rangan 2005). Inversely, Phoo-ngerhkam et al. (2017) found that high levels of SS:SH with respect to high calcium fly ash based geopolymers also resulted in reduced compressive strengths at later stages as the initial C-S-H bonds inhibited further geopolymerisation. Additionally, alkaline activators of high SS:SH ratios consist of lower amounts of sodium hydroxide, as such incomplete dissolution and leaching the aluminate species are believed to attribute due to reduced geopolymer bonds (Spano 2018, Spano et al. 2020).

Although sodium hydroxide and sodium silicate are typical primary and secondary alkaline activators, limited research has been conducted when combining the two with a third activator. Lau et al. (2019) suggested that Sodium Aluminate ($NaAlO_2$) could be a viable option in relation to increasing the presence of soluble alumina, in a similar manner to sodium silicate, to promote geopolymerisation. This premise was incited due to the slow leaching of Al from aluminosilicate source materials such as fly ash. Researchers (García-Lodeiro, Fernández-Jiménez, and Palomo 2013) have found that in the presence of aluminium, initial C-S-H bonds have been shown to evolve to C-A-S-H with respect to hybrid cements (Portland and GGBFS) at slow rates during the curing process. Nugteren et al. (2011) used waste sodium aluminate as a supplementary activator, demonstrating increased workability and settings times. However, compressive strength results were inconclusive as various other waste products were incorporated into the mixture. Research conducted by Spano et al. (2020) found that sodium aluminate inclusion had insignificant influence on compressive strength, in comparison to silica fume inclusion, alkaline activation concentration and alkaline activator composition. This insignificant result may be been due to the over bearing influence silica fume played on compressive strength. Incidentally, Spano (2018) theorised that high levels of sodium aluminate may act as an accelerator and furthermore increase the water demand on the system. In general, the inclusion of sodium aluminate to address shortfalls in aluminium content of fly ash stocks has not be investigating when examining geopolymer mixture design.

2.5 Mixture Design of Geopolymers

2.5.1 Bulk Composition Mix Design

Existing geopolymer mixture design and proportion formulation is currently undertaken by two means; the utilisation of constituent ratios and/or the prescription of bulk elemental ratios. Each of these methods only consider the total or bulk composition of the mixture constituents and ignore the existence of the unreactive crystalline phase during the mixture design process.

The formulation of geopolymers using constituent ratios is undertaken by specifying mixture ratios such as water:solids, liquid:fly ash, sodium silicate:sodium hydroxide and aggregate:binder. Research conducted solely utilising these ratios demonstrated significant inconsistencies, when using differing fly ashes, as these proportioning methods ignore the elemental composition of the mixture constituents. The alternative bulk mixture design process uses the bulk composition of the stock materials, obtained through XRF, to calculate the feedstock proportions by targeting specific elemental ratios. As stated earlier this method does not consider the inert crystalline composition of the feedstocks. As such, the majority of studies report incomplete dissolution of the fly ash feeder stocks (Williams 2015). The effect of this incomplete dissolution, specifically associated with fly ash geopolymers activated with sodium silicate, results in a decrease in the alumina and silica content of the formed geopolymer matrix (William 2015). This produces discrepancies associated with determined target elemental ratios and calculated bulk elemental ratios such as Si/Al and Na/Al. Rowles and O'Connor (2003) explored the effect that changing the bulk Na/Al and bulk Si/Al with reference to metakaolin (high pozzolanic man-made aluminosilicate material) geopolymers had on compressive strength. Extrapolative data determined that higher levels of bulk Si/Al and lower levels of Na/Al yielded higher compressive strength outcomes. This notion can be seen in Figure 2-8.

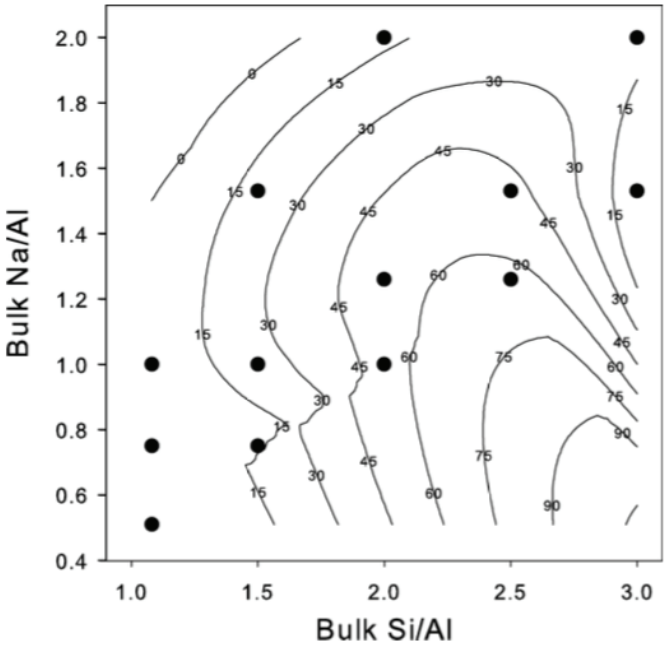

Figure 2-8 – Compressive strength outcomes of metakaolin geopolymers via changes to bulk Na/Al and bulk Si/Al.
Dots represent data values (Rowles and O'Connor 2003) and lines represent extrapolated values (William 2015).

Disparity between produced geopolymer binders, mortars and concretes can largely be attributed the lack of robustness the above methods demonstrate when considering the varied composition of the aluminosilicate source materials. This notion forms a large component of the issues outlined in *Section 2.2.3.1– Inconstancy.*

2.5.2 Amorphous Composition Mixture Design

To combat the underlying issues associated with inconsistency and poor fly ash reactivity, Williams and van Reisen (2010) proposed that an alternative approach to mixture design could be undertaken. This approach considered the amorphous composition of the reactive elements within the mixture constituents. This amorphous approach to mixture design was aimed to address the shortfalls of bulk mixture design, specifically focusing on the prescription of target elemental ratios, which originally included the non-reactive crystalline phase. By prescribing target elemental ratios utilising the amorphous composition of various fly ashes, Williams and van Riessen (2010) were able to produce geopolymers pastes with high compressive strength outcomes that those using bulk elemental ratios. Table 2-4 demonstrated the average compressive strength results of various fly ash stocks investigated and the improved results obtained through amorphous mixture design.

Table 2-4 - Average Compressive Strengths of Geopolymer Pastes (Williams and van Riessen 2010)

Fly Ash Source	Bulk Composition (MPa)	Amorphous Composition (MPa)
Collie	7	29
Port Augusta	24	48
Bayswater	Too weak to test	9.5

2.5.2.1 The amorphous mathematical framework

The formulation of mixture proportions utilising amorphous elemental ratios has been aided by a mathematical framework originally proposed by Williams and van Riessen (2010) (Figure 2-9)

$$W = \begin{bmatrix} F1_{wt} \\ F2_{wt} \\ F3_{wt} \\ F4_{wt} \end{bmatrix} = F^{-1} \cdot R$$

$$F = \begin{bmatrix} F1_{Si} & F2_{Si} & F3_{Si} & F4_{Si} \\ F1_{Al} & F2_{Al} & F3_{Al} & F4_{Al} \\ F1_{Na} & F2_{Na} & F3_{Na} & F1_{Na} \\ F1_{H} & F2_{H} & F3_{H} & F4_{H} \end{bmatrix}; \quad R = \begin{bmatrix} Si/Al \\ 1 \\ Na/Al \\ (Si/Al)(H/Si) \end{bmatrix}$$

Figure 2-9 - Mathematical Framework Originally Proposed by Williams and van Riessen (2010)

The W-matrix represents the weight percentage of each mix constituent, with each constituent being represented by F and a numeral (eg. F1= Fly Ash, F2 = Sodium Hydroxide, F3= Sodium Silicate, F4= Water). The W-matrix is generally determined once the F and R-matrix are set. The F-matrix refers to the reactive element composition of the feeder stocks, specifically the Si, Al, Na, and H; with each row representing a specific mix constituent and each column the specific element. The R-matrix refers to the desired amorphous elemental ratios of the geopolymer mixture.

The original framework was primarily developed for the formulation of unary geopolymers and used by Sweeney (2017) and Lau et al. (2019) to produce both fly ash and GGBFS unary geopolymers. Parnham (2016) expanded on the framework to allow for the development of mixture proportions relating to binary geopolymers.

$$F = \begin{matrix} \\ F1_{Si} \\ F1_{Al} \\ F1_{Na} \\ F1_{H} \\ F1_{Ca} \end{matrix} \begin{matrix} \begin{matrix} \textit{Fly-ash} & \textit{Sodium Silicate} & \textit{Sodium Hydroxide} & \textit{Water} & \textit{GGBFS} \end{matrix} \\ \begin{bmatrix} F2_{Si} & F3_{Si} & F4_{Si} & F5_{Si} \\ F2_{Al} & F3_{Al} & F4_{Al} & F5_{Al} \\ F2_{Na} & F3_{Na} & F4_{Na} & F5_{Na} \\ F2_{H} & F3_{H} & F4_{H} & F5_{H} \\ F2_{Ca} & F3_{Ca} & F4_{Ca} & F5_{Ca} \end{bmatrix} \end{matrix}; \quad R = \begin{bmatrix} Si/Al \\ 1 \\ Na/Al \\ (Si/Al)(H/Si) \\ (Ca/Si)(Si/Al) \end{bmatrix}$$

$$W(weight\ percentage) = \begin{bmatrix} F1_{wt} \\ F2_{wt} \\ F3_{wt} \\ F4_{wt} \\ F5_{wt} \end{bmatrix} = \% \begin{bmatrix} Fly\ Ash \\ Na_2SiO_3 \\ NaOH \\ H_2O \\ GGBFS \end{bmatrix} = F^{-1}.R$$

Figure 2-10 – Mathematical Mixture Design Framework (Parnham, 2016)

As seen in Figure 2-10 , the expanded framework included GGBFS and amorphous calcium content. In addition to utilising this framework to determine weight proportions, it was reverse engineered by Parnham (2016) and Spano (2018) to determine specific amorphous elemental ratios through variation to the W-matrix and F-matrix Figure 2-11.

$[W]$	x	$[F]$	=	$[R]$
Defined by Bulk Compostion and Weight to Produce Required Specimens		Determined for Each Mixture Design Based on Amorphous Content		Specific Elemental Ratios for Each Mixture

Figure 2-11 - Process of Determining Amorphous Atomic Ratios Using Mathematical Framework (Spano 2018)

Utilisation of the framework in this manners allowed for the determination of optimum amorphous ratios with reference to compressive strength outcomes, and variation to the weight composition of the constituents. Spano (2018) experimented to further expanded the mathematical framework to included additional mixture elements, however further expansion beyond that of Parnham (2016) is incomplete and only achievable using the reverse engineering approach and trial and error.

2.5.2.2 Amorphous elemental ratios

The prescription of elemental ratios are the leading mechanism behind the formulation of geopolymers using an amorphous approach. Reference to specific elements is driven by those elements which contribute the formation of the geopolymer matrix. As outlined in *Section 2.3 - Chemistry and Structure of Geopolymers* , C-S-H, C-A-S-H and N-A-S-H geopolymer bonds lend their formation to the availability of Ca, Na, Si, Al and H. Supply of these elements is dependent on the mixture components, amorphous content and quantities used. Table 2-5 defines the major and minor contribution of geopolymer mixture components with respect to the reactive elements.

Table 2-5 - Contribution of Amorphous Content to Geopolymer Formulation by Element

Reactive elements	Typical Binary Geopolymer Mixture Constituents					Additional Constituents	
	Fly Ash (Class F)	GGBFS	D-Grade Sodium Silicate	12M Sodium Hydroxide	Water	Silica Fume	Sodium Aluminate (Solids)
Si	+	o	o			+	
Al	-	-					+
Ca		+					
Na			-	+			o
H			+	+	+		

(+) major contribution (>40%)
(o) moderate contribution (20-40%)
(-) minor contribution (5-20%)

As seen above, the majority the Si content in binary fly ash and GGBFS geopolymer formulation is provided by the fly ash source material with minor contribution due to sodium silicate. These component typically influence amorphous Si/Al. Additional constituents such as silica fume can be used to increase the Si/Al ratio with minimal influence to other amorphous ratios, due to its predominantly Si composition. Similarly, as Al is supplied by either fly ash or GGFBS variation reducing the Si/Al is only achievable through the inclusion of sodium aluminate. Amorphous Na/Al is typical define and controlled by the type and concentration of the alkaline activators, however sodium hydroxide is predominately responsible for the majority of Na supplied to the geopolymerisation process. Likewise the liquid components all contribute to the designation of amorphous H/Si, which essentially refers to the water content of the system. Finally GGBFS is the sole providers of amorphous Ca to the system and responsible for the prescription of amorphous Ca/Al. It should be noted that fly ash stocks do have varied contribution with respect to Ca, depending on class and origin. However, compared to GGBFS its influence is negligible when considering Class-F fly ash.

In addition to the amorphous content available by each constituent, the mathematical framework allows for the prescription and determination of amorphous ratios such as Si/Al, Na/Al, Ca/Al and H/Si. Prescribed values associated with these amorphous ratios are still in their infancy, however several recent amorphous researchers have begun theorising and determine optimised values.

Works completed by Lau et al. (2019) associated with binary geopolymers yielded compressive strength outcomes of up to 70Mpa using both Eraring and Gladstone type fly ashes. It was theorised that optimum compressive strength results could be obtained when targeting amorphous Si/Al of 2.4-3, Na/Al of 0.65-0.8 and Ca/Al of 0.45. These theorised values did not examine amorphous Si/Al of 2.2-2.9 and Na/Al 0.65-0.8. Spano et al. (2020) aimed to address the gaps left by Lau et al. (2019) using Eraring fly ash, refining the optimum compressive strength range of amorphous Si/Al to 2.7-3.0 and Na/Al 0.75. The results associated with amorphous Na/Al mirrored those suggested and seen by Sweeney (2017) and Lau et al. (2019). Spano's optimisation resulted in compressive strength of up to 70Mpa, an increase of 15Mpa above Lau et al. (2019) Eraring fly ash results. However, the increased reactivity of the optimised geopolymer mixtures was paired with compaction issues and increased setting times. Investigation of optimum values associated with alternative fly ash sources was not addressed by Spano (2018) and Spano et al. (2020) and demonstrates a gap in the literature. Additionally, Lau et al. (2019) did little to balance the difference in amorphous content of each fly ash and investigate similar amorphous ratios for mixtures which used differing fly ash stocks. As such, neither researcher addressed the notion that specific elemental amorphous ratios can be targeted to produce geopolymers of consistent compressive strengths. This fact is one of the main premises behind adopting an amorphous approach, with Williams (2015) proposing that targeted elemental ratio could lead to geopolymers of comparable mechanical properties irrespective of fly ash origin.

3. METHODOLOGY

The experimental methodology of this research consists of four distinct phases, each of which being designed to contribute and address the objectives of the research. Of the four experimental phases, one is associated with the preparation and characterisation of the material constituents, examining the varied composition of the fly ash stock materials and developing mixture designs. The subsequent three experimental phases involve the production, testing and analysis of geopolymer specimens whilst examining various amorphous ratios and geopolymers configurations. The various preparation procedures and experimental phases of the research scope have been highlighted in Figure 3-1.

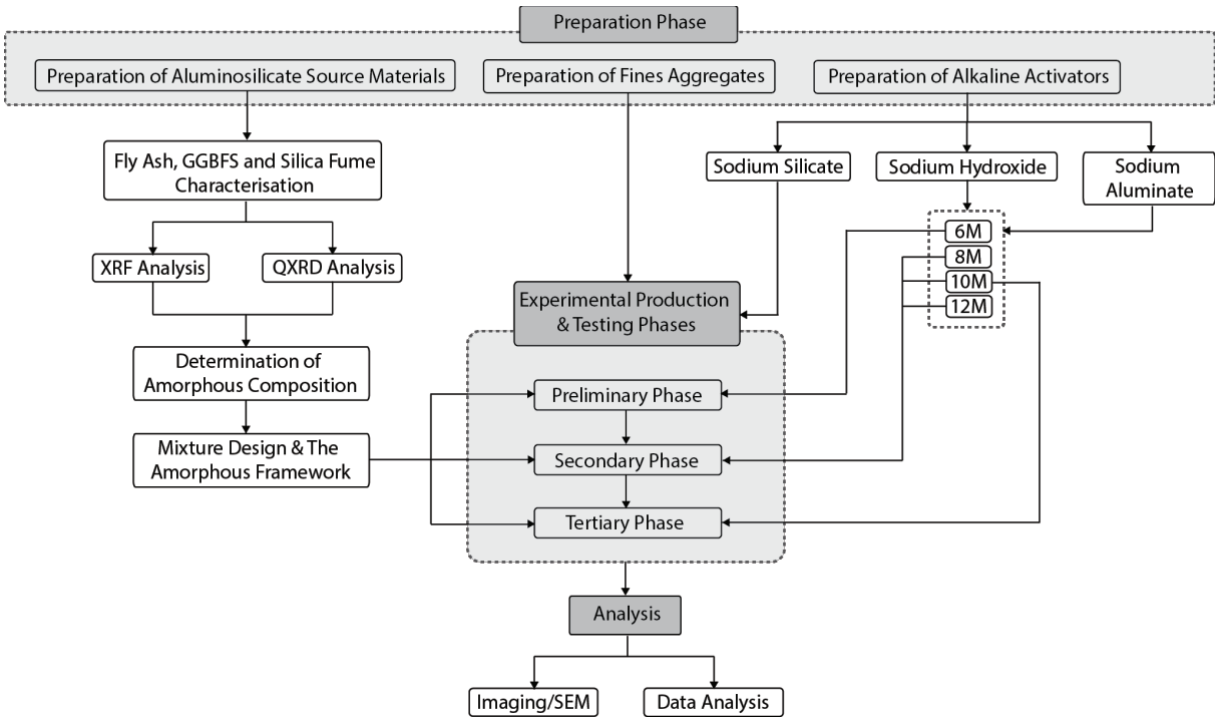

Figure 3-1 - Overview of Research Experimental Processes

This frame work adopted the use of Eraring and Gladstone fly ash, GGBFS and silica fume as aluminosilicate source materials and; sodium silicate, sodium hydroxide and sodium aluminate as alkaline activating constituents. These constituents formed the binder component of the mixtures. Fillers constituents included water and silica sand. For the purpose of this research silica sand was considered as inert and did not contribute to the amorphous content of the mixture.

All experimental mixtures produced adopted an ambient curing regime. Specimen testing with in the experimental phases included flow and compressive strength testing, whilst SEM imaging was undertaken to examine the crack surface morphology of specific specimens. Were applicable, data analysis techniques such as the Interquartile Rule (IQR) and Analysis of Variance (ANOVA) were employed to identify outliers and determine result significance.

The subsequent sections of this chapter outline the design and scope of each experimental phase including their respective variables, preparation procedures, geopolymer production processes, testing requirements and data analysis tools.

3.1 Design of Experiments

Four research phases defined the scope of this research, each phase aimed to address the objectives of the research. These phases were defined to independently explore specific experimental variables whilst holistically contributing to the research scope and each subsequent phase. Specific interphase variables have been omitted from the subsequent sections of this chapter. These interphase considerations and variables can be found within each specific phase chapter.

3.1.1 Preparatory Phase

This phase served as the precursor for the subsequent experimental phases which required specimen and mixture production. As such, the preparatory phase involved the determination of the chemical composition of each mixture constituent, utilisation of the mathematical framework for the development of mixture proportions and comparative analysis of the two fly ash stocks involved.

As an amorphous approach to mixture design formed one of the major pillars of this research, the mathematical framework was an integral tool in the determination of amorphous ratios and mixture proportions. Alterations to the framework used by Parnham (2016), were undertaken similarly to Spano (2018). This was done so to mirror the previous methodologies undertaken by Spano (2018) of which this research endeavoured to expand.

3.1.1.1 Mathematical mixture framework

As the scope of this research aimed to utilise supplementary constituents to address shortfalls in the amorphous content of fly ash stocks, as well as investigate the influence various amorphous ratio have on the mechanical properties of geopolymers, the adaptions made by Spano (2018) to Parnham's (2016) binary geopolymer matrix were adopted. The framework adopted within this research is expressed in Figure 3-2.

$$F = \begin{bmatrix} \text{Fly Ash} & \text{Sodium Aluminate} & \text{Silica Fume} & \text{Sodium Silicate} & \text{Sodium Hydroxide} & \text{Water} & \text{GGBFS} \\ F1_{Si} & F2_{Si} & F3_{Si} & F4_{Si} & F5_{Si} & F6_{Si} & F7_{Si} \\ F1_{Al} & F2_{Al} & F3_{Al} & F4_{Al} & F5_{Al} & F6_{Al} & F7_{Al} \\ F1_{Na} & F2_{Na} & F3_{Na} & F4_{Na} & F5_{Na} & F6_{Na} & F7_{Na} \\ F1_{H} & F2_{H} & F3_{H} & F4_{H} & F5_{H} & F6_{H} & F7_{H} \\ F1_{Ca} & F2_{Ca} & F3_{Ca} & F4_{Ca} & F5_{Ca} & F6_{Ca} & F7_{Ca} \end{bmatrix}; \quad R = \begin{bmatrix} Si/Al \\ 1 \\ Na/Al \\ (Si/Al)(H/Si) \\ (Ca/Si)(Si/Al) \end{bmatrix}$$

$$W\ (weight\ percentage) = \begin{bmatrix} F1_{wt} \\ F2_{wt} \\ F3_{wt} \\ F4_{wt} \\ F5_{wt} \\ F6_{wt} \\ F7_{wt} \end{bmatrix} = \% \begin{bmatrix} Fly\ Ash \\ NaAlO_2 \\ Silica\ Fume \\ Na_2SiO_3 \\ NaOH \\ H_2O \\ GGBFS \end{bmatrix} = F^{-1}.R$$

Additions to Parnham's (2016) framework have been highlighted in **blue*

Figure 3-2 – Experimental Mixture Framework (Spano 2018)

The mathematical framework was used to design and batch mixture proportions whilst considering the amorphous composition of the binder elements. The additional columns of the F and W matrix were removed when either sodium aluminate or silica fume were not implemented.

The feedstock matrix or F-matrix relates to the amorphous content of each mixture constituent and is a measure of the 'reactive mol' per g of each reactive element (Parnham 2016). In selected cases, specifically the development of mixture design using blended geopolymers, the fly ash columns was a combination of the reactive mol per g of the blended fly ash, determined through weight proportioning of the reactive composition. The W-matrix refers to the weight proportions of each constituent and is measured in grams. The R-matrix is a measure of the number of moles of each element, and reformed to produce the matrix highlighted above, which stipulates the targeted amorphous ratios of the mixture.

As outlined by Spano (2018), the addition of silica fume and sodium aluminate to the F-matrix without the inclusion of additional reactive elements, leave the matrix incomplete. This results in the frame work being limited that defined in Figure 3-3.

Figure 3-3 – Determination of R-Matrix (Spano 2018)

In its current state the F-matrix cannot be inverted, therefore the framework cannot be fully utilised without an iterative process. This notion was overcome by reducing the framework back to the original state proposed by Parnham (2016), with any additional constituents used to address the shortfall in the fly ashes amorphous composition being included within the fly ash F-matrix column. This process utilised were continued variation to mixtures was not required, specifically the preliminary phase and tertiary phase. However, this required separate F-matrix columns to be developed for each fly ash blend when proportion each mixture. Both the alteration made by Spano (2018) and the framework proposed by Parnham (2016) served their purpose of this research.

3.1.2 Preliminary Phase

The preliminary phase was designed to explore the influence amorphous H/Si had on the flow and compressive strength of binary geopolymers, which utilise Gladstone fly ash. This phase mirrored the amorphous ratios used by Spano et al. (2018) when examining Eraring fly ash binary geopolymers. Within this phase binary Gladstone fly ash geopolymers developed and tested with varied levels of H/Si, though the inclusion of free water. Additionally, the inclusion of free water was also examined in relation to pre and post activation similarly to Spano et al. (2018). The Gladstone mixture formulated and produced within this phase were then compared to the Eraring mixtures formulated by Spano (2018). SEM imaging was undertaken to conduct quantitative analysis of the samples produced within this phase.

3.1.2.1 Designation of variables

The main experimental variable of this phase was the amount of free water incorporated into the mixture, this in turn influences the amorphous H/Si of each mixture. Parnham (2016) found that differing fly ashes required differing free water quantities to achieve similar flow results, however these fly ash stocks did vary in chemical composition. Parnham did not correct the differences in amorphous composition between each fly ash stock and examine if free water requirements were similar in regards to flow or compressive strength.

As previously stated, the mixture proportions utilised within this experimental phase were to mirror those adopted by Spano (2018) with the exception of the fly ash stock. As such, mixtures were designed using the mathematical framework with the following amorphous ratios:

- Si/Al: 2.9 ± 0.2
- Na/Al: 0.56 ± 0.02
- Ca/Al: 0.48 ± 0.01
- H/Si: 7.0 – 8.5

In conjunction with above amorphous ratios, the following mixture parameters were also adopted:

- an aggregate : binder ratio of 1.4
- 6M sodium hydroxide solution as the primary activator
- a sodium silicate : sodium hydroxide (SS:SH) ratio of 2.5

These mixture proportions were adopted based on the previous research conducted by Harjito and Rangan (2005), Ng and Foster (2013), Lau et al. (2019) and Spano et al. (2020).

3.1.2.2 Preliminary Phase Mixture Proportions

The following set of mixture configurations defined in Table 3-1, aimed to compliment the works conducted by Spano (2018) whilst utilising Gladstone fly ash. This was undertaken through utilising the amorphous framework to develop mixture designs with comparable amorphous ratios.

Table 3-1 - Preliminary Phase Mix Configurations

Mix	Free Water Added Pre Activation (mL)	Free Water Added Post Activation (mL)	Amorphous H/Si	Fly Stock
PG1	400	-	7.7	Gladstone
PG2	450	-	8.2	
PG3	500	-	8.5	
PG4	600	-	9.7	
PG5	400	200	9.7	
PG6	450	150	9.7	
PG7	500	100	9.7	

Gladstone fly ash proportions were prescribed through the utilisation of the mathematical framework and analysis conducted within the Preparatory Phase.

3.1.3 Secondary Phase

The preliminary phase was designed to explore the influence amorphous Na/Al and Si/Al had on the flow and compressive strength of ternary geopolymers, which utilise Gladstone fly ash in combination with supplementary constituents. Similarly to the preliminary phase, this phase aimed to mirror those amorphous ratios examined by Spano (2018), with reference to Eraring fly ash geopolymers. The results of this phase were used to examine and compare optimum amorphous ratios, with those of previous literature. Flow and compressive strength data were collected and analysed with in this phase. In addition, the optimum geopolymer mixture determined by Spano (2018) was reproduced and used as a comparison mixture for SEM and data analysis.

3.1.3.1 Designation of variables

The two key variables associated with this phase were the amorphous ratios of Na/Al and Si/Al. The targeted ranges for each value were as follows:

- Si/Al: 2.65 - 3.50
- Na/Al: 0.57 - 0.83

These value were utilised to mirror those examine by Spano (2018), and bridge the gap in literature which Parnham (2016) did not investigate with relation to an amorphous approach to geopolymers.

The amorphous ratios of Hi/Si and Ca/Si were held constant at the following values:

- Ca/Al: 0.48 ± 0.01
- Na/Al: 8.43 ± 0.53

Variation of amorphous Na/Al and Si/Al was conducted in two sub-phases whereby each variable was held constant whilst the other was varied. Constant values of Na/Al = 0.73 and Si/Al = 3.11 were used with reference to previous literature.

The mixture configurations and related atomic ratios of secondary phase can be seen in Table 3-2.

Table 3-2 – Secondary Phase Binder Mix Configurations

Mix ID	Amorphous				Comment
	Si/Al	Na/Al	Ca/Si	H/Si	
SG1	3.15	0.57	0.48	8.43±0.53	Examining the Influence of Na/Al
SG2		0.65			
SG3		0.74			
SG4		0.83			
SG5	2.65	0.76			Examining the Influence of Si/Al
SG6	2.86				
SG7	3.10				
SG8	3.37				
SG9	3.50				
SE1	3.01	0.73	0.44	7.46	Optimum Eraring Mixture (Spano 2018)

3.1.3.2 Development of mixture proportions

Development of the mixture proportions for this phase were undertaken with reference to the mathematical framework outlined in *3.1.1.1 – Mathematical mixture framework*. Due to the previously outlined limitations of the amended framework, a iterative process was adopted to refine the mixture proportions outlined in Table 3-2. Variation of the experimental variables of Na/Al and Si/Al was undertaken either by varying the concentration of sodium hydroxide – influencing Na/Al or varying the silica fume or sodium aluminate content – influencing Si/Al. This was enabled due to the sodium (Na) content present in sodium hydroxide, the mainly silicon (Si) composition of silica fume and the aluminium (Al) present in sodium aluminate. Mixture proportions relating to SS:SH and aggregate:paste ratios were held constant and reflect those employed in the preliminary phase.

3.1.4 Tertiary Phase

The tertiary phase of this research was developed to investigate compressive strength outcomes associated with blended geopolymers which utilise varied amounts of differing fly ash stocks. The aim of this phase was to determine if an amorphous approach to geopolymer formulation can be used to produce geopolymers of consistent compressive strength. Similarly to the subsequent phases, flow and compressive strength data was collected and analysed, with SEM being undertaken to examine to cracked surface morphology of specific specimens.

3.1.4.1 Designation of variables

The main experimental variable associated with this phase was the composition of the fly ash blend utilised within each mixture. To examine if blended geopolymers can be formulated to produce consistent compressive strength outcome using an amorphous approach, the mixtures outlined in Table 3-3, were defined to examine a combination of fly ash blends. The two main fly ash stocks utilised with in this phase were consistent with the scope of the research and were Eraring and Gladstone fly ash. The amorphous ratio of each mixture were held constant as outlined in Table 3-3, with these values being determined with reference to the previous experimental phases and past literature.

Table 3-3 – Tertiary Phase Binder Mix Configurations

Mix ID	Gladstone Fly Ash %	Eraring Fly Ash %	Amorphous			
			Si/Al	Na/Al	Ca/Si	H/Si
TGE1	10	90	3.04	0.60	0.47	8.5
TGE2	25	75				
TGE3	50	50				
TGE4	75	25				
TGE5	90	10				

3.1.4.2 Development of mixture proportions

The mixture proportions of this phase were developed with reference to *3.1.1.1 – Mathematical mixture framework,* and the previously mention iterative process. An F-Matrix for each blended fly ash combination was developed and utilised for the formulation of mixture proportions. Due to the varied chemical composition of the independent fly ash stocks each fly ash blend differed in amorphous content. As such, similarly to the secondary phase, supplementary constituents such as silica fume and sodium aluminate were used to ensure the amorphous composition of the mixtures were maintained in line with the values stipulated in Table 3-3. Sodium hydroxide concentration was limited to 12M, with mixture proportion ratios such as SS:SH and aggregate:binder ratio limited to those values utilised throughout the experimental scope.

3.2 Preparation of Experimental Components

3.2.1 Preparation of Fine Aggregates

The use of fine aggregates with in this research has been dictated by the scope, the production of geopolymer mortars and previous research. Mortars consist of binder constituents and fine aggregates, such as sand or fine gravels. The addition of fines can influence the workability and water demand on the system due to their absorptive properties and moisture content. This in turn has the ability to influence mixture strength outputs. However, the finer natures of mortars compared to that of concretes, result in more homogeneous mixtures when considering smaller specimens. Larger aggregates present in small concrete specimens can lead to results subjected to higher standard deviations and potential experimental errors, due to uncontrollable variations in aggregate particle arrangements within each sample. These notions further support the utilisation of mortars in contrast to concretes with in this research.

The moisture content of the aggregates used with in the production of traditional concrete and mortars is an influencing factor in their rheological and hydraulic properties. This is also reflective in geopolymer production. During traditional concrete production, aggregates are incorporated into the mixture when in a state of saturated surface dry (SSD). SSD is favourable as aggregates are assumed to be non-absorptive, and therefore do not present an increased the demand for additional water or alkaline activator on the system. However, determination of SSD for fine aggregates is at the discretion of the individual and difficult to maintain. This notion can lead to increased risks associated with repeatability and continuity of the mixtures developed. Therefore, SSD was not adopted for this research.

In retrospect, oven dried silica sand was adopted for the development of all geopolymer mortars within this research. Silica sand was initially washed to remove foreign organic matter, and then oven dried at 105°C for 24 hours. This was undertaken with reference to *ASTM C330/C330M-17a Standard Specification for Lightweight (Sand) Aggregates for Structural Concrete* (ASTM 2017). Once dried, the sand aggregated were allowed to cool under ambient conditions before being place in dry sealed containers.

3.2.2 Preparation of Aluminosilicate Source Materials

The aluminosilicate solids used within this research consisted of Gladstone and Eraring fly ash, Westbuild GGBFS and Ecotec silica fume. The fly ash and silica fume stocks were supplied by Curtin University, were as the GGBFS stock was procured from Westbuild Perth.

The fine/powdered nature of the source materials was sufficient for mixture production and no physical preparation tasks were required. However, x-ray compositional analysis and particle laser sizing (PLS), were undertaken in line with the amorphous scope of the research.

To ensure representative samples of each source material was taken, each source material was stockpiled at the start of the research. This stockpile was sufficient in size to meet the material requirements of the entire scope. Prior to sampling the stockpile of material was combined and mixed. Sampling was undertaken with reference to *AS1141-1974 – Methods For Sampling and Testing Aggregates* (Standards-Australia 1974), to ensure a representative sample was obtained. Sample were then used to determine the amorphous content of each aluminosilicate materials and PLS analysis.

3.2.2.1 Determination of the amorphous content of the aluminosilicate materials

As outlined within *Section 2*, aluminosilicate materials are composed of an amorphous and crystalline phase. The scope this research is associated with the development of mixtures utilising the amorphous phase. As such, determination of the amorphous phase requires the utilisation of two separate x-ray analysis processes. The two processes utilised within this research were; x-ray fluorescence (XRF) and quantitative x-ray diffraction (QXRD). XRF was utilised to determine the total chemical composition, were as QXRD was utilised to determine to crystalline content. Through a subtraction process of each elemental oxide the amorphous content was then determined. This process is outlined in Figure 3-4.

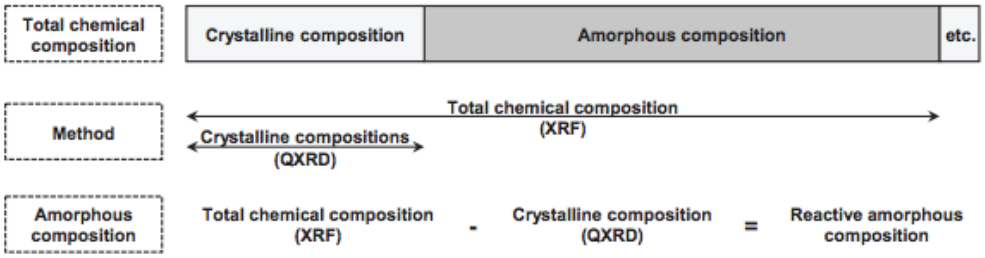

Figure 3-4 – Calculation Method of the Amorphous Composition of the Aluminosilicate Source Materials (Lee et al. 2017)

3.2.2.2 Determination of Bulk Chemical Compositions via X-Ray Fluorescence

Analysis of the total or bulk chemical composition of each aluminosilicate material was undertaken by Bureau Veritas (Canning Vale WA). The elemental oxide composition of each material was determined by initially oven drying each sample at 105°C. Each sample was cast using x-ray flux type 66:34 which consisted of 4% lithium nitrate. X-ray fluorescence spectrometry was undertaken using a Bruker AXS's S4 Pioneer machine. In addition to x-ray fluorescence spectrometry, robotic thermogravity analysis was undertaken to obtain loss of ignition (LOI) results. LOI analysis was undertaken to determine the amount of unburned carbon present in each sample due to the combustion process. XRF and LOI results defined the outputs related to the bulk chemical composition of each aluminosilicate material.

3.2.2.3 Determination of Crystalline Composition via Quantitative X-Ray Diffraction

Quantification of the crystalline composition of the aluminosilicate materials was undertaken utilising a two-step analysis process. This process used obtained x-ray diffraction data and quantitative analysis to determine the crystalline phase of each material. The quantification method used within this research was that associated with the internal standard method. The internal standard method, uses a known amount of stable crystalline material, to aid in the quantification and concentration of other crystalline oxides. The accuracy of this method has been found to be sufficient for the analysis of fly ash and GGBFS due to its stability (Hill and Howard 1987).

XRD data was obtained using a Bragg-Brentano designed Bruker-AXS D8 Discover powder diffractometer located within the John de Laeter Centre at Curtin University (Bentley WA). A representative 3g sample of aluminosilicate material was combined with 0.3g of fluorite powder (internal standard material). Fluorite was selected over corundum due to peak overlaps of corundum with the crystalline composition of the aluminosilicate material (Williams and van Riessen 2010). The mixture was then ground for 10 minutes using McCrone Micronizing Mill with 48 individual grinding elements, to reduce the average particle size to 10microns. Ethanol was added into the mixture prior to micronizing to produce a slurry. This was undertaken to limit heat generated during the grinding process and avoid possible sample decomposition. Upon the completion of grinding, the micronized slurry was washed from the grinder with ethanol and dried overnight at 40°C. Finally, the dried powder was packed into XRD sample holders via the side loading method to ensure the particles are oriented randomly in the holder. XRD data collection was undertaken using the Bruker-AXS D8 Discover powder diffractometer fitted with a 40mA copper element x-ray tube, 3° LynxEye linear detector, 0.3° divergence silts and two 2.5° Soller Silts. Instrumental quantification parameters of the diffractometer were set to 7 to 120° 2theta, with a step size of 0.015 for a total running time of 90 minutes per sample.

Once the XRD scanning was complete, qaulification analysis of the obtained crystalline data commenced by searching for the crystalline phases present using computer software known as DiffracEVA 11.0. Within DiffracEVA, the position and intensity of the crystalline peaks observed during XRD, were superimposed with the known crystalline peaks and position data to ICDD PDF4+ (International Centre for Diffraction Data Powdered Diffraction File) database. The ICDD add diffraction patterns of crystals to the Powdered Diffraction File (PDF) for phase matching. Quantification software known as TOPAS, was used to determine the specific crystalline phases of each stock material using Rietveld quantitative phase analysis (Coelho 2018). The Rietveld method employs profile intensities directly from the XRD powder diagram, then, uses the least-square refinement procedure to add linear or quadratic constraints between parameters. The

fundamental equation of Rietveld method for phase quantification: the Rietveld weight fraction, *W* of a particular phase *p* is given by Equation 1,

$$W_p = \frac{S_p(ZMW)_p}{\sum_i S_i(ZMV)_i}$$

W is the Rietveld weight fraction
S is the Rietveld scale factor
Z is the number of formula units per unit cell
M is mass of formula unit
V is unit-cell volume

(Equation 1)

The relative Rietveld weight fractions were converted to absolute values via internal standard method to obtain the crystalline composition in a weight percentage (Rietveld 1969). Rietveld analysis was utilised as it examines the whole spectrum of the crystalline data, resulting in more accurate phase analysis and identification.

Crystalline quantification via the above processes was undertaken with the assistance of Dr Matthew Rowles (Curtin Physical Sciences) and postgraduate research fellow Chee Keong Lau.

3.2.2.4 Particle Laser Sizing

With respect to some fine materials, sieve analysis is sufficient to determine the gradation of particles, however for particles ranging below 100µm sieving can be inaccurate. This is due to the increased effort required to pass the particles through the sieves and particle interaction. Particle Laser Sizing (PLS) was employed to measure the volume of the independent particles and was done so due to the increased accuracy of results. Particle size analysis using laser diffraction was conducted in accordance with *AS4863.1 - Particle size analysis—Laser diffraction methods* (Standards-Australia 2000) on each aluminosilicate source material and undertaken by Australian Laboratory Services (ALS) using a Mastersizer 2000.

3.2.3 Preparation of Alkaline Activators

Sodium based alkaline activators were selected for this research to mirror those utilised by previous amorphous geopolymer researchers (Parnham 2016, Spano 2018). Additionally they have shown a greater ability to dissociate the reactive elements within the aluminosilicate source material, over potassium based activators (Duxon et al. 2007). Three sodium activators were utilised, these included; sodium hydroxide, sodium silicate (D-grade) and sodium aluminate (Sigma Aldrich). Sodium hydroxide and sodium silicate were used as the main activating solutions, whereas sodium aluminate was used as a supplementary constituent to increase the Al content of the mixture.

Sodium hydroxide activating solution was prepared using solid sodium hydroxide mini pearls (98%) (supplied by Curtin University) and distilled water; and batched in molar concentrations of 8, 10, 12 and 14M. Preparation of sodium hydroxide activating solutions were conducted within an ice bath, as the combination of sodium hydroxide solids and distilled water produce high temperatures through an exothermic reaction. Solution was left to cool to an ambient temperature before being sealed and stored. D-grade sodium silicate solution was provided by Curtin University, as such no preparatory task were required.

Sigma Aldrich sodium aluminate granules were batched and combined with the required amount of sodium silicate and sodium hydroxide for each mixture, 24 hours prior to liquid activation. This ensured that no exothermic heat was present during the mixing process.

Table 3-4 outlines the use of each alkaline activator within each experimental phase.

Table 3-4 – Alkaline Activation Utilisation

Experimental Phase	Sodium Hydroxide Conc. (M)				Sodium Silicate D-grade	Sodium Aluminate
	6	8	10	12		
Preliminary	✓				✓	
Secondary	✓	✓	✓	✓	✓	✓
Tertiary		✓			✓	

Utilisation of the various molar concentrations and activator types was dependant on the targeted amorphous ratios of each experimental phase. This was also influenced by experimental observations and recommendations.

3.3 Production & Testing of Geopolymer Mortar Specimens

Once the preparation of the fine aggregates, alkaline activators and aluminosilicate source materials had been completed, mixture constituents were batched individually using electric scale to an accuracy of 0.01g. Each mixture was proportioned with reference to the specific mixture designs of each phase.

The production and testing of the geopolymer produced in each phase was undertaken with reference to *ASTM – C192/ C192M -19a Standard Practice for Making and Curing Concrete Test Specimens in the Laboratory* (ASTM 2019-1). This was done to mirror the methods and procedures undertaken by Spano (2018).

Table 3-5 summarises the production and testing schedule of each experimental phase.

Table 3-5 – Production and Testing Requirements

Experimental Phase	Number of Mixes	Number of Specimens/Mix	Flow Testing	No. of Compression Tests	
				7 Days	28 Days
Preliminary	7	6	✓	3	3
Secondary	10	12	✓	6	6
Tertiary	5	12	✓	6	6

3.3.1 Geopolymer Mortar Mixing Process

Due to the investigative nature of this research and number of mixture designs to be examined, batch sizes were limited to <5.00kg. This was due to limitations associated with the preparation of fine aggregates and alkaline activator supply and costs. As such, the primary mixing apparatus used was a 10L Hobart mixer.

The mixture process was undertaken inline with the methodology adopted by Spano (2018) whereby; the fines and dry binder constituents (fly ash, GGBFS and silica fume, if applicable) were mixed for 4 minutes, ensuring the dry constituents were well combined. Next, free water was then combined with the dry constituents and then allowed to mix for an additional 4 minutes. This was undertaken to reduce clumping when the activator solution was added and promote homogeneity. Finally, the activating solution (sodium hydroxide and sodium silicate, inclusive of sodium aluminate, if applicable) were then incorporated and allowed to mix for an additional 5 minutes. Upon the competition of the final mixing stage, if required additional free water was incorporated and mixed for a further 2 minutes. This was only undertaken when flow results were insufficient for casting.

3.3.2 Flow Testing

Although not the primary experimental output, flow results were undertaken to observe and compare the workability of each mixture during each experimental phase. This was undertaken as an ongoing quality control measure ensuring each mixture had sufficient flow and workability to be compacted in line with *ASTM – C192/C192M* (ASTM 2019-1). As such, flow testing was undertaken inline with *ASTM C1437-15 Standard Test Method for Flow of Hydraulic Cement Mortar* (ASTM 2020-1). Parnham (2016) and Spano (2018), found that flow values between 70 and 120% for binary and ternary geopolymers was sufficient to facilitate casting and compacting. However, flow values below 50% exhibited significant large voids due to poor compacting and resulted in low compressive strengths. Figure 3-5, shows the flow testing apparatus used throughout this research.

Figure 3-5 - Flow Testing Apparatus

3.3.3 Casting and Curing

The specification of specimen casting sizes was undertaken to reflect those utilised by previous amorphous mixture design researchers. 50mm cube specimen moulds were used as this aligned with the works undertaken by Parnham (2016) and Spano (2018) and supported a much more robust compression testing methodology and procedure (refer to *3.7.4 – Compressive Strength Testing)*.

Specimen moulds were initially lubricated with silicone spray, prior to casting, to limit cohesion between the samples and moulds. This ensured demolding could be undertaken without damaging the freshly cured specimens. Compaction was undertaken via tamping rod and vibration compaction table. Mechanical vibration was limited to 5-10 seconds with reference to *ASTM – C192/ C192M* (ASTM 2019-1). Excessive and aggressive use of mechanical vibration can result in segregation of the fines, whereas insufficient application can result in trapped air voids. An ambient curing regime was adopted for all experimental phases, with each specimen was cured under controlled conditions with the Curtin University of Technology Civil Laboratory at a constant 23°C and 50% humidity.

Table 3-6 summarises the number of mixtures and specimens cast for each experimental phase.

Table 3-6 – Number of Mixes and Specimens

Experimental Phase	Number of Mixes	Number of Specimens/Mix
Preliminary	7	6
Secondary	10	12
Tertiary	5	12

3.3.4 Compressive Strength Testing

As outlined in *3.3.3 – Casting and Curing*, specimen casting sizes were dictated by previous research and a more robust compressive strength testing methodology. *ASTM C109/C109M - Standard Method for Compressive Strength of Hydraulic Cement Mortars (Using 50mm Cube Specimens)* (ASTM 2020-2), was utilised in contrast to *AS1012.9 - Methods of Testing Concrete: Compressive Strength Tests of Concrete, Mortar and Grout Specimens* (Standards Australia 2014), due to these two notions. This allowed for the comparison of compressive strength results with previous research without the influence of dimensional or shape effects.

Destructive compressive strength testing was conducted on each specimen inline with *ASTM C109/C109M* (ASTM 2020-2). Each batch and respective specimens were tested at 7 and 28 days, utilising a 300kN Shimadzu AGS-X universal testing machine. All compressive strength tests was conducted within the Curtin University of Technology Civil Engineering Laboratory.

Table 3-7 defines the number of specimens tested at 7 and 28 days with respect to each mixture batch and experimental phase.

Table 3-7 – Number of Specimens Tested for Each Mixture Batch

Experimental Phase	7 Days	28 Days
Preliminary	3	3
Secondary	6	6
Tertiary	6	6

3.4 Data Analysis

3.4.1 Interquartile Rule

Whilst analysing the raw experimental data, outliers were identified and removed using the interquartile rule. This was undertaken through the following process:

- Determine the interquartile range: IQR = $Q_3 – Q_2$
- Multiply the interquartile range (IQR) by 1.5
- Add 1.5IQR to Q_3 to give the outliner upper bound
- Minus 1.5IQR to Q_3 to give the outliner lower bound

This process utilises the interquartile range of the experimental data to define upper and lower bound values and determine outlying results. The first quartile (Q_1) bounds 25% of the values below it and the third quartile (Q_3) bounds 25% above it. The above-mentioned process was adopted to identify and remove outlying results associated with the 7 and 28 days compressive strength results associated with each mixture, with in each phase.

3.5 Specimen Analysis

3.5.1 Scanning Electron Microscopy

Specimen analysis was undertaken after the production and testing of samples utilising Scanning Electron Microscopy (SEM) imaging. SEM imaging was undertaken by a representative of the John de Laeter Centre at Curtin University (Bentley WA). This research utilised a TESCAN MIRA SEM with LVSTD (Low Vacuum Secondary Tescan Detector).

The focus of the SEM imaging conducted within this research, was to explore and investigate the topography and morphology of the geopolymer samples. As such, Back Scatter Electron (BSE) detection was not utilised as BSE's have a tendency to obscure sample topography. Additionally due to the similar atomic numbers of silicone, calcium, aluminium and sodium (primary elements associated with geopolymer bonds) BSE provides limited contrast between compositional elements. With these considerations Secondary Election (SE) detection was conducted.

Low-vacuum mode was adopted when conducting SEM imaging in contrast to High vacuum mode. This was due to the need to oven dry samples when producing high vacuum images. Oven drying of geopolymer samples is used to increase geopolymerisation and curing processes. As the scope of this research is associated with ambient cured geopolymerisation, the oven drying process during sample preparation for SEM, could influence the topography and morphology of the samples and alter the constraints of this research.

Utilisation of low vacuum mode and the SE TESCAN detector, can result in reduced image quality and "grainy-ness" as the presence of air in the chamber causes minor interference. This is primarily due to a reduction in the surface charge of the insulated sample and increased scatter cause by the presence of air particles. This is specifically prevalent when undertaken high magnification imaging. Magnification was limited to <2000x, as such this effect was not prevalent.

4. PREPARTORY PHASE

As defined within *Section-3.1.1,* this phase served as the precursor to the subsequent experimental phases. This phase examined the difference in reactive composition of Eraring and Gladstone fly ash stocks, as well as West build GGBFS, whilst also aiming to investigate if amorphic shortfalls in specific elements such Si and Al could be address of through supplementary constituents. The acquired results, calculations and analysis within this phase have been further discussed and addressed within this phase and subsequent phases as they were integral to the whole scope of the research. The specific items associated with this phase consisted of the following.

- PLS and SEM of aluminosilicate binder materials*
- XRF total elemental composition of binder aluminosilicate binder materials
- QXRD crystalline phase characterisation of aluminosilicate binder materials
- Calculation of amorphous composition of aluminosilicate binder materials
- Analysis and discussion of results associated with PLS, SEM and amorphous composition determination.
- Determination of mixture design matrices associated with amorphous mathematical framework.

** Aluminosilicate Binder Materials were limited to; Eraring Fly Ash, Gladstone Fly Ash and Westbuild GGBFS*

4.1 Particle Laser Sizing and SEM of Aluminosilicate Materials

Particle laser sizing and SEM were undertaken in an effort to capture the particle size and shapes associated with each binder aluminosilicate material. As stated in *Section-2.4.1.1* and *2.4.1.2,* particle size and morphology of fly ash and GGBFS materials can influence factors such as reactivity, workability, packing and compaction, all of which can influence geopolymer matrix densification and compressive strength.

Particle laser sizing was complete by a representative sample by Beau Veritas (Canning Vale, Perth, WA). Each sample was analysed using a Malvern Mastersizer 2000. The material particles were passed through a laser and scattering the light. The scatter angle is inversely proportional to their size. The intensity of the scattered light is used to determine the volume and particle size distribution. Table 4-1 outlines the nominal particles sizes of each sample in terms of d_{10}, d_{50} and d_{80}.

Table 4-1 – Summary of Particle Laser Sizing Analysis

Sample	d_{10} (µm)	d_{50} (µm)	d_{80} (µm)	% Passing 75µm
Eraring Fly Ash	3.95	22.26	54.87	87.79
Gladstone Fly Ash	1.19	7.79	27.75	94.39
West Build GGBFS	1.93	14.96	31.06	96.97

Full particle size distribution data can be found in APPENDIX A

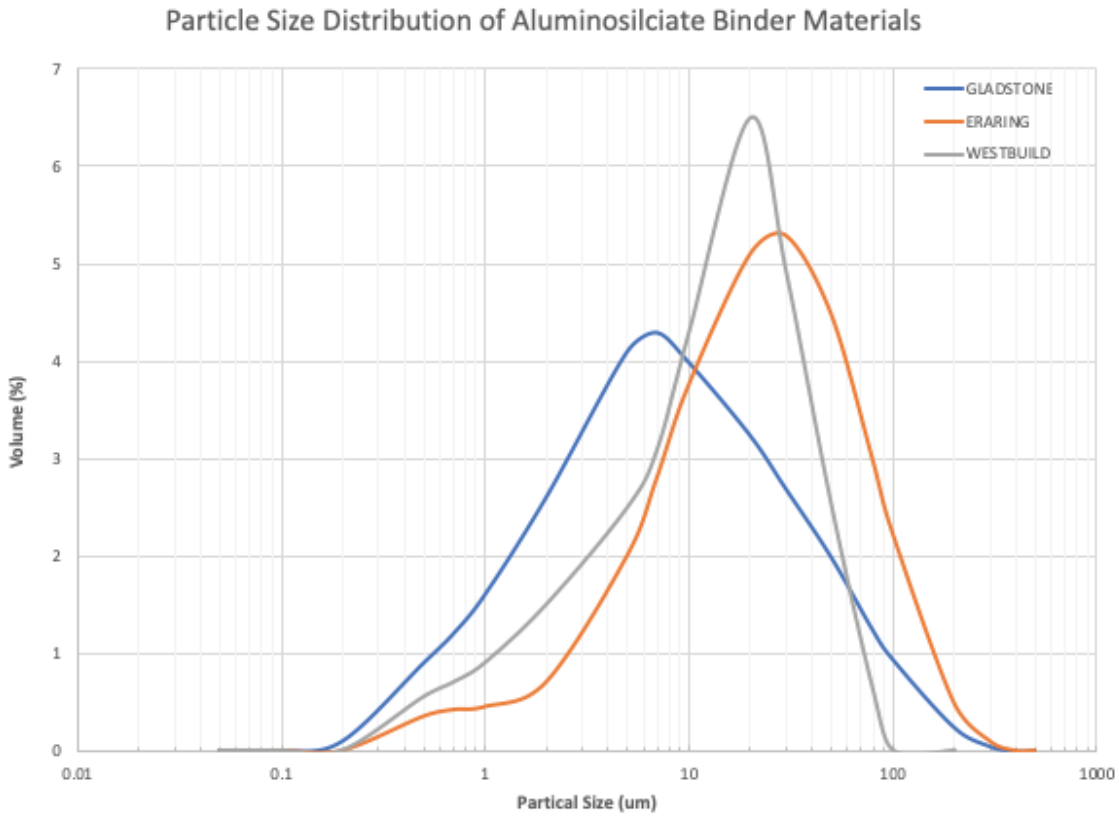

Figure 4-1 – Particle Size Distribution from PLS of Aluminosilicate Binder Materials

As defined with Table 4.1, it can be seen that the Gladstone fly ash sample was determined to be finer than both the Eraring fly ash and Westbuild GGBFS across d10, d50 and d80. This demonstrated that the particle range of Gladstone fly ash sample generally consisted of finer particles. This notion was further reiterated with in Figure 4.1, as the particle distribution curve for Gladstone sample was offset toward the finer range of particle sizes, with the largest volume % of particles located at 7-8 µm.

Figure 4.1 also demonstrates that the Eraring fly ash and Westbuild GGBFS exhibited similar particle size distributions between 0.1-10µm, with the largest volume % particles being sized at 20-30 µm. Furthermore the Eraring fly ash sample exhibited a larger percentage of larger particles compared to both the Gladstone and Westbuild samples, however the maximum particle sizes of both fly ashes did not differ significantly. The % Passing 75µm results defined in Table 4.1 show that the Westbuild GGBFS contained marginally finer particles overall, compared to Gladstone fly ash. This can be attributed to the maximum particle size of the GGBFS sample not exceeding 100 µm, compared to maximums of 300µm measure for the fly ash samples.

As outlined in *3.5.1.*, SEM analysis was undertaken by a representative of the John de Laeter Centre at Curtin University (Bentley WA) using TESCAN MIRA SEM with LVSTD. SEM imaging of the Eraring and Gladstone fly ashes, as well as Westbuild GGFBS was conducted to observe the particle shape, size and morphology of these stock materials. Figure 4-2 presents SEM imaging of Eraring fly ash, Gladstone fly ash and Westbuild GGFBS.

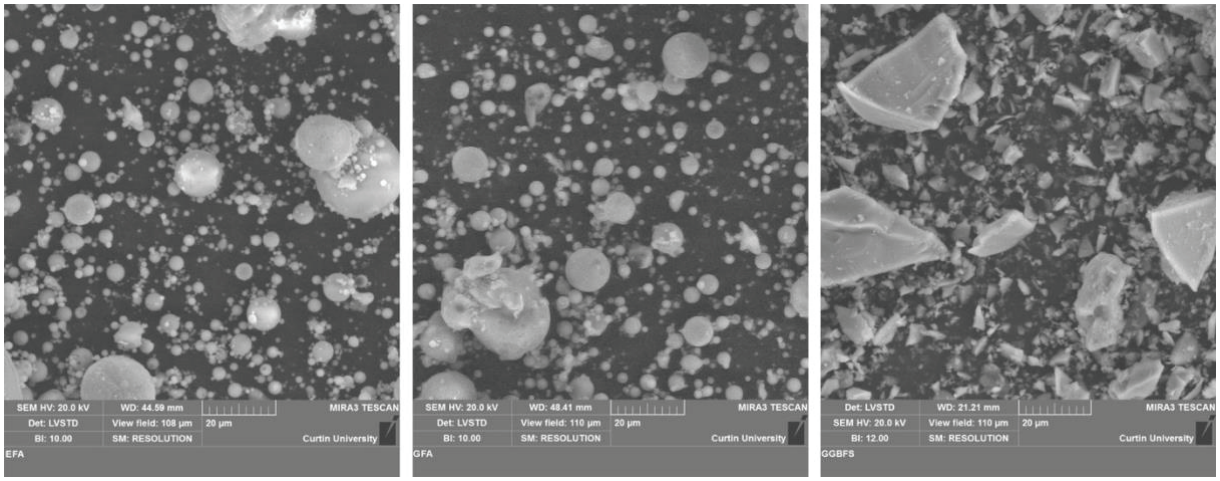

Figure 4-2 - SEM Imaging of Eraring Fly Ash (Left), Gladstone Fly Ash (Middle) & Westbuild GGBFS (Right)

As seen in Figure 4-2, the morphology observed for both fly ash samples was that of smooth surfaced spheres of various sizes. In contrast, the GGFBS sample demonstrates angular prismatic particle shapes of varying sizes. Differentiation between the fineness of each sample could not be undertaken from the above SEM imaging. However, all three samples presented partial sizes less than 20µm. This was in line with recorded PLS data.

4.2 Aluminosilicate Composition via X-Ray Techniques

4.2.1 Bulk Composition and X-Ray Fluorescence Results

Bulk compositional analysis of the aluminosilicate source materials was undertaken via x-ray fluorescence analysis (XRF) by Bureau Veritas (Canning Vale, Perth, WA). Analysis was undertaken on Gladstone and Eraring Fly ash, Westbuild GGBFS and Ecotec Silica Fume. Table 4-2 summarises the XRF elemental oxide results related to Si, Al, C, and Na. Iron oxides (Fe_2O_3) were also been included for reference and further discussion.

Table 4-2 – XRF Bulk Oxide Composition Summary of Aluminosilicate Materials

Compound	Sample (wt%)			
	Gladstone Fly Ash	Eraring Fly Ash	Westbuild GGBFS	Ecotec Silica Fume
SiO_2	45.26	60.03	33.24	89.75
Al_2O_3	26.99	22.75	13.20	0.45
Na_2O	0.42	0.05	0.03	0.68
CaO	5.45	6.78	40.90	0.9
Fe_2O_3	14.30	3.80	0.94	1.16

Full XRF analysis results (inclusive of trace elements) can be found within APPENDIX B

As defined above both the Gladstone and Eraring fly ashes can be deemed to be Class F fly ashes (ASTM 2019-3), due to the sum of the silicon, aluminium and iron content of each sample being greater than 70%. Additionally, both samples were identified to be comprised mainly of silicon followed by aluminium. However, there was some disparity between the bulk elemental composition of each fly ash. The Gladstone fly ash exhibited higher aluminium and iron oxide content compared to that of the Eraring fly ash. In retrospect, the Eraring sample exhibited higher levels of silicon. Other bulk elemental oxides within these sample demonstrated little disparity and were present in trace amounts (refer to Appendix A). Analysis of the GGBFS and silica fume samples yielded results which reflected those examined from previous research. The Westbuild GGFBS sample was mainly comprised of calcium (40.9wt%), silicon (33.24wt%) and aluminium (13.2wt%). The Ecotec silica fume consisted of 89.75% silicon with negligible amount (>1wt%) of trace elements, including aluminium and calcium.

4.2.2 Crystalline Composition and Quantitative X-Ray Diffraction Results

Quantitative x-ray diffraction (Q-XRD) analysis was conducted on the Gladstone and Eraring fly ashes, as well as Westbuild GGBFS. The crystalline composition of each material was obtained using the facilities within the John de Laeter Centre at Curtin University and the methodology outlined within *3.2.2.3 - Crystalline composition via Quantitative X-Ray Diffraction (Q-XRD)*

X-ray diffraction analysis identified the crystalline peaks within each aluminosilicate sample, with phases identification being undertaken within DiffractEVA 11.0. Figures 4-3 and 4-4 display the crystalline peaks and phases within the Gladstone and Eraring fly ashes, whereas Figures 4-5 and 4-6 displays those associated with Westbuild GGBFS and Ecotec silica fume.

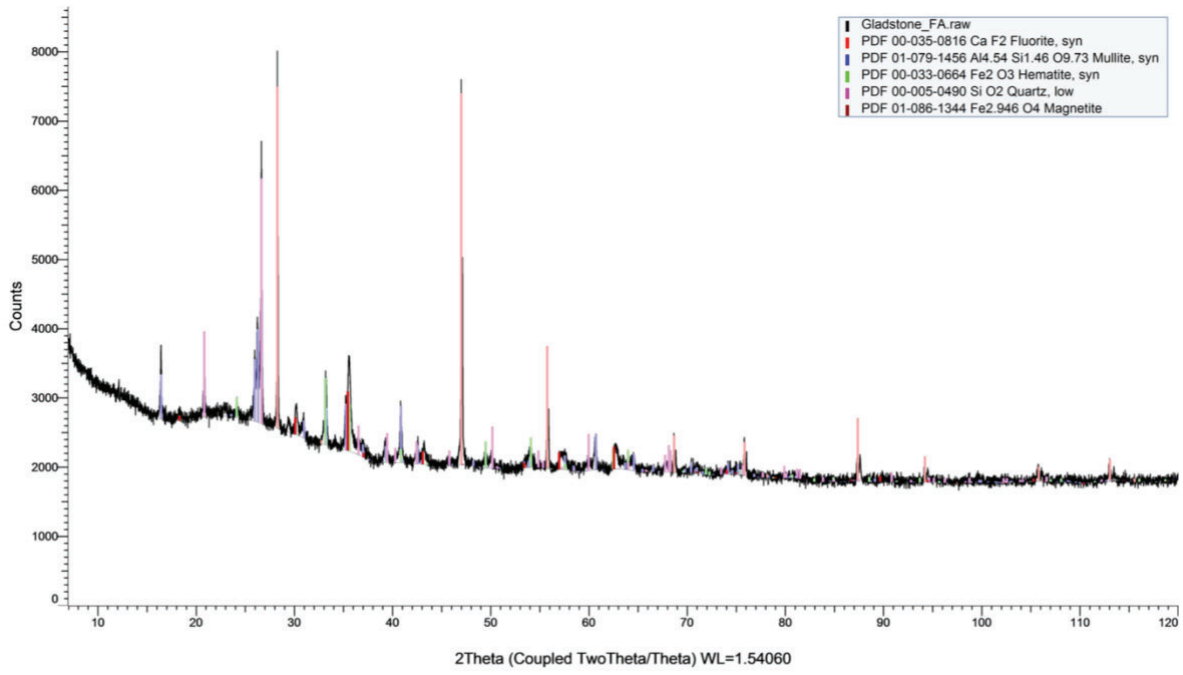

Figure 4-3 - Crystalline Peaks of Gladstone Fly Ash

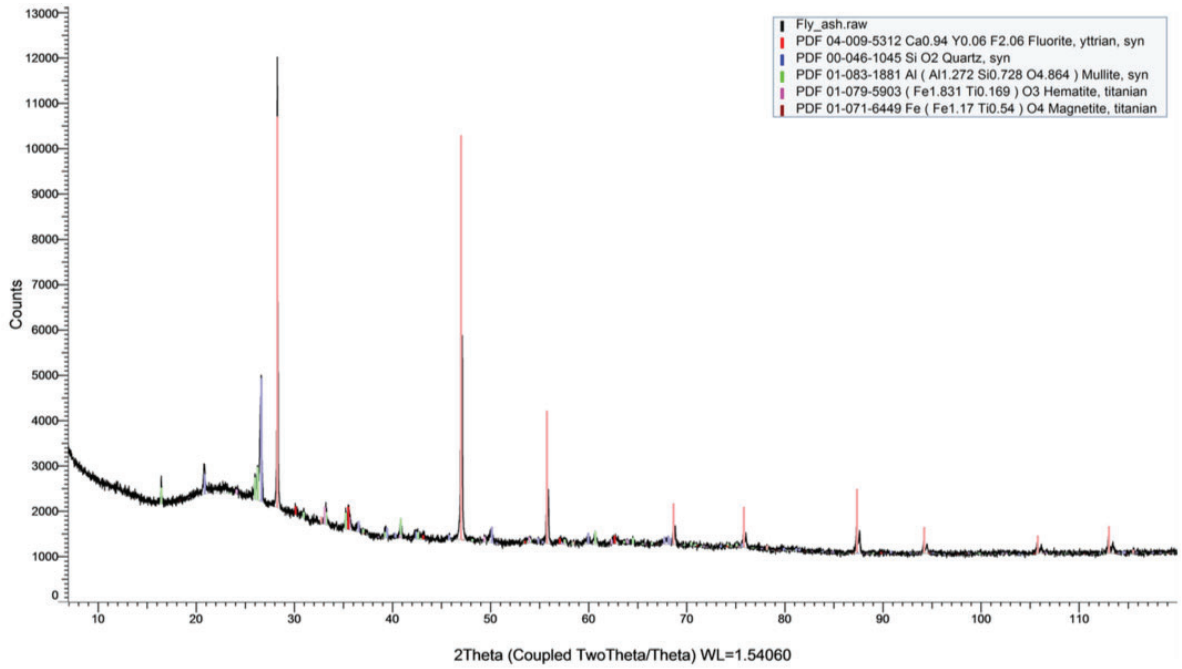

Figure 4-4 - Crystalline Peaks of Eraring Fly Ash

Within both the Gladstone and Eraring fly ash samples similar crystalline peaks were observed. These peaks correlated to phases which included Fluorite and Quartz as well as several iron oxides such as Mullite, Hermatite and Magnetite. The identification of Fluorite in both samples is expect due to the prescribed methodology associated with the internal standard method. The use of Fluorite aids the quantification process as it acts a base line for determining the quantities of the crystalline content present. The trio of iron oxides identified within both samples was also expected, with previous works conducted by Parnham (2016) and Spano (2018) also encountering such compounds. Due to the crystalline nature of these iron oxides as well as that of Quartz, it is believed that these compounds essentially act as fillers and do not contribute to the formation of geopolymer bonds.

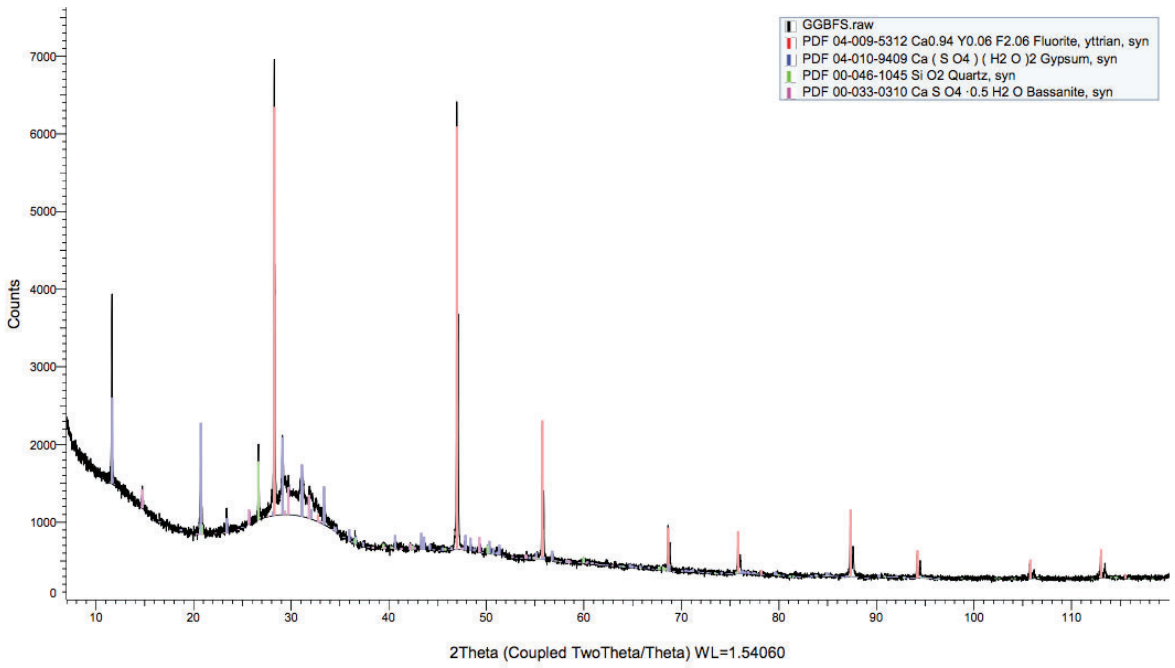

Figure 4-5 - Crystalline Peaks of Westbuild GGBFS

Crystalline phase analysis of the Westbuild GGBFS sample resulted in the identification of Fluorite and Quartz crystalline phases, similar to the fly ash samples, as well as calcium sulphates such as Gysum and Bassanite. Similarly, Fluorite again was anticipated due to the methodology associated with the analysis, whereas Quartz was expected based on results obtained by past researchers (Parnham 2016, Sweeney 2017, Spano 2018). The presents of calcium sulphates within the GGBFS sample are believed to be attributed to two cause. The first is due to the presence of limestone within the slag production process and the second, being the addition of Gypsum to GGBFS after the grinding process. Yip et al. (2008) highlighted that Gysum is typically added to GGBFS to aid the hydration process when employed as SMC during the production of OPC concretes within Australia.

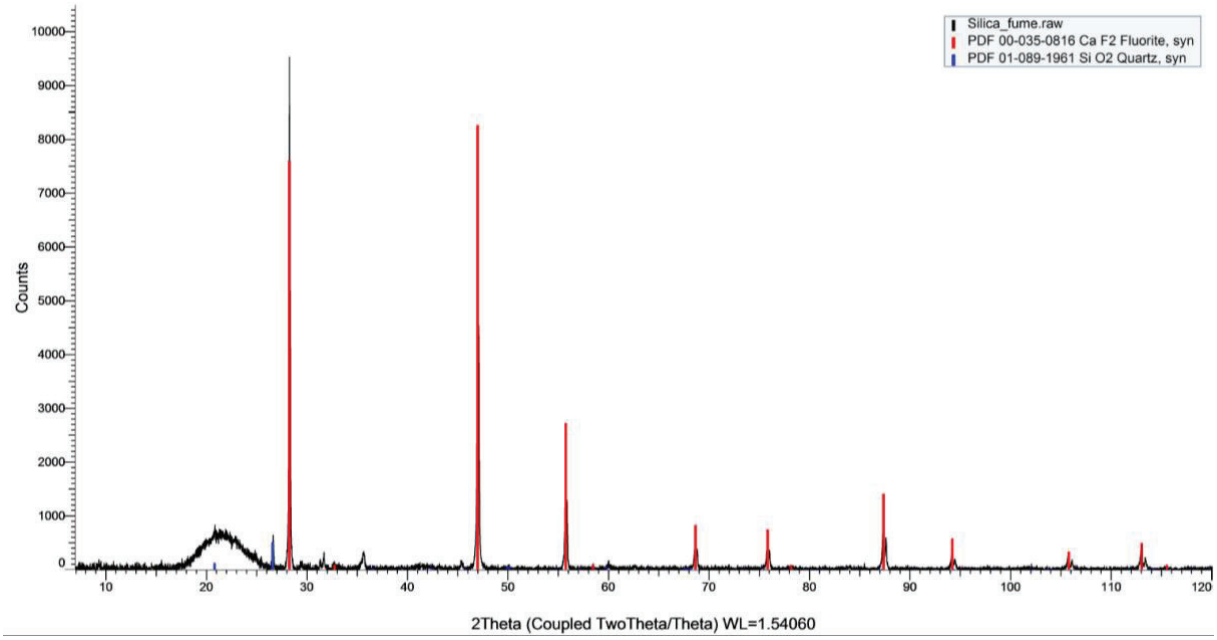

Figure 4-6 - Crystalline Peaks of Ecotec Silica Fume

Crystalline phase analysis of the Ecotec silica fume sample resulted in the identification of Fluorite and Quartz crystalline phases. Similarly to all samples examined, the large crystalline peaks associated with Fluorite is reflective of the internal standard material. Trace amounts of crystalline quartz where also identified, believed to be attributed to traces left from micronizing through the utilisation of agate milling material. Based on the XRD pattern it can be assumed that silica fume was fully amorphous.

Upon the completion of crystalline phase analysis and identification, quantification of the crystalline content within the aluminosilicate samples was undertaken. Quantitative analysis was conducted using the Reitfield method and computer software known as TOPAS. Table 4-3 summarises the weight percentage (wt%) of each crystalline phase identified during QXRD analysis.

Table 4-3 - Crystalline Composition Result Summary of Aluminosilicate Materials Conducted via QXRD

Phase	Compound	Sample (wt%)		
		Gladstone Fly Ash	Eraring Fly Ash	Westbuild GGBFS
Quartz	SiO_2	8.44	6.10	1.31
Mullite	$Al_{4.5}Si1_{0.5}O_{9.74}$	22.51	6.32	-
Hematite	Fe_2O_3	3.15	0.71	-
Magnetite	Fe_3O_4	6.71	1.50	-
Gypsum	$CaSO_4$	-	-	4.20
Bassanite	$CaSO_4.0.5(H_2O)$	-	-	2.50

Refer to APPENDIX C for full set of calculated values.

As outlined in Table 4-3, the Gladstone fly ash contained the most crystalline content (40.8wt%), followed by the Eraring fly ash (14.6wt%) and then the Westbuild GGBFS (8.0wt%). The most notable difference with reference to the two fly ash samples was the higher levels of Mullite within the Gladstone sample as well as Hematite and Magnetite. The combination of these three crystalline ferric oxides contributed to 79% of the Gladstone crystalline content compared to 58% for the Eraring sample. Both fly ash samples contained similar levels of Quartz, with the Westbuild GGBFS only containing minimal levels. In contrast, the GGBSF sample contained crystalline calcium sulphates such as Gysum and Bassanite, unlike the fly ash samples. These calcium sulphates formed the majority of the crystalline content of the GGBFS (83.75%).

4.3 Determination of the Amorphous Phase

Utilisation of the amorphous content within each aluminosilicate source material forms one of the main pillars of this research. As such, the determination of the amorphous content of these source materials was undertaken utilising the data obtained via XRF and Q-XRD. The following process below has been adopted by geopolymer amorphous researchers to calculate the amorphous content of fly ash and GGBFS materials. The methodology and process listed below has been sourced from the works conducted by Spano (2018), as this research aims to further develop the amorphous approach to mixture design.

The following process was undertaken for each aluminosilicate material of which the amorphous composition was to be calculated.

Analysis of crystalline compound data obtained from Q-XRD

a) *The crystalline compounds within each sample are reduced to their elemental state and the relative proportions of each element are determined, with respect to their molecular weight.*
b) *The weight percentage of the crystalline compound are proportioned into its respective elemental crystalline composition utilising Equation 2:*

$$\boldsymbol{Cryst.\ Comp_{\cdot(Element)} = Cryst.\ Comp_{\cdot(Compound)} \times Relative\ Prop_{\cdot(Element)}}$$

(Equation 2)

c) *The elemental crystalline composition of each separate crystalline compound for each sample is combined, yielding the total crystalline weight percentage of each element.*
d) *Determination of the equivalent crystalline oxide component*

Determination of the amorphous composition is essentially undertaken by subtracting the bulk oxide composition from crystalline elemental composition. This cannot be undertaken until the crystalline elemental composition is converted to an equivalent oxide. the equivalent crystalline oxide of each elemental component must be obtained with respect to the compounds identified within XRF analysis. This is undertaken via Equation 3.

$$\boldsymbol{Eq.Crystalline\ Oxide = \left(\frac{Crystalline\ elemental\ component}{MW_{(element)}}\right) \times MW_{(oxide\ compound)}}$$

MW = Molecular Weight

(Equation 3)

Utilisation of the total chemical composition data obtained from XRF

The data obtained from the XRF analysis results does not require any correction as it is reported in oxide form. This data will be used in correlation with calculated Equivalent crystalline oxides to determine the amorphous composition of each material.

Determination of the amorphous (reactive) composition

Determination of the amorphous composition is then obtain via subtraction Equation 4.

$$\boldsymbol{Amorphous\ Content = Total\ Oxide\ Compostion - Eq.Crystalline\ Oxide}$$

(Equation 4)

(Extract from: Spano 2018)

Based on the above methodology, the amorphous composition of the Gladstone and Eraring fly ash as well as the Westbuild GGBFS was calculated. The results of which can be seen in Table 4-4.

Table 4-4 – Amorphous Composition of Gladstone Fly Ash, Eraring Fly Ash and Westbuild GGBFS

Oxide Compound	Gladstone Fly Ash (wt%)	Eraring Fly Ash (wt%)	Westbuild GGBFS (wt%)
SiO_2	38.35	52.15	31.94
Al_2O_3	10.82	18.23	13.20
Na_2O	0.42	0.05	0.03
CaO	5.45	6.78	37.92
TOTAL	**55.04**	**77.21**	**83.08**

Refer to APPENDIX D for full set of calculated values.

Calculation of the amorphous composition of the Ecotec Silica fume has been omitted due to its characteristically complete amorphous composition. As such, XRF analysis results have been utilised for the amorphous content of the silica fume material. This methodology aligned with previous research, whilst being supported by research conducted by Mostafa et al. (2001) and confirmed by Figure 4-6, whereby through QXRF analysis, silica fume exhibits extensive scatter peaks with negligible crystalline peaks.

4.4 The Application of the Amorphous Mathematical Framework

Utilisation of the mathematical framework was conducted with the amorphous content of each material to develop mixture designs throughout this research. This was undertaken to define and examine specific amorphous ratios whilst determining the specific weight proportions of each mixture constituent. This research utilised the mathematical framework through Equation 5.

$$[\boldsymbol{W}][\boldsymbol{F}] = [\boldsymbol{R}]$$

Equation 5

An iterative process was adopted though specifying the weight proportion [W] of the constituents. This in turn allowed for specific elemental ratios [R] to be targeted, whilst the amorphous content of the mixture constituents [F] were constant.

4.4.1 Determination of the Elemental Proportion of the F-Matrix

The F-matrix (Figure 4-7) reflects the amorphous composition of the constituents within a particular mixture.

$$F = \begin{bmatrix} F1_{Si} & F2_{Si} & F3_{Si} & F4_{Si} & F5_{Si} & F6_{Si} & F7_{Si} \\ F1_{Al} & F2_{Al} & F3_{Al} & F4_{Al} & F5_{Al} & F6_{Al} & F7_{Al} \\ F1_{Na} & F2_{Na} & F3_{Na} & F4_{Na} & F5_{Na} & F6_{Na} & F7_{Na} \\ F1_{H} & F2_{H} & F3_{H} & F4_{H} & F5_{H} & F6_{H} & F7_{H} \\ F1_{Ca} & F2_{Ca} & F3_{Ca} & F4_{Ca} & F5_{Ca} & F6_{Ca} & F7_{Ca} \end{bmatrix}$$

Fly Ash *Sodium Aluminate* *Silica Fume* *Sodium Silicate* *Sodium Hydroxide* *Water* *GGBFS*

Figure 4-7 – F-Matrix : Feeder Stock Matrix

As the F-Matrix presents the amorphous composition of each constituent in its reactive elemental proportions, these portions must be determined prior to its utilisation. These proportions were determined using the following process, as defined by Spano (2018):

Determination of the Elemental Proportions of the F-Matrix:

I. Each constituent was reduced into its corresponding compounds.

II. Each compound was then proportioned with respect to the respective elemental molarity using Equation 6.

$$\boldsymbol{F_{(Element)} = No.of\ Atoms\ in\ Compound_{(Element)} \times \left(\frac{Amorphous\ Content_{(compound)}}{MW_{(compound)}}\right) = (mol/g)}$$

(Equation 6)

III. The elemental molarity of each constituent was then combined to form the overall F-matrix for that particular mix.

Except from Spano (2018)

Sample calculations can be found in APPENDIX E in relation to the above process.

This process was undertaken for the following mixture constituents:

- F1 = Fly ash (Eraring and Gladstone)
- F2 = Sodium aluminate (Granules)
- F3 = Silica fume (Ecotec)
- F4 = Sodium silicate solution (Type D- Solution)
- F5 = Sodium hydroxide (6, 8, 10, 12 & 14M)
- F6 = Water
- F7 = Grounded granulated blast furnace flag (Westbuild)

Each material F-matrix component can be found within APPENDIX F

In relation to the F-matrix for a mixture, the above components are combined in relation to the constituents utilised within a specific mixture. The total F-matrix configuration did vary between specific mixtures when differing aluminosilicate stock materials were utilised, such as Gladstone or Eraring fly ash, or varied concentrations of sodium hydroxide activating solution are adopted. Varied activator concentrations were used in correlation with the F-matrix to manipulate the amorphous Na/Al ratio during the mixture design process.

Corresponding F-matrixes for each phases mixtures can be found in APPENDIX G, I, K.

4.4.2 Prescription of the W-matrix

As previously outlined, the W-matrix relates to the weight proportions of each mixture constituent and as defined in Figure 4-8.

$$W\ (grams) = \begin{bmatrix} F1_{wt} \\ F2_{wt} \\ F3_{wt} \\ F4_{wt} \\ F5_{wt} \\ F6_{wt} \\ F7_{wt} \end{bmatrix} = \begin{bmatrix} Fly\ Ash \\ NaAlO_2 \\ Silica\ Fume \\ Na_2SiO_3 \\ NaOH \\ H_2O \\ GGBFS \end{bmatrix}$$

Figure 4-8 – W-Matrix : Weight Proportion Matrix

The values within the W-matrix were initially prescribed based on previous research to determine approximate bulk mixture proportions, as defined in *3.1 - Design of Experiments*. An iterative process was conducted whereby specific weight proportions within the W-matrix were varied to target specific elemental ratios. This was undertaken with reference to *2.5.2.2 - Amorphous elemental ratios*, using the following criteria:

- silica fume and sodium aluminate content was used to alter the amorphous Si/Al ratio,
- sodium hydroxide and sodium silicate content was used to alter the amorphous Na/Al ratio,
- GGBFS content used to alter amorphous Ca/Si ratio

Mixture proportions varied with respect to the targeted elemental ratios of each phase and mixture. The W-matrixes for each mixture and phase can be found in APPENDIX G, I, K.

4.4.3 The R-Matrix and Amorphous Ratios

Through the prescription of the W-matrix and determination of the F-matrix, the R-matrix was calculated using Equation 7.

$$[\boldsymbol{W}][\boldsymbol{F}] = [\boldsymbol{R}]$$

(Equation 7)

The R-matrix is defined as the number of moles of each reactive element within the mixture. As expresses above, manipulation of the W-matrix directly influences the amorphous moles within the R-matrix, whilst the F-matrix is held constant. The values within the R-matrix are then converted to specific amorphous atomic ratios of interest. This process can be seen in the example below.

$$[\boldsymbol{W}][\boldsymbol{F}](\boldsymbol{Mix_{PG}}) = [\boldsymbol{R}]$$

$$[R] = \begin{bmatrix} 841 \\ — \\ 392 \\ 158 \\ 500 \\ 672 \end{bmatrix} \begin{bmatrix} 0.00638 & - & 0.01494 & 0.00489 & - & - & 0.00532 \\ 0.00212 & 0.00549 & 0.00008 & - & - & - & 0.00259 \\ 0.00014 & 0.00565 & 0.00564 & 0.00237 & 0.00600 & - & 0.00001 \\ - & - & - & 0.06206 & 0.09038 & 0.11101 & - \\ 0.00097 & - & 0.00017 & - & - & - & 0.00676 \end{bmatrix}$$

$$[R](Mix_{PG}) = \begin{bmatrix} 10.858 \\ 3.526 \\ 1.997 \\ 94.116 \\ 5.361 \end{bmatrix} = \begin{bmatrix} Si \\ Al \\ Na \\ H \\ Ca \end{bmatrix} (mol)\ (Elemental\ Moles)$$

$$Amorphous\ Ratios\ (Mix_{PG}) = \begin{bmatrix} 3.08 \\ 1.00 \\ 0.56 \\ 8.50 \\ 0.49 \end{bmatrix} = \begin{bmatrix} Si/Al \\ Al/Al \\ Na/Al \\ (H/Si) \\ (Ca/Si) \end{bmatrix}$$

Specific amorphous ratios were targeted depending on the experimental phase and used to proportion the weight proportions of each mixture. As stated previously, an iterative process was adopted whilst examining the R-matrix and synonymous amorphous ratios until desired values were obtained during the mixture design process.

The R-matrix and amorphous ratios associated with each mixture design can be found in APPENDIX G, I, K.

4.5 Discussion

4.5.1 Particle size and Fineness

As identified within Table 4-1 the two fly ash samples median particle size (d50) differed in significantly, with Gladstone demonstrating a value of 7.79 µm compared to Eraring with 22.26 µm. Typically particle size results for fly ash samples range from 0.3 to 250 µm with the major fraction being within 20-25 µm. The d_{50} value observed with respect to the Gladstone fly ash sample was well below the major fraction values of 20-25 µm, as demonstrated by the peak presented in Figure 4-1. The Gladstone d_{50} values were significantly smaller than those presented by the Eraring fly ash stock, which reflected more typical d_{50} values through PSL analysis. In general these results pertained to the Gladstone fly ash being finer overall compared to Eraring fly ash stock. This was reflected further as Gladstone demonstrated smaller d_{10} and d_{80} values, and higher % Passing 75µm values compared to the Eraring sample. When referring to Figure 4-1 the Gladstone particle size distribution curve tends towards smaller and finer particles compared to Eraring. This shift can lend itself to several benefits and implications associated with geopolymer production and compressive strength outcomes.

Increased fineness is associated with the fly ash particles having an increased surface area, which in turn, can results in increased alkaline activator dosing and water demand on the system, to facilitate sufficient workability for production, casting and compacting (Singh et al. 2015). Enhancement of fly ash reactivity has been examined in several studies (Temuujin, Williams, and Van Riessen 2009, Hela and Orsáková. 2013, Lau et al. 2019) through methods of mechanical activation (grinding) in an effort to reduce to average particle size of the fly ash stock material. Although mechanical activation is said to release additional amorphous content encased with the fly ash spheres, it also leads to particle size reduction and increased fly ash particle surface area. This is said to contribute to reduced workability and diminish the rheological properties of the geopolymer binder. Quantification of the effects of particle size on workability and compressive strength are difficult to assess as they are typical concurrent with the effects of increased reactivity and the geopolymerisation reaction itself. However, increased fly ash particle surface area is said promote dissolution of the aluminosilicate stock material resulting in a faster and more extensive polycondensation reaction, which inherently requires additional free water to facilitate ionic transportation (Brough and Atkinson 2002).

As demonstrated in Figure 4-2 the morphology of the aluminosilicate samples is reflective of current and past literature. The fly ash particles resemble smooth spherical shaped elements, whereas GGBFS particles are angular and course in nature. The smooth spherical shape of the fly ash particles typically promote workability and liquid-like rheological behaviour in mortars and concretes, inversely high levels of GGBFS reduce workability due to the nature of the course particles and their interaction.

When examining both the PLS data and SEM imagery associated with Westbuild GGBFS, it was found that the GGBFS of this research was reflective of that observed by numerous researchers previously, including Sweeney (2017) Lau et al. (2019), and Spano (2018). As defined in *Section - 2.4.1.2*, the morphology of the particles and their angular shapes could lead to reduced workability, specifically when incorporated into binary or ternary geopolymer production in high levels. Chindaprasirt, P, T Chareerat, and Vute Sirivivatnanon. (2007) found that levels up to 30% resulted in reduced workability by up to 20% and that levels above 50% induced increased micro-cracks within the geopolymer matrix. Additionally the incorporation of Westbuild GGBFS with the finer Gladstone fly ash of this research may result in increased setting times and significant water/activator demand as both sample demonstrated similar PLS results.

4.5.2 Difference in Gladstone and Eraring Fly Ash Amorphous and Crystalline Content

As defined with *Section - 4.2* both XRF and QXRD analysis was undertaken on each aluminosilicate stock material (Gladstone and Eraring fly ash and Westbuild GGFBS). These results were used to determine the bulk mixture proportions of each mixture via the amorphous frame work as outlined in *Section - 3.1.1.1*. Additionally, x-ray analysis results were also used to examine the extent of difference in reactive composition of the two fly ash stocks, and ascertain the influence each might play when considering the mixture design and production of ternary and blended geopolymer mortars.

Through XRF analysis reulst defined in Table 4-2, it was found that both fly ash samples contain >70% of SiO_2, Al_2O_3 and Fe_2O_3 combined, as well as lose of ignition (LOI) of <6%, therefore being classified as Class-F fly ash in accordance with *ASTM C618* (ASTM 2019-3). In line with Harjito and Rangan (2005), such fly ashes are favourable due to their high aluminosilicate content. With reference to Table 4-2, significant differences between the two fly ashes bulk compositions were associated with SiO_2 and Fe_2O_3. These results simply show the that Eraring fly ash contains more total silicone and Gladstone more iron. When referencing Table 4-3 the crystalline content of both fly ashes associated with quartz (SiO_2) was similar (±2wt% of sample), however Gladstone contained significantly higher crystalline content associated with Mullite (Al and Si crystalline compound) and iron oxide compounds of Hematite (Fe_2O_3) and Magnetite(Fe_3O_4). Gladstone's reduced bulk silicon content and high levels of Mullite resulted in less total amorphous Si and Al. As defined with Table 4-4, it can been seen that Gladstone fly ash contains less total amorphous content, and therefore is theoretically less reactive compared to Eraring. As highlighted in Table 4-4, Eraring fly ash exhibits increased amorphous content compared to the Gladstone fly ash, in all oxide compounds, except Na_2O. The Na_2O content in both sample was deemed to be negligible and is provided via the inclusion of alkaline activators in the geopolymerisation reaction.

Fly ash samples containing lower levels of amorphous content have been found have less reactivity, producing weaker geopolymers, as the reduced presence of reactive elements do not facilitate substantial geopolymerisation (Williams 2015).The reduced presence of both Al and Si (with reference to the Gladstone fly ash) have the potential to impact both N-A-S-H bond for geopolymers, as well as slow forming C-A-S-H geopolymer bonds and early stage C-S-H bonds associated with binary and ternary geopolymers which incorporate GGBFS. Inversely higher levels of amorphous content, as observed with respect to Eraring Flay ash, can attribute to increased water demand which leads to reduced compressive strength as ion transportation is inhibited during the formation of N-A-S-H and C-A-S-H geopolymer bonds (Zuhua et al. 2009). However, as the dissolution of the fly ash stock material is generally not complete, higher levels of available amorphous content is favourable in the production higher strength geopolymers, yet this tends to lead to reduced setting times and the possibility of flash setting. In contrast, less reactive fly ash stock

materials and those with lower levels of amorphous content may also be favourable in producing geopolymers with sufficient workability and increase setting time to facilitated adequate compaction and increased densification.

This research also observed that the Gladstone fly ash contained high levels of iron oxide compounds (14.3 bulk wt%) compared to the Eraring fly ash (3.8 bulk wt%). Chen-Tan (2010) observed that both crystalline and amorphous iron compounds do not play a significant role in geopolymerisation, primarily due to their extremely slow dissolution rate. As such, it should be considered as an inert filler. This notion paired with the higher crystalline content of the Gladstone fly ash, may hinder the geopolymerisation process since the crystalline content is mostly embedded within the amorphous content of the fly ash (Chen-Tan 2010). High filler content although typically paired with lower reactivity, may have benefits associated with densification and reduction of air void, specifically paired with the Gladstone fly ashes extreme fineness.

4.5.3 Supplementation of Amorphous Content through Additional Aluminosilicate Material and Alternative Activators.

One of the defined objectives of this research was to determine if complementary constituents could be used to supplement short falls in the reactive composition of fly ash stock materials. This objective was to be investigated from an amorphous mixture design and geopolymer production perspective. As discussed in *Section-4.5.2*., the extent of difference in amorphous composition between the two examined fly ash stocks was significant with respect to Si and Al. The Gladstone fly ash of this research contains considerably less amorphous silicon and aluminium in contrast to, the Eraring fly ash of this research and that utilised by Spano (2018). Due to the reduced presence of amorphous Si and Al within the Gladstone fly ash stock two supplementary constituents were identified, these being silica fume and sodium aluminate. Each of which were identified due to their ability to provide amorphous Si or Al to the system, as well as their previous use in geopolymer formulation and production.

To address short falls in amorphous Si content, silica fume supplementation was deemed appropriate due to its previous use in both concrete and geopolymer production, as highlighted in *2.4.1.3. – Silica Fume.* The inclusion of silica fume specifically influences the amorphous Si/Al ratio due its predominately Si and non-crystalline composition (Refer to Table 4-2). As such, utilisation of silica fume to "balance out" shortfalls in Si content between two differing fly ash stocks or increase the amorphous Si/Al ratio is possible from an amorphous mixture design and formulation perspective. Utilisation of the amorphous mathematical framework and the methodology proposed in *Section - 3.1.1.1*, demonstrates that silica fume inclusion can be incorporated into the amorphous framework to target specific amorphous ratios with little influence on other reactive elements. From an experimental and production perspective silica fume inclusion has the potential to exhibit both benefits and challenges based on its utilisation in previous geopolymer production. Dutta et al. (2010) and Adek et al. (2014) found the inclusion of up to 10wt % was favourable to increases in compressive strength. Spano (2018) found the inclusion of 7wt% of silica fume provided significant contribution to compressive strength, compared to activator concentration and composition. However, Okoye, Durgaprasad and Singh (2015) found that increased levels resulted in reduced workability due to the increased water demand for ion transportation and the fine nature of silica fume. This also attributed to the formation of agglomerates which also attributed to reduced compressive strengths and inhibition of geopolymerisation. Due silica fumes high Si content and completely amorphous nature, it was found to be favoured over the less reactive fly ash stock, resulting in C-S-H bonds, typical to concrete hydration rather than favourable N-A-S-H and C-A-S-H bonds which lend themselves to geopolymers durability properties. This is specifically prevalent in the presence of amorphous calcium, provided by GGBFS in binary geopolymers.

To address short falls identified in amorphous Al content within the Gladstone fly ash sample, sodium aluminate was selected. Although not classed as an aluminosilicate material (similarly to silica fume, fly ash or GGBFS), previous research has investigated the use of sodium aluminate as an alternative alkaline activator in lieu of sodium silicate and sodium aluminate (Nugteren et al. (2011). When incorporating sodium aluminate into the amorphous mixture design process and the mathematical framework, the presence of both Na and Al within its composition results in underlying influences to both the Si/Al and Na/Al ratios. As the amorphous Na/Al ratio is typically associated with the concentration of the alkaline activators adopted, considerations regarding sodium hydroxide concentrations rather than sodium silicate are required specifically when targeting/maintaining specific Si/Al ratios. This adds an additional complexity in targeting specific elemental ratios when trying to address Al supplementation only.

From an experimental and production perspective the inclusion of sodium aluminate is believe to promote early stage geopolymerisation, by initially providing Al ions in lieu of slowly dissociating Al species within the aluminosilicate stock, therefore producing improved physical properties. This concept is believed to be apparent with low calcium fly ash stock materials. Heo, Park and Kim (2019) reported in the inclusion of up to 2%wt of sodium aluminate improved the compressive strength of geopolymer samples at ambient and elevated temperatures. Improvement of early age compressive strength associated with sodium aluminate inclusion in concrete mixtures was observed by Han et al. (2014) at the detriment of later stage strength. In the presence of calcium, typical to high calcium fly ash geopolymers, alkali activated GGBFS and binary geopolymers which incorporate GGFBS, sodium aluminate inclusion is believed to contribute to the rapid formation of calcium hydroaluminate (C-A-H). The formation of C-A-H is facilitated in cement production through the inclusion of alkaline accelerators, such as sodium aluminate, to reduced setting times (Kropyvnytska et al. 2019). This notion is believed to be apparent with calcium rich geopolymers as Spano (2018) theorised that the inclusion of sodium aluminate contributed to accelerated setting and the phenomenon of flash setting.

4.6 Phase Conclusions

The extent of difference between the Gladstone and Eraring fly ash stock were examined with reference to particle size and morphology as well as bulk, amorphous and crystalline composition. Examination of these properties were undertaken to identify differences in chemical composition of each fly ash material; and ascertain if substitution of amorphous content was possible through the inclusion of supplementary constituents, within the amorphous mixture design framework.

Particle laser sizing was undertaken to examine the particle size distribution of both fly ash materials and the potential effect fineness may have on production and geopolymerisation. Significant differences was observed between the two samples, with Gladstone demonstrating increased fineness compared to Eraring (Gladstone d_{50}= 7.8µm, Eraring d_{50}= 22.3µm). Interestingly, the Gladstone fly ash exhibited similar fineness values compared to the Westbuild GGBFS. SEM micrographs confirmed the expected sphere-like particles of the fly ash sample and angular/course shaped particles associated with the Westbuild GGBFS.

The bulk, crystalline and amorphous composition of the two fly ashes was determined using x-ray fluorescence (XRF) and quantitative x-ray diffraction (QXRD). Significant differences in the bulk composition of the two fly ashes bulk compositions were identified with reference to SiO_2 and Fe_2O_3. Gladstone contained significantly higher crystalline content associated with Mullite, and iron oxide filler compounds of Hematite and Magnetite. This lead to lower amorphous content levels compared to the Eraring fly ash. Differences in the amorphous Si/Al values of each fly ash were determined with Gladstone = 3.8 and Eraring = 2.9. This demonstrated that aluminium inclusion could reduce the amorphous Si/Al of geopolymer using Gladstone fly ash, and silica fume inclusion could increase the Si/Al of geopolymers using Eraring fly ash. All done in an effort to target specific Si/Al values through the amorphous framework. Silica fume and sodium aluminate were identified as possible constituents which could be utilised for Si or Al inclusion. Inclusion of high levels of either silica fume or sodium aluminate were identified as detrimental to production and compressive strength.

5. PRELIMINARY PHASE

The aim of the preliminary phase was to investigate the interaction between amorphous H and Si, in the form of the amorphous ratio H/Si. The amorphous H/Si content of a mixture is directly related to the amount of free water incorporated into the mixture. This phase examined the amount of free water required to produce binary geopolymers of sufficient workability; investigate the effect that the inclusion of addition free water (prior and post activation) has on workability and compressive strength; and determine optimum compressive strength values associated with amorphous H/Si. This was undertaken through the production of a full set binary Gladstone fly ash geopolymers.

The results of this experimental phase were compared to the works conducted by Spano et al. (2018), which involved an identical approach using solely Eraring fly ash and Westbuild GGBFS as the main binder stocks. This was undertaken to determine common amorphous H/Si values could lead to similar flow and compressive strength outcomes. Additionally, the outcomes of this phase aided in the prescription of H/Si values associated with subsequent phases.

5.1 Mixture Proportions

As defined within *Section-3.1.1*. binary Gladstone fly ash geopolymers were produced with in this phase, of which the main variable was the amount of free water incorporated prior and post activation. Table 5-1 defines the mixture proportions adopted during this experimental phase.

Table 5-1 – Bulk Mixture Proportions - Preliminary Phase

Mix ID	Bulk Mixture Proportions (g)						
	Sand	FA	GGBFS	SS	SH	Water (Prior to Activation)	Water (Post Activation)
PG1	3000	840.9 (Gladstone)	672.0	392.1	158.2 (6M)	400	-
PG2						450	-
PG3						500	-
PG4						600	-
PG5						400	200
PG6						450	150
PG7						500	100

FA= Fly Ash
GGBFS = Westbuild GGBFS
SS = Sodium Silicate Solution
SH = Sodium Hydroxide Solution

5.2 Observations

5.2.1 Mixing

During the production of the mortar samples the following observation were noted.

- Mixture consistencies varied, with contrasting properties being observed between PG2 and PG4. Figure 5-1, shows the extreme consistencies experience within this phase. PG2 was extremely sticky with stiff clay like properties, whereas PG4 demonstrated liquid-like and watery properties. Aggregate separation was observed with reference to PG4.

Figure 5-1: Contrasting Mortar Consistencies. (Left– PG2, Right PG4)

- The mixtures which incorporated additional free water post activation exhibited similar mortar like consistencies which were workable and soft, without exhibiting liquid-like properties.

5.2.2 Flow and Casting

Upon the completion of mixing, the mortars underwent flow testing to immediately ascertain flow results prior to casting. Figure 5-2, highlights the observed and recorded changes in flow with respect the mixtures P1-P4.

Figure 5-2: Mortar Flows Observed Immediately after Mixing

It was observed that PG1 and PG2 experienced very low flow results. During flow testing the mortar of PG2 was observed to be extremely unworkable, as such difficulty was experienced when placing the mortar into the flow apparatus. This resulted in low flow results and non-uniform flow spread. Placement of PG1 and PG2 into the 50mm specimen cube moulds was possible, however increased mechanical vibration was required to settle the mortar into the moulds and reduce the presence of air voids. The mortar produced with respect to PG3 exhibited mortar like flow characteristics, whilst still being slightly stiffer than the ideal flow value of 110, as stipulated in *ASTM C1437-15* (ASTM 2020-1). This being said, no issues were observed when casting the specimen samples. The extremely liquid state of PG4, which was observed during production, resulted in high flow results were by the required amount of repetitions for the flow testing procedure was limited as the mortar began to overflow the limits of the apparatus.

P5-P7, demonstrated ideal to high flow results , however due to the mortar like mixture consistencies observed upon the completion of mixing, these batches were cast with no implications and in line with the experimental methodology.

5.3 Flow and Compression Results

Table 5-2, defines the average flow results prior to casting, and compressive strength outcomes at 7 and 28 days. The amorphous H/Si ratio for each mixture has been refenced in conjunction with mixture specific elemental ratios for further analysis and discussion.

Table 5-2 – Summary of Flow Results – Preliminary Phase

MIX ID	Flow Prior to Casting (%)	Compressive Strength		Amorphous Elemental Ratios			
		Av. 7 Days (MPa)	Av. 28 Days (MPa)	H/Si	Si/Al	Na/Al	Ca/Si
PG1	40	40.3	57.7	7.70	3.08	0.56	0.49
PG2	50	39.0	49.0	8.20			
PG3	80	44.2	55.4	8.70			
PG4	150	30.3	53.6	9.70			
PG5	120	28.6	44.1				
PG6	110	33.3	47.4				
PG7	140	33.7	49.4				

Refer to APPENDIX H for the full set of experimental data inclusive of the outliers remove through the IQR.

5.4 Analysis

Figure 5-3, demonstrates the recorded flow (%) of each mixture prior to casting with respect to amorphous H/Si.

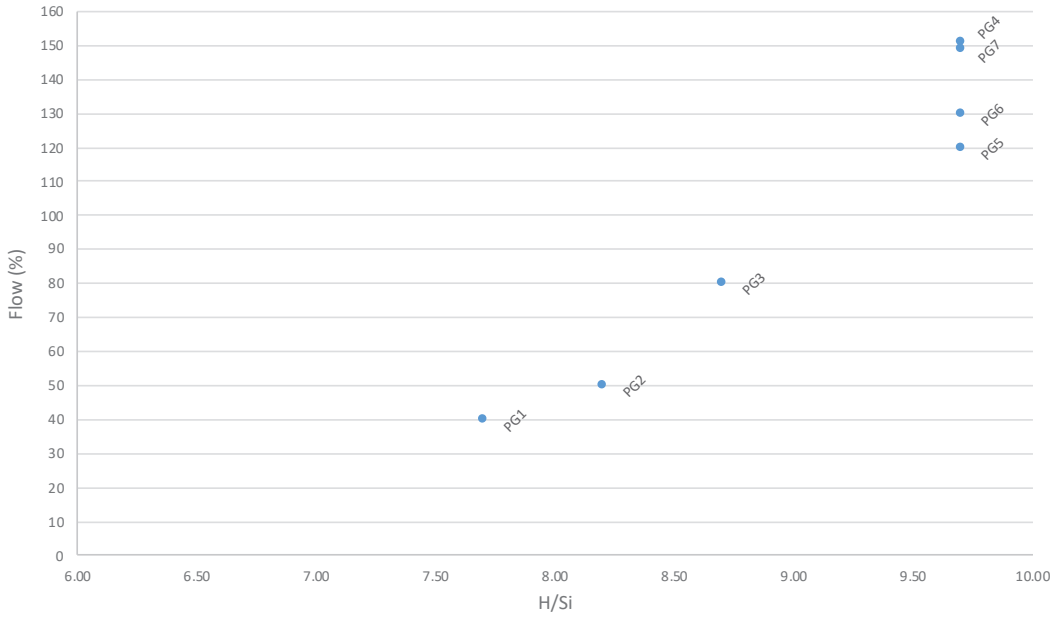

Figure 5-3 - Flow (%) vs Amorphous H/Si

As defined in Figure 5-3, the addition of water pre-activation promotes increased flow during casting. This tread is apparent with mixtures PG1-4, and is demonstrated through a rise in the amorphous H/Si Ratio. Higher levels of H/Si are synonymous with increased levels of free water therefore resulting in higher flowing mortars.

Mixtures PG4-7 all adopted the same H/Si values, however displayed differing flow values. These mixtures contained differing pre and post activation water inclusion values. The mixture which contained highest level of pre-activation water resulted in highest flow (PG4 – 500mL) compared to the mixture with lowest pre activation water and highest post activation water (PG5 – 400mL + 200mL). Although the flow results of these mixtures varied from 120-150%, their flow values were deemed sufficient for casting (>110%) in line with *ASTM C1437-15* (ASTM 2020-1).

Based on Figure 5-3, an H/Si of >9.2 would likely provide sufficient free water (550mL) to obtaining flow values of >110% with respect to the Gladstone fly ash binary geopolymer used within this phase.

Figure 5-4, presents the average 7 and 28 days compressive strengths of each mixture, as well as average strength gain (%) between 7 and 28 days.

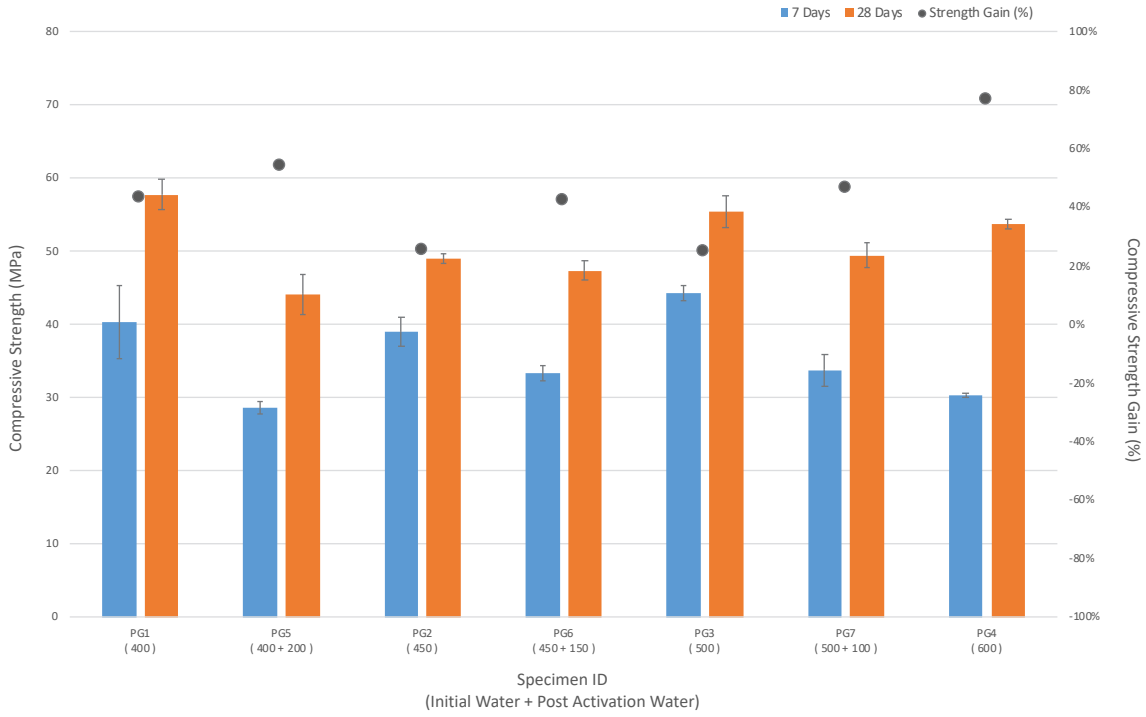

Figure 5-4 – Primary Phase Average 7 & 28 Days Compressive Strength and Strength Gain (%) (Error Bars Signify 95% Confidence Interval)

As demonstrated in Figure 5-4, upper bound compressive strength results of 40 and 43MPa were obtained by PG1 and PG3 at 7 days, compared to lower bound values of 29 and 30 MPa achieved by PG5 and PG4. At 28 days similarly, upper bound results were achieved by PG1 and PG3 with 58MPa and 55MPa and lower bound compressive strengths of 44MPa and 48MPa were achieved by PG5 and PG6.

Although PG4 achieved low compressive strength results at 7 days, at 28 days the mixture specimens achieved >50MPa. This resulted in PG4 achieving a strength gain of >80% between 7 and 28 days. This was the most significant results observed. This was preceded by PG5 with a strength gain of 62%. Inversely, PG3 demonstrated the worst performance in terms of strength gain (%) with 23%.

As observed above, the mixtures which incorporated post activation water (PG5, PG6, PG7) expressed reduced compressive strength results compared to their pre-activation only equivalents (PG1, PG2, PG3). However, these mixtures demonstrated increased strength gain (%) in all case (up to +20%), over the 7 to 28 day period. This resulted in a 3% difference in compressive strength between PG2 and PG6 at 28 days (best performer) and 22% difference between PG1 and PG5 (worst performer).

5.5 Discussion

5.5.1 The Influence of H/Si on Flow

As observed and confirmed through the examination of Figure 5-3 increases to the amorphous H/Si through increased water dosing results in higher flow values, specifically with regards to those mixture only dosed initially with water. Post activation dosing did result in increased flow values whilst amorphous H/Si was observed to be constant. These results were reflective of those observed by Spano et al. (2018) with respect to Eraring based fly ash binary geopolymers.

Figure 5-5 compares the flow and amorphous H/Si values of the Gladstone fly ash binary geopolymer mortars of this research and those obtained by Spano et al. (2018), with respect to Eraring fly ash binary geopolymer mortars of similar amorphous ratios.

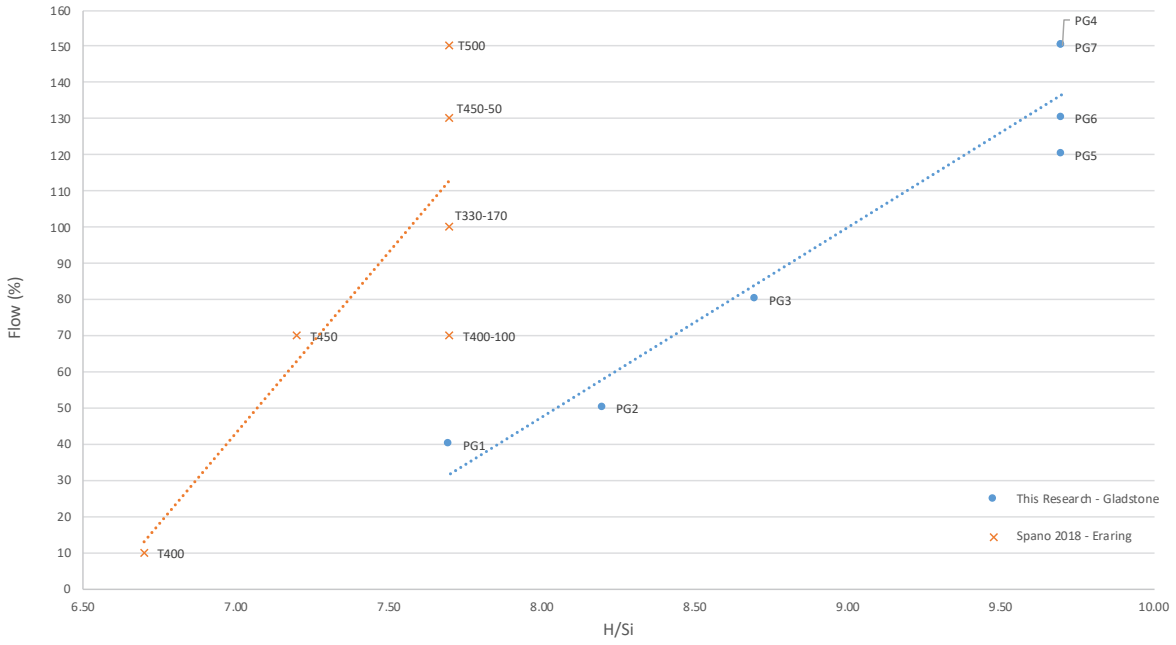

Figure 5-5 - Flow (%) vs H/Si Comparison
Between Gladstone Based Binary Geopolymer Mortars of This Research and Eraring Based Binary Geopolymer Mortars (Spano 2018)

From inspection of Figure 5-5, it can be seen that initially dosed mixtures for the Gladstone (PG1-4) and Eraring (T400,T450,T500) demonstrate increase workability as overall H content increases. This is expected as increase water content promotes workability. Additionally for those mixtures were free water was increased at post activation stage workability also increased (PG5-7 – Gladstone Mixtures and T450-50,T400-100,T330-170 – Eraring Mixtures]. This further supports the notions suggest by Spano et al. (2018),

that initial free water dosing of binary geopolymers provides sufficient water to address aggregate absorption, facilitate mixing and provide a mechanism for ionic transportation. Whereas, post activation dosing attributes to the lubrication of the newly forming geopolymers oligomers, therefore promoting workability, however inhibiting the slowing of geopolymerisation through dilution (Barbosa et al. 2000).

Although the Gladstone mixtures of this research aimed to achieve similar Amorphous Si/Al, Na/Al and Ca/Al; and volumetric measurements of water to those prescribed by Spano (2018) , disparity between the H/Si trends of the Gladstone and Eraring geopolymer mortars was observed. As such as a commonly prescribed optimum H/Si value to achieve sufficient flow for casting could not be prescribed. To achieve mortars flow of >110% targeted amorphous H/Si values of >9.2 and >7.6 for the Gladstone and Eraring binary geopolymer mixture would be necessary. This disparity is primarily attributed to the reduced Si content within the Gladstone samples as outlined with *Section - 4.3*, this results in higher H/Si values in contrast to Eraring mixtures with identical bulk volumetric water contents. This can be seen specifically with respect to T500 and P3 which both adopted a dosing methodology of 500ml of free water pre-activation, with H/Si values of 7.6 and 8.7. Similarly, although both mixture adopted the same dosing quantities, dosing methodology and exhibit similar Si/Al, Na/Al and Ca/Al values, a significant difference in flow values (70%) can be seen in Figure 5-5. The reduced flow values associated with the Gladstone mixture (P3) could be attributed to the observed finer overall PSD recorded and discussed in *Section - 4.5.1*. Generally, finer fly ash materials result in a higher degree of reactivity and increased geopolymerisation due to increased surface area attained by finer materials (Cheah, Part, Mahyuddin 2017). These notions lend themselves to a reduction in flow values. Inversely the higher amorphous content of the Eraring fly ash mixture (T500) of which is believed to attribute to reduced workability (Williams 2010), did not seem to play a observable role in this instance. This may have been due to the dilution of the activating solution through high levels of initial water dosing and the availability of amorphous content encapsulated within the fly ash spheres (Temuujin, Williams, Van Riessen 2009). Disparity between flow values of the mixtures adopting the same dosing methodology with reduced water, such as T450 and P2, did show reduced levels of flow disparity (20%), however the extent and quantification that reactivity and fly ash morphology attribute to flow is difficult to independently quantify (Temuujin, Williams, Van Riessen. 2009).

5.5.2 The Influence of H/Si on Compressive Strength

As outlined in *Section - 5.4*, an optimum compressive strength of 58MPa (PG1) was obtained within this phase of the research using Gladstone binary geopolymer mortars when tested at 28 days. This value was achieved through the utilisation of 400mL of free water incorporated pre-activation with an H/Si of 7.6. The lower bound H/Si value of 7.6 utilised for this mixture also resulted in low flow values of 40%. The low flow values yet high compressive strength achieved by the optimum mixture is believed to be attributed to the high alkalinity present during the dissolution stage, as reduced level of free water available to dilute the alkalinity of the system. As such, accelerated and increased geopolymerisation was facilitated by presences of a larger amount dissociated ions, causing a faster forming and less workable geopolymer mortar. The high compressive strength value reflects a more complete geopolymer matrix. However, low flow values and reduced workability can promote the development of voids which are unable to be removed during the compaction stage of production. With reference to the Eraring binary geopolymer mortars produced by Spano et al. (2018), T400 adopted the same dosing methodology and similar Si/Al, Na/Al and Ca/Al values (H/Si = 6.8) and was found to be approximately 10% stronger (62MPa achieved at 28 days). Overall, the Eraring mixtures which investigated free water dosing and various amorphous H/Si levels conducted by Spano et al. (2018) demonstrated higher compressive strengths compared to the Gladstone mixture of this phase. These higher compressive strength results are believed to be attributed to the increased presence of amorphous silicon and aluminium present in the Eraring fly ash compared to that of the Gladstone (as outlined in Table 4-4). The increased dissolution of both silicon and more specifically the slower leaching aluminium from the fly ash stock attributes to the increased formation of N/C-A-S-H bonds resulting faster gelling and extensive polycondensation, as such fostering high compressive strengths.

Of the Gladstone mixtures examined within this phase, the inclusion of increased levels of free water was observed to impact the compressive strength the mixtures initially dosed with free water and those dosed with additional free water post activation. Figure 5-6 presents the achieved compressive strengths and graphically demonstrates trends associated with the Gladstone mixtures of this phase; specifically in relation to those mixtures which adopted a pre-activation only dosing methodology (PG1-PG4) and those in which free water dosing was conducted pre and post activation (PG5-PG7).

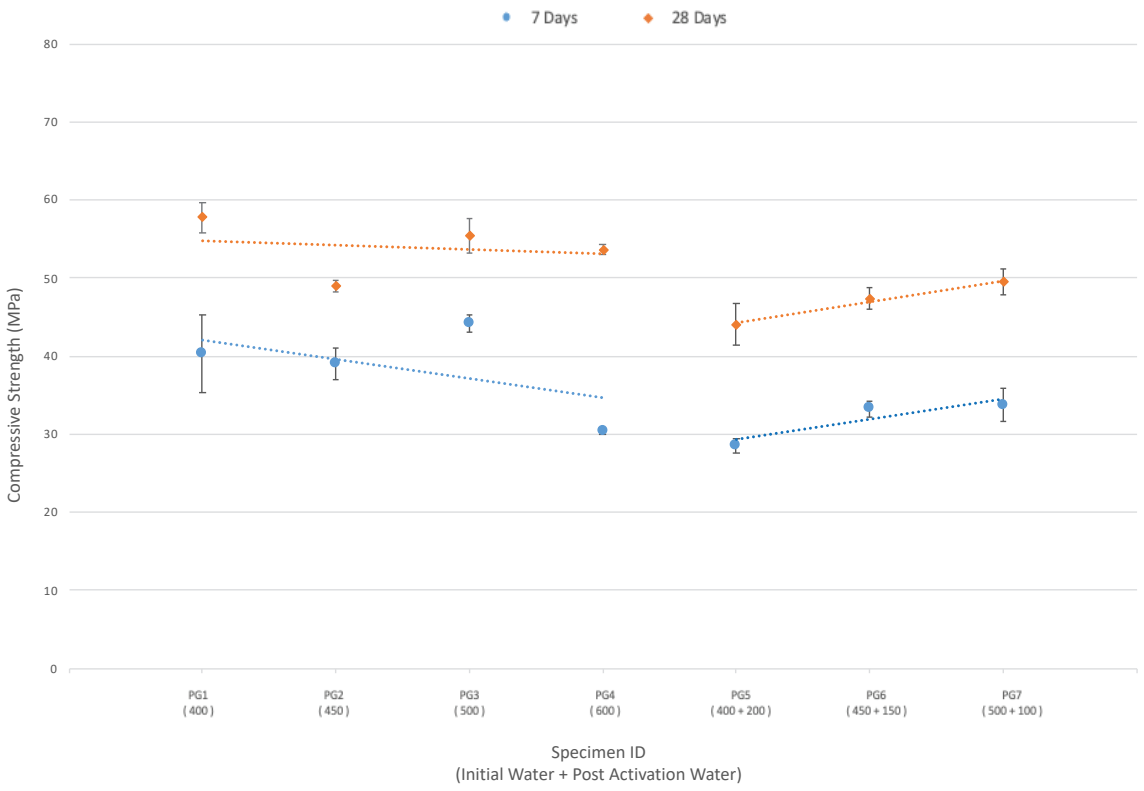

Figure 5-6 - Primary Phase Average 7 & 28 Days Compressive Strength and Graphical Trends (Error Bars Signify 95% Confidence Interval)

As defined in Figure 5-6 general downward trends related to compressive strength at 7 and 28 days were observed for PG1 to PG4. This demonstrates that increased levels of pre-activation free water attributes to reduced compressive strengths. Similarly, those mixtures which incorporated increased levels of post activation demonstrated trends lines associated with a reduction in compressive strength whilst maintain a constant H/Si value. This further reiterates that the amorphous H/Si ratio is reflective of the initial reactive process. These trends can be primarily attributed to the dilution of the alkaline activating solution through increased free water content inhibiting the dissolution process and/or the transportation of newly dissociated ions away from the activation zone. This results in a limited amount of dissociated ions available for coagulation and gelling, which in turn limits the polycondensation and solidification of these oxide gels, producing a less vast 3D silico-aluminate geopolymer structure. Reduction in compressive strength results due to increased water inclusion was observed by Rangan (2008) and Spano et al. (2018). SEM imaging of mixtures PG1 and PG4 (Figure 5-7) was undertaken to observe the difference in the microstructure of mixtures influenced by increased free water content.

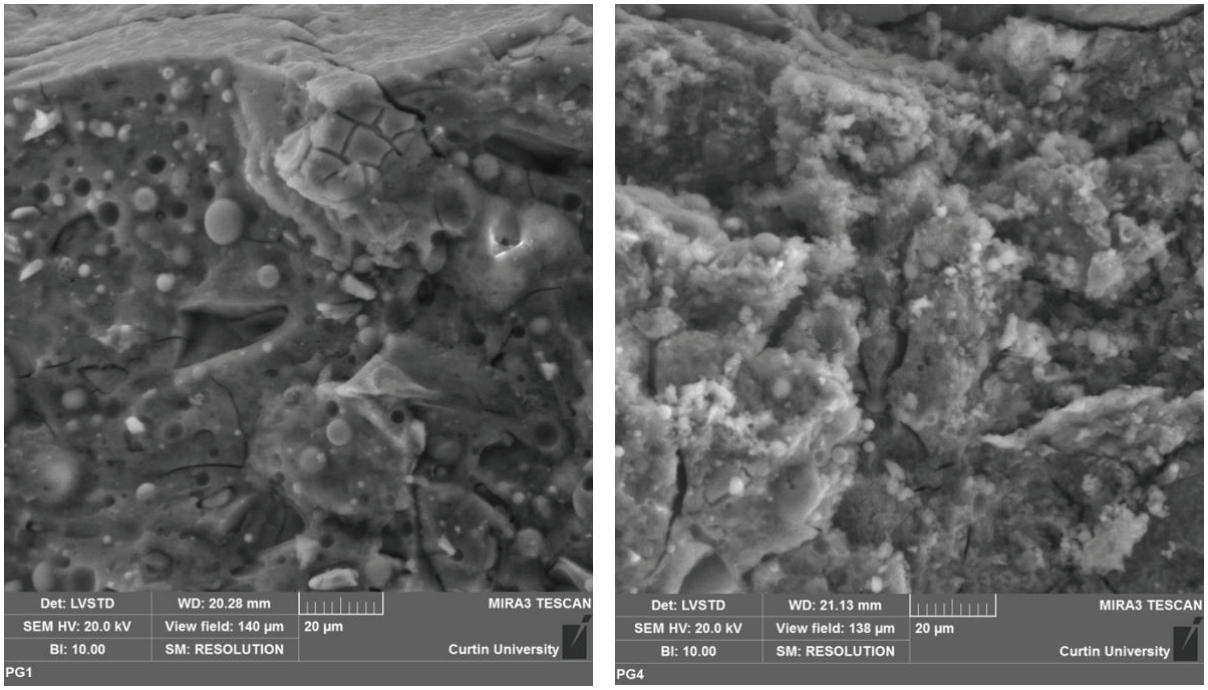

Figure 5-7 – SEM micrographs of PG1 (Left) and PG4 (Right) at 2000x Magnification.

SEM analysis undertaken in Figure 5-7 demonstrates that morphology of PG1 and PG4 differ both in smoothness and completeness. The topography of PG1 is observably smoother demonstrating a more complete and cohesive geopolymer binder. In contrast, the grainy and course topography of the PG4 sample demonstrates incomplete geopolymerisation and reduced dissolution. An increased amount of micro-cracks were observed within the PG4 sample. These observations further reiterate that increased levels of free water content and increased H/Si result in reduced compressive strength due to activator dilution and reduced dissolution.

It should be noted that although whilst excess free water content is detrimental to mechanical properties such as compressive strength, sufficient amounts are not only crucial when considering the hydrolysis of dissolved ions, but also production and casting. As such, the dosing methodology of PG3 (500mL at pre-activation) was deemed superior due to higher flow values (80%) and increased workability. Although an additional 100mL of free water was incorporated into the mixture, in contrast to PG1, PG3 still achieved compressive strength values averaging 52MPa (-3MPa compared to PG3). It is believed that the reduction in compressive strength attributed to activator dilution was supplemented by the improved densification and compaction aided by higher flow values. Free water content and dosing in line with the production of PG3 was prescribed as the minimum benchmark for production of the mixtures of subsequent phases, with considerations associated with achieving sufficient flow for casting taking precedence.

5.6 Phase Conclusions

Free water inclusion and the assessment of amorphous H/Si was undertaken to investigate the effect water had on workability and compressive strength. Free water inclusion is directly related to amorphous H/Si values, however the point at which free water is included within the production process does not have any bearing on the amorphous framework, yet has the potential to influence both flow and compressive strength. Development of Gladstone binary geopolymers and the comparison to Eraring binary geopolymers of previous research served as the platform for the conclusions of this phase.

The influence amorphous H/Si values played on flow results highlighted that increased levels of H/Si (free water) resulted in increased flow values with respect to mixtures dosed prior to activation. However, when amorphous H/Si values were maintained (H/Si = 7.6) and levels of free water increased post activation, flow values also increased. This further supports the notion that targeting amorphous H/Si with respect to flow is reflective of the initial dosing of water.

Disparity in flow between amorphic similar Gladstone geopolymers (PG3) of this phase and Eraring geopolymers (T500) of previous research was believed to attributed to observed differences in the particle sizes (as discussed in *Section - 4.5.1).* The reduced flow values of the Gladstone geopolymers were believed to be attributed to the increased fineness, therefore exhibiting a higher water demand to facilitate, initial aggregate absorption and lubrication of newly formed geopolymer oligomers.

The observed role amorphous H/Si played in compressive strength outcomes was similar to past research. Increased levels of free water and amorphous H/Si of the mixtures dosed pre-activation, resulted in reduced compressive strength outcomes. Increased micro-cracks and a less complete geopolymer binder paste was observed through comparison of PG1 and PG4 via SEM qualitative analysis. The geopolymers which maintained amorphous H/Si values and utilised increased post-activation free water dosing also experienced reductions in compressive strength.

6. SECONDARY PHASE

The focus of the secondary phase was targeted towards investigating the interaction between Na, Si and Al, via the amorphous ratios of Na/Al and Si/Al. Examination of these two amorphous ratios were undertaken through maintaining one while varying the other. Variation of the amorphous Na/Al ratio was undertaken through the prescription of sodium hydroxide concertation (6-12M), whereas variation of the amorphous Si/Al ratio was achieved through the inclusion of sodium aluminate and silica fume. This aimed to address if supplementary constituents such as silica fume and sodium aluminate could address shortfalls in amorphous content within differing fly as stocks.

Within this phase, the mixtures designed and produced were Gladstone fly ash geopolymers, and compared to equivalent Eraring fly ash geopolymer mixtures (Spano 2018). This phase utilised ternary geopolymers due to the inclusion of silica fume and sodium aluminate granules. Compressive strength and flow results were collected to determine optimum values associated with Na/Al and Si/Al, and examined with reference to past research. SEM was undertaken to further examine the cracked surface morphology, orientation of materials, crystalline structure and presence of micro-cracks of the solid geopolymer samples.

Optimum values determined within this phase were utilised for the mixture design associated with the subsequent tertiary phase.

6.1 Mixture Proportions

The mixture proportions adopted within the secondary phase can be seen in Table 6-1. The mixtures which investigated amorphous Na/Al comprised of SG1-SG4 and those which investigated Si/Al comprised of mixtures SG5-SG9. Mixture SE1 represented an comparison Eraring fly ash mixture produced inline with Spano (2018).

Table 6-1 – Bulk Mixture Proportions - Secondary Phase

<table>
<tr><th rowspan="2">Mix ID</th><th colspan="9">Bulk Mixture Proportions (g)</th></tr>
<tr><th>Sand</th><th>FA</th><th>GGBFS</th><th>SS</th><th>SH</th><th>[SH]</th><th>SA</th><th>SF</th><th>Water</th></tr>
<tr><td>SG1</td><td rowspan="10">3000.0</td><td rowspan="4">845.0
(Gladstone)</td><td rowspan="4">678.0</td><td rowspan="4">395.5</td><td>158.2</td><td>6M</td><td rowspan="4">0</td><td rowspan="4">15.0</td><td rowspan="4">550.0</td></tr>
<tr><td>SG2</td><td>158.2</td><td>8M</td></tr>
<tr><td>SG3</td><td>158.2</td><td>10M</td></tr>
<tr><td>SG4</td><td>158.2</td><td>12M</td></tr>
<tr><td>SG5</td><td rowspan="2">845.0
(Gladstone)</td><td rowspan="2">650.0</td><td>372.9</td><td>149.2</td><td rowspan="5">10M</td><td>100</td><td rowspan="3">0</td><td rowspan="2">550+450*</td></tr>
<tr><td>SG6</td><td>384.2</td><td>153.0</td><td>50</td></tr>
<tr><td>SG7</td><td>665.0</td><td rowspan="3">400.0</td><td rowspan="3">160.00</td><td>0</td><td rowspan="3">550.0</td></tr>
<tr><td>SG8</td><td>775.0
(Gladstone)</td><td>725.0</td><td></td><td>75.0</td></tr>
<tr><td>SG9</td><td>700.0
(Gladstone)</td><td>750.0</td><td></td><td>125.0</td></tr>
<tr><td>SE1</td><td>676.0
(Eraring)</td><td>720.0</td><td>429.0</td><td>171.6</td><td>12M</td><td></td><td>75.0</td></tr>
</table>

FA = Fly Ash *GGBFS = Westbuild GGBFS* *SS = Sodium Silicate Solution*
SH = Sodium Hydroxide *SA = Sodium Aluminate* *SF = Silica Fume*

** Additional water required above that defined by the H/Si values of Table 3-2 – Secondary Phase Binder Mix Configurations, as per observations.*

Specifics relating to each mixture design can be found within APPENDIX I.

6.2 Observations

6.2.1 Mixing, Flow & Casting

During the production of the mortar samples the following observations were noted.

- Increased water demand and apparent accelerated setting observed with respect to SG5 and SG6. As demonstrated in Figure 6-1 (Left), each mixture was observed to begin setting and clumping within the mixing bowl approximately 2 minutes after the liquid activation and sodium aluminate inclusion.

Figure 6-1: Observations of SG5 and SG6

(Left: Mortar experiencing rapid setting in Hobart Mixing Bowl, Middle: Mixture consistency after the addition of free water and additional mixing, Right: Flow table observation of mixture with minor clumping.)

Free water was incrementally added until the mortar was observed to be of a castable consistency (Figure 6-1– Middle). Both mixtures required an additional 450ml of water. Upon the completion of mixing, it was observed that clumping had occurred and the mixtures were not entirely homogeneous (Figure 6-1– Right). Flow result for both mixtures exceeded nominal values and casting was undertaken in line with the methodology.

- The flow of SG4, experience accelerated degradation over the cast process. Initial flow results were reflective of a castable mortar (<100%). Whilst casting, the mortar did begin to stiffen. Although still workable enough to facilitate casting and compaction, shortly after the mixture exhibited semi-solid plastic-like properties. This occurred over an approximate 5 minute period after the mixing process ceased. Flow results post-casting were unable to be taken.

6.3 Flow and Compression Results

Table 6-2 outlines the flow and compressive strength results, as well as amorphous ratios of Na/Al and Si/Al of each mixture.

Table 6-2 – Summary of Results – Secondary Phase

MIX ID	Flow (%)	Compressive Strength		Amorphous Elemental Ratios	
		Av. 7 Days (MPa)	Av. 28 Days (MPa)	Si/Al	Na/Al
SG1	90	38.6	53.7	3.15	0.57
SG2	101	36.2	54.9		0.66
SG3	88	33.6	56.4		0.74
SG4	110	31.3	49.8		0.83
SG5	130	3.6	9.6	2.65	0.76
SG6	139	9.7	22.6	2.86	
SG7	90	32.6	52.9	3.10	
SG8	79	32.6	52.7	3.37	
SG9	88	39.5	52.0	3.50	
SE1	70	37.8	59.8	3.01	0.73

Refer to APPENDIX J for the full set of experimental data inclusive of the outliers remove through the IQR.

6.4 Analysis

Figure 6-2 highlights the flow results obtained from the geopolymers produced within this phase.

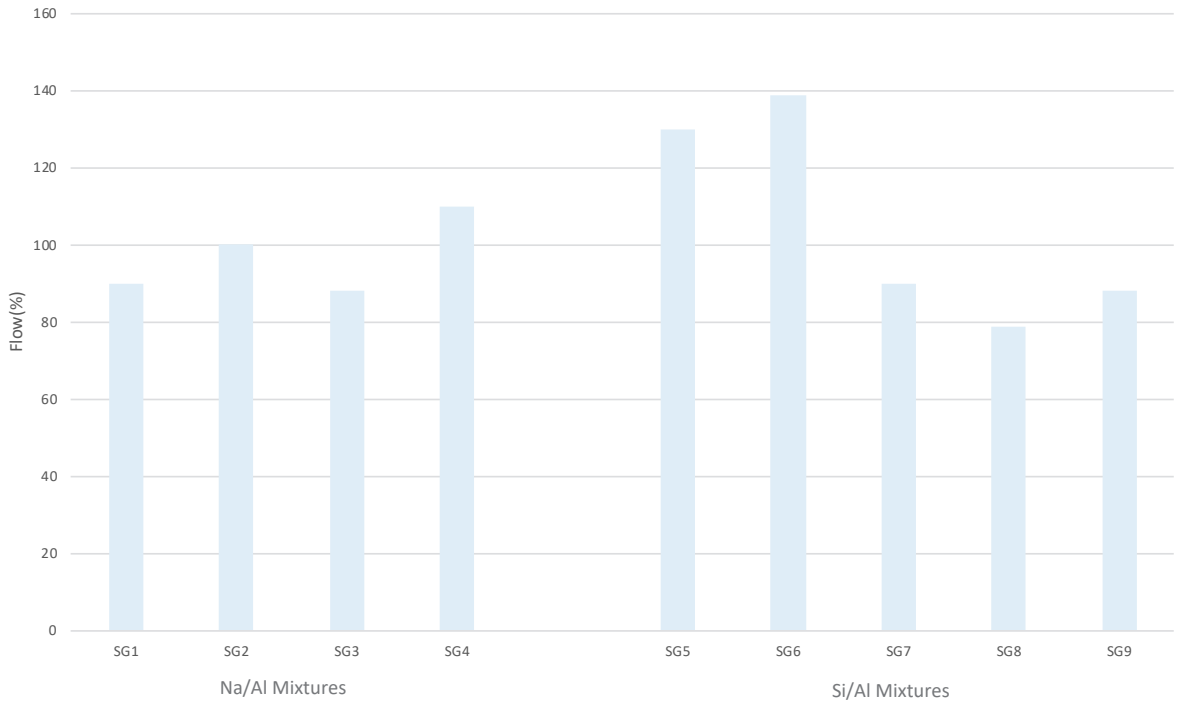

Figure 6-2 - Flow Results of the Secondary Phase Mixtures Prior to Casting

As defined in Figure 6-2, the flow results of the Na/Al mixtures (SG1-SG4) ranged from 90 – 110% when measured prior to casting. Whereas the Si/Al mixtures (SG5-SG9) varied from 80 – 140%. The high flow values of SG5 and SG6 are representative of those mixtures which required additional free water (post activation) during the production process as defined in 6.2.1. This was due to the onset of rapid setting. With the exception of SG5 and SG6, mixture SG4 was the only sample to meet the flow benchmark of 110% deemed appropriate within *ASTM C1437-15* (ASTM 2020-1) for casting cementitious mortars. No distinct correlations were observed with respect to the Na/Al or Si/Al mixtures as defined within Figure 6-2, however mixtures SG3 and SG8 did exhibit the least flow of each group. In contrast , SG4 exhibited the highest flow whilst only being initially dosed with water prior to activation.

Figure 6-3, presents the average compressive strength results of mixtures SG1-SG4 and their respective amorphous Na/Al ratios.

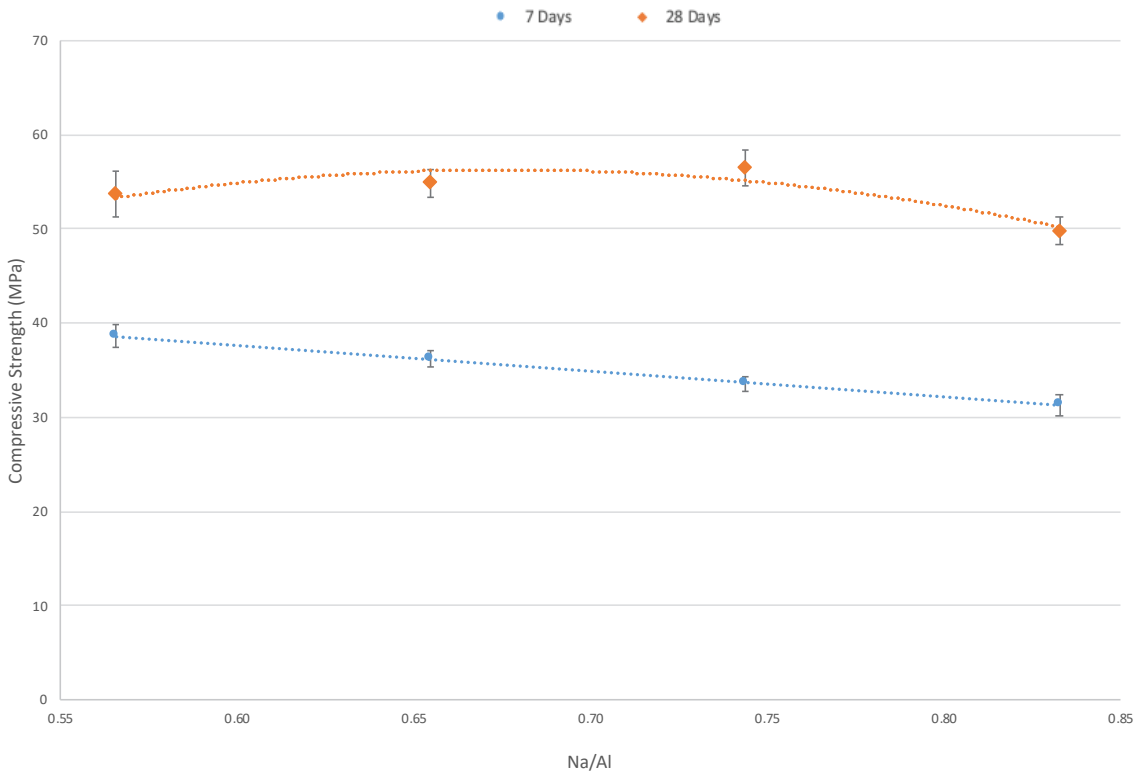

Figure 6-3 - Comparison of Compressive Strength and Amorphous Na/Al (Error Bars Signify 95% Confidence Interval)

As demonstrated in Figure 6-3, trends associated with the compressive strength of the Na/Al mixtures varied at 7 and 28 days. With respect to the 7 days compressive strength results, optimum strength values tended towards Na/Al = 0.57 (SG1). The 28 days results demonstrated optimum strength values of up to 56MPa, at Na/Al of 0.75 (SG3), with optimum values being observed between 0.65 - 0.75. The average spread of compressive strength results within both 7 days and 28 days results were similar, with the 7 days data being larger (7 days : ±3.7Mpa or 11%, 28 days : ±3.3MPa or 6%).

Figure 6-4, presents the average compressive strength results of mixtures SG5-SG9 and their respective amorphous Si/Al ratios.

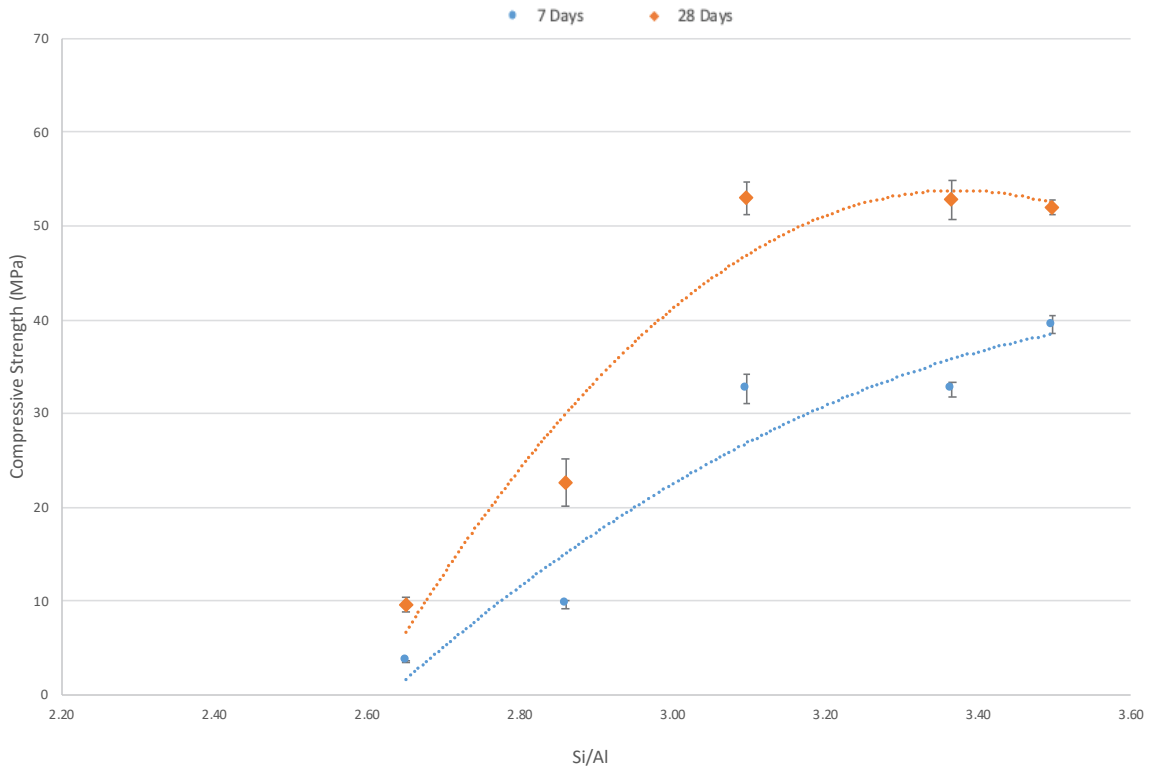

Figure 6-4 - Comparison of Compressive Strength and Amorphous Si/Al (Error Bars Signify 95% Confidence Interval)

As defined in Figure 6-4, amorphous Si/Al values of <3.0 (SG5 and SG6) yielded significantly lower compressive strength values than those which adopted an amorphous Si/Al of 3.1-3.5. These results were reflective of the mixtures which required additional free water during the production process. These mixture were deemed outliers and not considered in the trends associated with the Si/Al mixtures due to the increase water content provided.

Optimum compressive strength values varied between the 7 and 28 days compressive strength results. At 7 days, optimum compressive strength results of 39.5 MPa were obtained by SG9 with an Si/Al of 3.5. At 28 days, SG7 and SG8 achieved comparable optimum compressive strength results of 52.9MPa with Si/Al values of 3.1-3.4. Similarly at 7 days, SG7 and SG8 achieved the same average compressive strength value of 32.6MPa.

6.5 Discussion

6.5.1 Influence of Na/Al on Ternary Geopolymers

Modification and variation of the amorphous Na/Al ratio associated with this phase, was undertaken through the variation of the molar concentration of the primary alkaline activator, sodium hydroxide (NaOH). As defined in 2.4.2.1, alkaline activator concentration plays a pivotal role in the extent of dissolution which is attributed to the completeness and extent of geopolymerisation. General trends of past research defined in 2.4.2.1, highlight that increased molar concentrations of NaOH lead to increased compressive strength in various geopolymers under various curing regimes. Optimum amorphous Na/Al values theorised by Parnham (2016) were stated to be 0.65 – 0.80 when examining the 28 days compressive strength of Eraring binary geopolymers. These values were confirmed by Spano (2018), with an observed optimum of Na/Al = 0.74 achieving 70MPa at 28 days, when examining Eraring ternary geopolymers.

As defined in Figure 6-3, optimum 7 days compressive strengths were achieved at Na/Al of 0.54 utilising 6M NaOH, which tended towards the lower bound values explored in this phase. Similarly, Spano (2018) found that lower levels of Na/Al achieved higher 7 days compressive strengths comparted to higher Na/Al levels, with optimum values of 46MPa being achieved when also targeting Na/Al of 0.54. Rationale of these optimum results being achieved at the lower bound values of amorphous Na/Al is believed to be associated with the formation of early stage C-S-H, which typically favour lower pH levels. High levels of early forming C-S-H are synonymous of alkaline activated slag, due to the primary dissolution of the Ca species. This notion is believed to be reflective of binary and ternary geopolymer which utilise GGBFS as an aluminosilicate feeder stock. Chen and Brouwers (2007) predicted that up to 57.7% of GGBFS alkaline activation consisted of the C-S-H phase, and 12.8% of the slower forming C-A-S-H phase. It is theorised that the presence of both silica fume and GGBFS within the geopolymers of this phase, reacted with the low molar activating solution to produce C-S-H, contributing the higher observed compressive strength at 7 days when targeting at lower Na/Al values. As the Na/Al value was increased and high molar concentrations of alkaline activator were utilised, the pH of the system became further alkaline. As such, increased dissociation of the aluminium species from the fly ash stock and increased presence of Na, provided by the higher molar concentration activators, facilitated the development of slower forming N-A-S-H and C-A-S-H bonds, in lieu of C-S-H. This notion is reflective of alkali-activated slag systems, whereby high pH environments attribute to the increased the uptake of alkalis changing the composition of the initial C-S-H phase (Ye and Aleksandra 2017). Garcia-Lodeiro et al. (2011), found that the stability and extent of N-A-S-H bonds was also heavily dependent on the pH of the system. These slower forming bonds and reduced presence of C-S-H are believed to have attributed to the observed reduction in 7 days compressive strength values as the molar concentration and amorphous Na/Si was increased.

With reference to optimum 28 days compressive strength values, SG3 achieved a maximum average of 56.4Mpa. This was achieved by targeting an amorphous Na/Al of 0.74 whilst utilising an 10M NaOH alkaline activator. These values reflected optimum Na/Al values observed by Spano (2018) of 0.74. However, the equivalent Eraring ternary geopolymer mixture produced by Spano (2018) reached average 28 days compressive strength of 70Mpa whilst experiencing increased setting rates. The optimum values achieved in this phase, specific to Gladstone ternary geopolymers are believed to be attributed to concurrent formation of C-S-H, N-A-S-H and C-A-S-H, although quantification of the extent is difficult to quantify and differentiate. As stated in 2.4.2.1, increased concentrations of NaOH and higher levels of dissolution of slower dissociating Al species are believed to have attributed to the formation of increased geopolymer bonds. The amplified presence of alumina is also believed to attributed to the uptake of Al in C-S-H, further promoting later stage compressive strength. Discrepancies associated with these notions were seen in the reduced 28 days strength of SG4, which targeted an amorphous Na/Al of 0.83, utilising 12M NaOH. As defined in Figure 6-5, qualitative examination of SEM micrographs of SG3 and SG4 demonstrate similar geopolymer surface topography, geopolymer morphology and extent of micro-cracks.

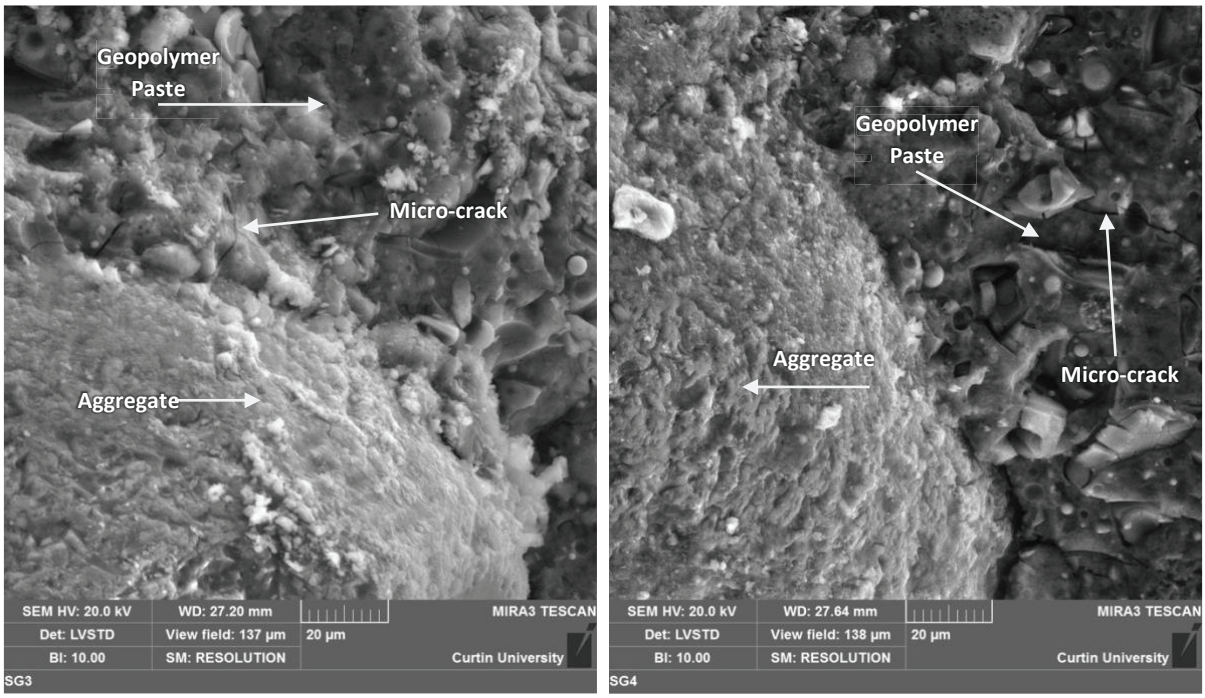

Figure 6-5 - SEM Micrographs of SG3 (Left) and SG4 (Right) at 2000x Magnification

The reduction compressive strength observed with SG4 is believed to be associated with the rapid deterioration of flow and workability during the casting stage as noted in *6.2.1*. This deterioration in flow and accelerated setting is sign of the increased presence of reactive content and the rapid formation of geopolymer bonds, due to the utilisation of high molar concentration activators. Reduced compressive strength results may have been attributed to the lack of free water to facilitate ionic transportation as the dissolution-hydrolysis process draws free water out of the system, and/or, due to limited packing and compaction as the mixture began exhibit sign of hardening during the casting process. Verification the completeness and extent of the geopolymer bonds formed fell outside of the scope of this research. Yet, the optimum values observed and recorded with respect to amorphous Na/Al reflected the general consensus previous research associated with binary and ternary geopolymer adopting Eraring and Gladstone fly ash.

6.5.2 Influence of Si/Al on Ternary Geopolymers

6.5.2.1 Reduction of Amorphous Si/Al Through Sodium Aluminate Inclusion

Both mixtures which received sodium aluminate inclusion (SG5 and SG6) were observed to experience increased water demand and accelerated setting. This notion was previously observed by Spano (2018) when targeting Si/Al ratios of >2.5 using Eraring fly ash and sodium aluminate. It was previously theorised that inclusion of high levels of sodium aluminate reduced workability due to the accelerated development of N/C-A-S-H bonds through supplementation of ionic Al, which is typically dissociated as slow rates through the leaching of the aluminium species within the aluminosilicate materials. This phenomena was similarly observed with respect to both SG5 and SG6 whilst utilising Gladstone fly ash. These observations correlate with the adoption of aluminium oxide accelerators used in concrete production to facilitate the rapid hardening. More specifically, alkaline accelerators such as sodium aluminate have been incorporated into cement system to facilitate accelerated setting and increased water resistance (Kropyvnytska et al. 2019). The inclusion of sodium aluminate in cement systems leads to the rapid formation of calcium hydroaluminate (C-A-H), resulting in reduced resistance to water (Xu, Stark, Finger 2008). However, sodium aluminate inclusion in cement systems leads to an increased water demand of the binder as the amount of the aluminate component increases (Han et al. 2014). This notions were witnessed with respect to the ternary geopolymer mixtures of this research and Spano (2018). It is believed that the rapid setting experience was not only attributed to the accelerate formation of N/C-A-S-H bonds but also the formation of C-A-H. The presence of these hydration reaction bonds are facilitated due to the dissociate calcium ions supplied by the GGBFS stock, synonymous with binary and ternary geopolymers.

Both SG5 and SG6, experience significantly lower compressive strength values, believed to be due to the inclusion of 450ml additional free water. Spano (2018) similarly observed reduced compressive strength values of mixtures which contained high levels of sodium aluminate, due to the inclusion of additional free water (+200mL) to facilitate casting and compaction. A comparison of mixtures utilising similar Si/Al ratios with respect to this research and Spano (2018) can be seen in Table 6-3.

Table 6-3 - Comparison Between Mixtures Targeting Si/Al < 3.0 From This Research and Spano (2018)

MIX ID	Compressive Strength		Sodium Aluminate Inclusion (g)	Si/Al	Additional Free H_2O (mL)	Study
	Av. 7 Days (MPa)	Av. 28 Days (MPa)				
SG5	3.6	9.6	100	2.7	450	This Research
SG6	9.7	22.6	50	2.9	450	
EX5	24.3	49.4	84	2.5	200	Spano (2018)
EX6	43.9	69.5	0	2.8	0	

As shown in Table 6-3, EX6 did not utilise any sodium aluminate and whilst targeting an Si/Al of 2.8, in contrast, SG6 which required 50g of sodium aluminate to target an Si/Al of 2.9. This is prevalent as the Gladstone fly ash of this research was comprised of higher amorphous Si/Al (3.8), compared to Eraring (2.9) as defined in *Section - 4.5* . Therefore when targeting Si/Al values <3.0, whilst maintaining Na/Al value, Al inclusion was required with respect to the Gladstone mixtures. Table 6-3 also highlights that the inclusion of sodium aluminate increased the demand for free water regardless of fly ash stock. This increased demand is reflective of targeting low Si/Al values through sodium aluminate inclusion. The mixtures of this research and Spano (2018) demonstrated a reduction in compression strength due to the increased presence of free water regardless of additional sodium aluminate. Dilution of the primary alkaline activator is believed to be attributed to this reduction in compressive strength as highlighted and discussed in *Section - 5.5*. Qualitative examination of the morphology and topography of SG5 and SG6 was undertaking using SEM micrography shown in Figure 6-6.

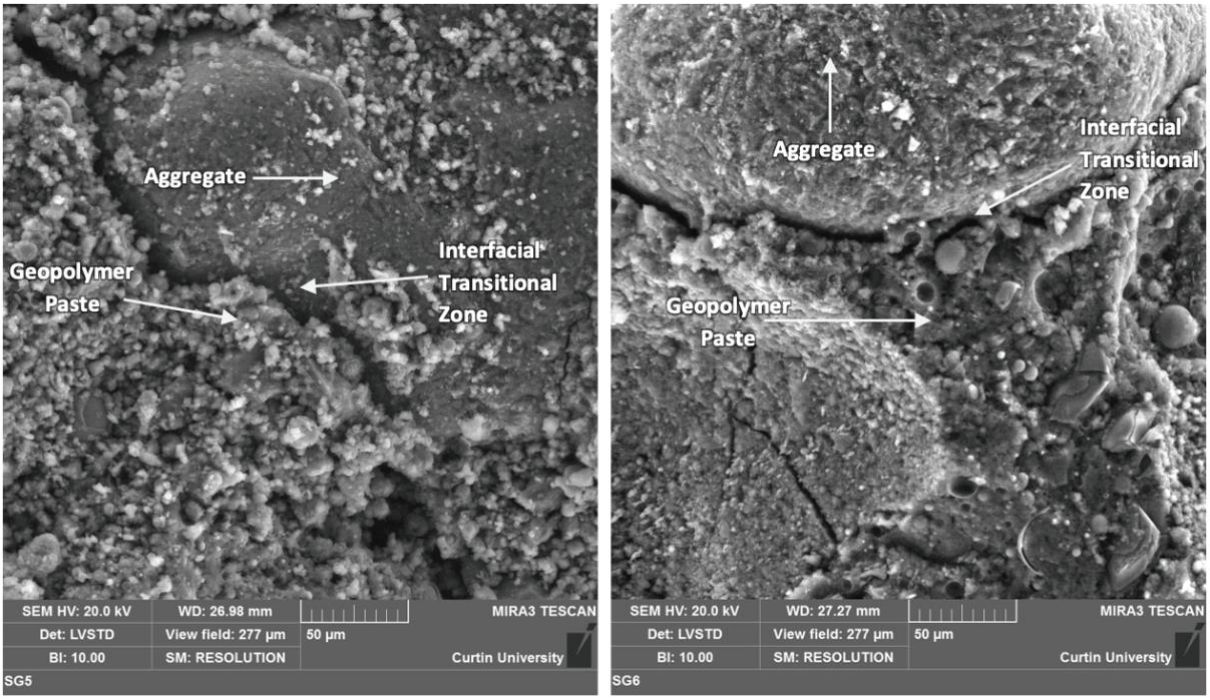

Figure 6-6 - SEM Micrographs of SG5 (Left) and SG6 (Right) at 1000x Magnification

Qualitative analysis of the micrographs in Figure 6-6, demonstrate a highly complex morphology consisting of a combination of unreacted, partially reacted and completely reacted GGBFS and fly ash particles. More apparent is the coarse and grainy surface topography of each geopolymer specimen, which is typically associated with incomplete aluminosilicate dissolution and incomplete geopolymerisation. More specifically attributed to coagulated spheres and particles of unreacted fly ash and GGBFS. This is reflective of the dilution of the primary alkaline activator due to the increased presence of free water added to both SG5 and SG6.

Additionally, qualitative analysis of the interfacial transition zone (ITZ) was undertaken on both samples. In both cement based concretes and self-compacting geopolymer concretes, the ITZ is caused by the disorder of packing of anhydrous cement grains or unreacted fly ash microspheres at the transition between geopolymer paste and aggregate. Typically the ITZ is a region which is highly varied and changes from point to point along the face of each aggregate particle (Nuruddin et al. 2011). Typically, specimens which demonstrate highly discontinuous and narrow ITZ micro-cracks, experience high compressive strength and increased densification. As demonstrated in Figure 6-6, a clear discontinuity between the aggregate and geopolymer paste can been seen in both specimens along the ITZ, with the presence of large forming continuous micro-cracks . Both specimens experienced significant reductions in compressive strength, believed to attributed to the incomplete dissolution of aluminosilicate stock materials leading to the poor formation of geopolymers bonds, incomplete packing at the ITZ and a less dense microstructure. This is prevalent as the ITZ tends to act as “the weak link” between the geopolymer paste and aggregate. The significant size and continuity of micro-cracks along the ITZ of these samples reflect the poor compressive strength outcomes.

6.5.2.2 Increase of Amorphous Si/Al Through Silica Fume Inclusion

As defined in Figure 6-4, optimum 7 days compressive strength results were obtained by SG9 whilst targeting an amorphous Si/Al of 3.5 at 39.55Mpa. This value was a 21% increase on 7 days results recorded for SG7and SG8. The addition of 125g of silica fume reflective of SG9, was theorised have contributed to the compressive strength values achieved. This was believed to be due to the formation of C-S-H, as quickly dissociated silicon and calcium species are heavily present due to the use of silica fume and GGBFS. Interestingly, SG8 which was also provided with 75 g of silica fume to target an amorphous Si/Al of 3.3, did not demonstrate an increase in average compressive strength compared to SG7 (no silica fume inclusion).

Inversely at 28 days, SG9 marginally achieved a lower average compressive strength of 52MPa, compared to SG7 (52.9MPa) and SG8 (52.7MPa). Examination of the 95% confidence interval of each mixture demonstrate that the compressive strengths of all three mixtures are essentially the same. The slight reduction in 28 days compressive strength could be attributed to the limited development of slower forming N-A-S-H bonds due to the reduced availability of Si and H, captured within the formation of early stage C-S-H. Typically the formation of C-S-H is formed during the early stages of activation. Although the formation of both C-S-H and N-A-S-H bonds do occur concurrently (Garcia-Lodeiro et al. 2011), aluminium dissociation limits the formation of additional N-A-S-H bonds. García-Lodeiro, Fernández-Jiménez, and Palomo (2013) found that C-S-H was found to evolve in the presence of aluminium to C-A-S-H with respect to hybrid cements at slower rates during the curing process. The evolution of C-S-H to C-A-S-H is believed to negate the shortfall of N-A-S-H bonds at 28 days.

Additionally the seemingly similar compressive strength of these three mixtures at 28 days, may have been a result of the influence of amorphous H/Si. Although all three mixtures achieve comparable flow results (80-90% flow) and adopted the same free water dosing methodology and quantities, the amorphous H/Si of each mixture varied. These values can be seen in Table 6-4.

Table 6-4 - H/Si, 28 Days Compressive Strength (MPa) and Flow of SG7, SG8 and SG9

MIX ID	H/Si	Av. 28 Days Comp, Strength (MPa)	Flow
SG7	9.0	52.9	90
SG8	8.3	52.7	79
SG9	7.9	52.0	88

As flow values were the primary focus to producing a castable and compactable mixture free water reduction of was not considered; and free water addition was limited due to potential activator dilution. As noted previously, higher amorphous H/Si have been observed to reduce compressive strength. This notion may have resulted in the strength outcomes of SG7 and SG8 to be aligned with SG9.

As defined in *Section - 2.4.1.3*, silica fume inclusion attribute to increasing compressive strength due to mechanisms associated with increased packaging and densification, however over supplementation of silica fume can have negative effects. High levels of silica fume contribute to high Si/Al values. As such it was expected that this would increase the presence of micro-cracking as observed with by Rowles and O'Connor (2003) when examining the morphology of metakaolin geopolymers. Similarly , the utilisation of GGBFS was also thought to exacerbate the potential for micro-cracking. However, this was not the case and can be observed within SEM micrographs presented in Figure 6-7, when examining SG7 (no silica fume) and SG9 (125g silica fume).

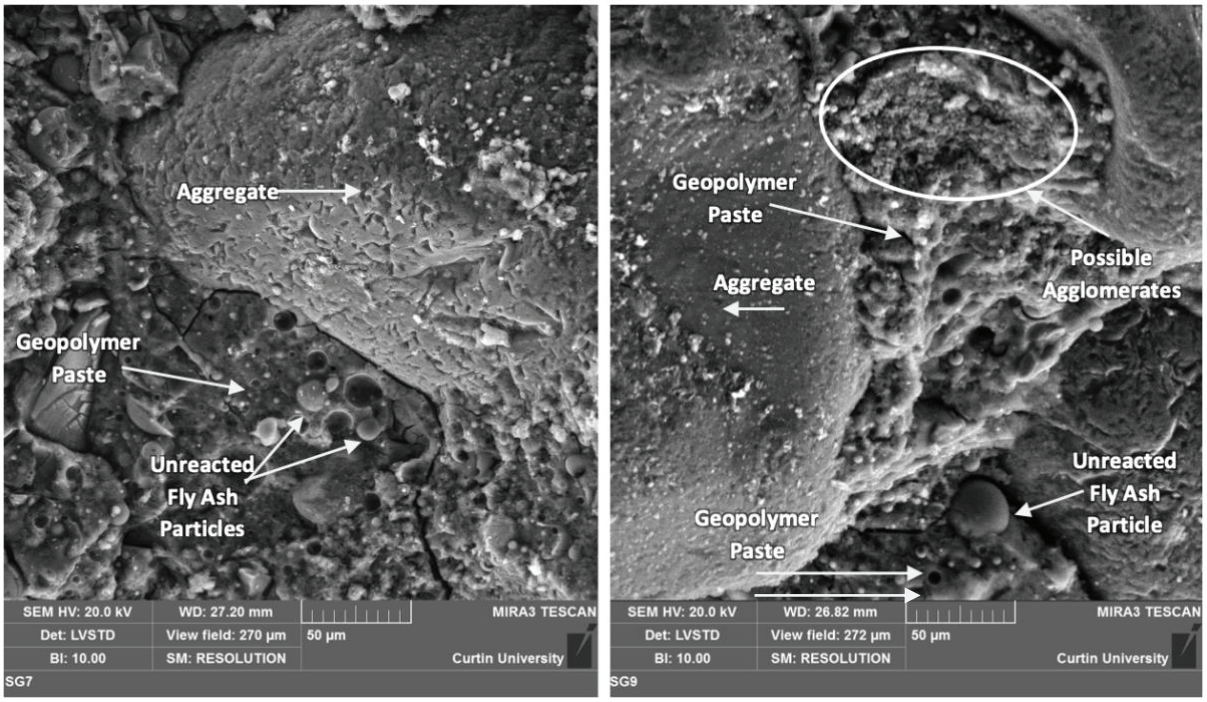

Figure 6-7 - SEM Micrographs of SG7 (Left) and SG9 (Right) at 1000x Magnification

Observations regarding minor levels of silica fume agglomeration have been highlighted in Figure 6-7 and SG9. This is believed to be apparent due to the high levels of silica fume inclusion adopt. Agglomerates are clusters of particles which are responsible for hindering the formation of geopolymer pastes. Khater (2013) found that inclusion of 10% silica fume resulted in the formation of agglomerates which required significantly more mixing energy to disperse than typical production processes. Spano et al. (2020), highlighted that geopolymer production whilst utilising a Hobart mixer does not have sufficient energy to break apart these agglomerate particle clusters. The highlighted fine cluster of particles and course poorly formed geopolymer paste is reflective of the surface topography of geopolymer pastes suffering dilution effects, as observed in *Section - 5.5.2*. Inversely, SG7 demonstrated a dense smooth geopolymer paste, with some signs of incomplete dissolution of larger fly ash spheres. Yet, no obvious signs of agglomeration were present, which was expects as silica fume was not incorporated into the mixture.

From the results highlighted in Table 6-2 optimum compressive strength outcomes referencing Gladstone ternary geopolymers were obtained for amorphous Si/Al values of 3.5 (7 days) and 3.1 - 3.5 (28 days). With respect to Eraring ternary geopolymers, Spano (2018) determined optimum compressive strength outcomes were achieved whilst targeting Si/Al values of 3.5 (7 days) and 2.8 – 3.2 (28 days). Maximum compressive strengths achieved by Spano (2018) reached up to 70Mpa (Si/Al = 3.0), were as those achieved within this phase reached a maximum of 52.9Mpa (Si/Al = 3.1). Disparity between Gladstone ternary geopolymers of this research and Eraring utilising by Spano (2018), can be potentially attributed to notion associated with fly ash fineness and differing amorphous compositions discussed in *Section - 4.5.1* and *4.5.2*. The increased amorphous content present in the Eraring fly ash is believed to attributed to increased geopolymer bonds, hence increased compressive strength compared to that of the Gladstone. Production of SE was undertaken to compare an equivalent Eraring ternary geopolymer produced by Spano (2018) with a Gladstone ternary geopolymer of this phase (SG7). Although each mixture adopted similar amorphous ratios, SE achieved higher compressive strength at both 7 and 28 days. Examination of the surface morphology and smoothness of geopolymer pastes of each of these mixtures (SE and SG7) was undertaken with reference to SEM micrographs presented in Figure 6-8

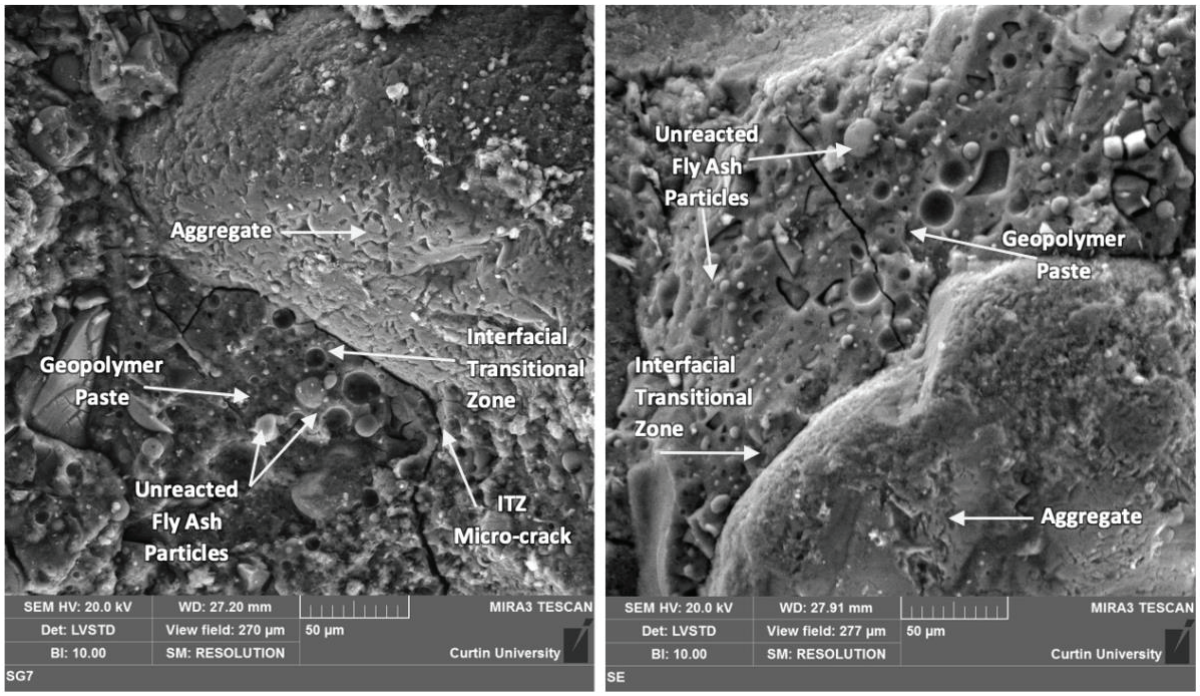

Figure 6-8 - SEM Micrographs of SG7 (Left) and SE1 (Right) at 1000x Magnification

As highlighted in Figure 6-8, both geopolymers produce smooth geopolymer pastes, however the SE sample demonstrates a more dense ITZ with less micro-cracks. However, both sample shown signs of unreacted fly ash particle demonstrating non-complete dissolution of the fly ash stock material. The finer nature of the Gladstone fly ash, although believed to potentially promote dissolution, and facilitate increased densification though packing, was not significant enough to overcome the difference in amorphous composition. This notion is believed to be paired with the high level of iron oxides fillers present in the Gladstone fly ash, which hinders the polymerisation process. Constituent particle fineness and filler effects are not accounted for in the amorphous framework, as such this demonstrates a weakness of the amorphous approach and mathematical framework.

With reference to mixture SE, although produced in an effort to mirror the compressive strength results obtained by Spano (2018), the mixture only achieved a 28 days compressive strength of 59.8 MPa (85% of 2018 equivalent). Although the same fly ash stock materials, amorphous ratios and production and curing methodology was adopted, disparity between previous literature was observed. It is believed environmental factors such as the ambient air temperature during casting may have attributed to such variations. This believed to have occurred as the formation and extent of the geopolymerisation reaction is sensitive to temperature variation. Neither the less, optimum ranges of Si/Al between both Gladstone ternary geopolymer of this research and Spano (2018) did coincide, yet reciprocal compressive strengths were not obtained.

6.6 Phase Conclusions

The focus of this phase was to investigate and report on the interaction between specific amorphous ratios and how they influence compressive strength. Investigation of amorphous Na/Al and Si/Al ratios was undertaken through the production of Gladstone ternary geopolymer mortars, and the comparison of Eraring ternary geopolymer mortars of previous research. Comparison between the two differing fly ash ternary geopolymers was undertaken to examine correlations between optimum Na/Al, Si/Al and compressive strength values. Additionally, an assessment of the suitability of supplementary constituents to be used to address shortfalls in amorphous content within geopolymer production was also undertaken.

With reference to the amorphous Na/Al examining mixtures, optimum 7 days compressive strength values were observed for the Gladstone geopolymers of this phase when targeting Na/Al = 0.54. This was reflective of the results obtained by Spano (2018) with respect to Eraring geopolymers. The higher strengths achieved at lower bound Na/Al values were believed to be attributed to early stage C-S-H, which favours lower PH values, and the limited availability of slowly leaching Al species. 28 days optimum Na/Al values for Gladstone geopolymers also correlated with previous research for Eraring geopolymers at Na/Al = 0.74. This was attributed to the slower forming nature of geopolymer bonds such as N-A-S-H and C-A-S-H.

With reference to amorphous Si/Al investigation, when targeting lower bound values (Si/Al<3.0) through sodium aluminate inclusion, mixtures experienced increase water demand and accelerated setting. This was prevalent with respect to the Gladstone mixtures of this phase and Eraring of previous research. Sodium aluminate was deemed to be alkaline accelerator through the increased rapid formation of N-A-S-H and C-A-S-H geopolymer bonds and/or rapid development of C-A-H. The application of increased water to combat rapid setting resulted in poorly formed geopolymer bonds, predominantly by limited dissolution and increased micro-cracks observed within the ITZ.

Optimum compressive strength values at 7 and 28 days were observed for Si/Al = 3.5 and Si/Al = 3.1 - 3.5. These Si/Al values correlated with those defined by Spano (2018) for Eraring mixtures. Disparity between the optimum compressive strengths achieved between Gladstone and Eraring geopolymer mortars was observed. The Eraring samples of previous research and the reference mixture produced within this phase, obtained higher compressive strength value whilst targeting the same amorphous values. Disparity is believed to be attributed to the differing reactivity and availability of amorphous content of the two fly ash materials, two aspects not captured within the amorphous framework.

7. TERTIARY PHASE

The directive of the tertiary phase was to investigate the compressive strength outcomes of blended geopolymer mortars, which utilised varied bulk ratios of Gladstone and Eraring fly ash. The amorphous ratios of all mixtures within this phase were held constant, with respect to Si/Al, Na/Al, Ca/Al and H/Si. The values of each amorphous ratio was determined via the observations, results and recommendations of the previous phases. The aim of this approach was to determine if an amorphous approach to geopolymer formulation can be used to produce geopolymers of consistent compressive strength, irrespective of the blended content of the fly ash stock material.

Similarly, to the previous experimental phases, flow and compressive strength data were collected during the experimental phase with SEM imaging and analysis being undertaken to further investigate geopolymer surface topography, morphology and specimen macrostructure.

7.1 Mixture Proportions

As outlined in 3.1.4, Gladstone and Eraring fly ash stocks were utilised in the formulation and production of the blended geopolymer specimens of this phase. The bulk mixture proportions within Table 7-1, were defined through the utilisation of the mathematical framework and the bulk ratios of Table 7-2. Variation of the mixture constituents (other than Fly ash) were used to ensure the amorphous ratios of all mixtures were held constant.

Table 7-1 – Bulk Mixture Proportions - Tertiary Phase

Mix ID	Bulk Mixture Proportions (g)								
	Sand	FA (Gladstone)	FA (Eraring)	GGBFS	SS	SH (8M)	SA	SF	Water
TGE1	3005	62.5	562.5	800.0	450.0	180.0	0	75.0	600
TGE2		177.5	532.5	740.0	440.0	170.0		60.0	600
TGE3		375.0	375.0	700.0	410.0	170.0		40.0	550
TGE4		618.7	206.3	675.0	400.0	160.0		20.0	550
TGE5		774.0	86.0	650.0	400.0	150.0		0	500

FA = Fly Ash *GGBFS = Westbuild GGBFS* *SS = Sodium Silicate Solution*
SH = Sodium Hydroxide *SA = Sodium Aluminate* *SF = Silica Fume*

Specifics relating to each mixture design can be found within APPENDIX K.

Table 7-2 – Fly Ash Bulk Percentages

Mix ID	Gladstone Fly Ash %	Eraring Fly Ash %
TGE1	10	90
TGE2	25	75
TGE3	50	50
TGE4	75	25
TGE5	90	10

7.2 Observations

During the production and casting process no significant discrepancies between each mixture were not observed. However, TG1 and TG2 did exhibit a noticeable reduction in flow, compared to the other mixtures (TG3,TG4 and TG5). TG1 and TG2 were observed to be thicker in consistency and did display reduced flow values when tested. Although the flow values observed and recorded for these two mixtures were less than the recommended values stated by *ASTM C1437-15* (ASTM 2013), they were still sufficient to cast and responded well to typical mechanical vibration compaction. No noticeable voids were observed during the production or testing of these two mixtures.

7.3 Flow and Compression Results

Table 7-3 defines the flow and compressive strength outcomes of each mixture within the Tertiary Phase.

Table 7-3 – Summary of Flow Results – Tertiary Phase

MIX ID	Flow (%)	Compressive Strength		Amorphous Elemental Ratios			
		Av. 7 Days (MPa)	Av. 28 Days (MPa)	H/SI	Si/Al	Na/Al	Ca/Si
TGE1	103	32.0	47.1	8.5	3.04	0.61	0.47
TGE2	91	31.2	48.1				
TGE3	131	33.9	49.0				
TGE4	140	31.9	51.2				
TGE5	130	31.5	49.8				

Refer to APPENIX L for the full set of experimental data inclusive of the outliers remove through the IQR.

7.4 Analysis

Figure 7-1 presents the average compressive strength results of the blend geopolymer mixtures of this phase.

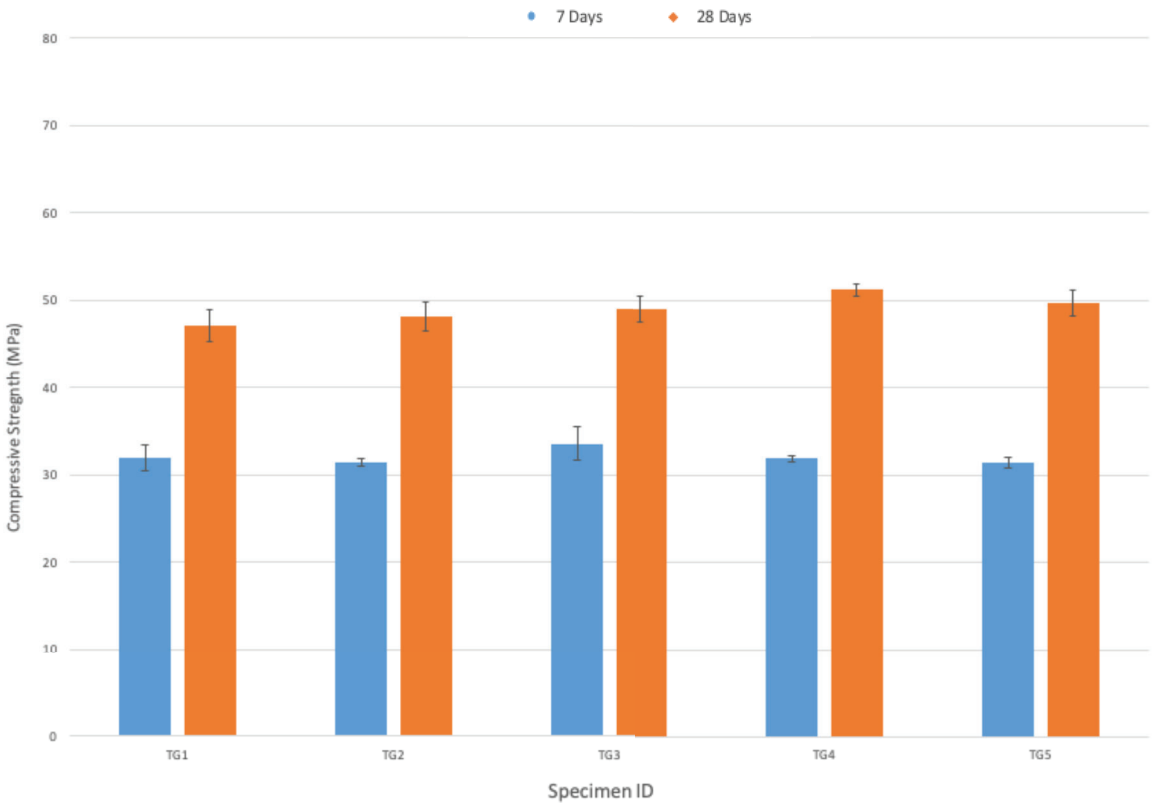

Figure 7-1 - Tertiary Phase Average 7 & 28 Days Compressive Strength
(Error Bars Signify 95% Confidence Interval)

As defined in Figure 7-1, the compressive strengths achieved at both 7 and 28 days of each mixture demonstrated minimal variance between each other. As such, further statistical analysis was undertaken to determine if the average compressive strength of each mixture could be deemed statically similar.

The maximum difference in 7 days compressive strengths values was observed to be 2.7MPa (7.9%) between TGE2 and TGE3. Analysis of Variance (ANOVA) of the 7 days results determined that the difference between the averages of all mixtures was not big enough to be statistically significant. ANOVA returned a p-value of 0.1398, greater than the significance level (α) of 0.05, thus demonstrating 95% confidence in rejecting the possibility of the means being significantly different. This confirms the notion that mixtures essentially achieved the same compressive strength.

With reference to the 28 days compressive strength results defined in Figure 7-1, the maximum difference in results was determined to be 4.2MPa (8.1%) between TGE1 and TGE4. ANOVA of the 28 days results yielded a p-value of $0.0049 < \alpha = 0.05$, therefore demonstrating that some of the mixtures' averages do vary significantly. As such, Tukey's (Honestly Significant Difference) HSD tests was undertaken to examine which mixtures demonstrated significant variance. Tukey's HSD results demonstrated that comparison between TGE1 and TGE4 as well as TGE2 and TGE4, were the only tests which returned p-values of < 0.05 (TGE1-TGE4, $p = 0.003$; TGE2-TGE4, $p = 0.038$). This demonstrated that the difference in the mean 28 days compressive strength of TGE4, with respect to TGE1 and TGE2 was statically significant. Inversely the difference between the means of other mixture pairs was not found to be statically significant.

7.5 Discussion

The aim of this phase was to determine if the amorphous approach and respective mathematical framework could be utilised to produce geopolymer mortars of comparable strength, regardless of the fly ash stock, whilst targeting specific amorphous ratios. This phase aimed to test the hypothesis that specific amorphous ratios can be targeted to achieve specific compressive strengths.

Analysis and testing of the formulated mixtures within this phase yielded compressive strengths of 32.1 ± 1.4 MPa and 49.0 ± 2.1 MPa at 7 and 28 days. Statistical analysis via ANOVA determined that there was no significant difference in compressive strength values of the mixtures at 7 days. Essentially labelling them as similar or the same value. Alternatively, when examining the statistical significance of the results associated with the 28 days results, it was determined that mean compressive strength of the TGE4 specimens did vary significantly. It should be noted that the maximum variance observed at 28 days was limited to 4.2 MPa between TGE4 and TGE1.

From the summarised analysis results, it can be said that there is no distinguishable difference between the compressive strength of the mixtures at 7 days, and little to marginal difference at 28 days. These results support the theory that targeting specific amorphous elemental ratios, through the amorphous framework, could yield consistent compressive strength outcomes.

Although the results observed throughout this phase supported the abovementioned hypotheses; the amorphous framework does not consider other contributing aspects to compressive strength and geopolymerisation. These aspects include fly ash reactivity, dissolution extent and particle fineness, as highlight in *Section - 4.* Although these elements are closely paired with each other, their contribution to the compressive strength of each mixture may differ with respect to each fly ash stock. This may be apparent through increased densification as a result of increased levels of finer less reactive Gladstone fly ash or inversely; increased amorphous content due to high levels of highly amorphous Eraring fly ash. As these mechanisms would be concurrent with respect to the blended geopolymers of this phase, the strength contribution of each is difficult to quantify.

In an effort to further investigate these mechanisms, SEM micrographs of the cured geopolymers of this phase were examined.

Figure 7-2 and Figure 7-3, show the topography of TGE1 and TGE5 to examine the extent of geopolymerisation and dissolution between mixtures which contained high levels of either Gladstone or Eraring fly ash.

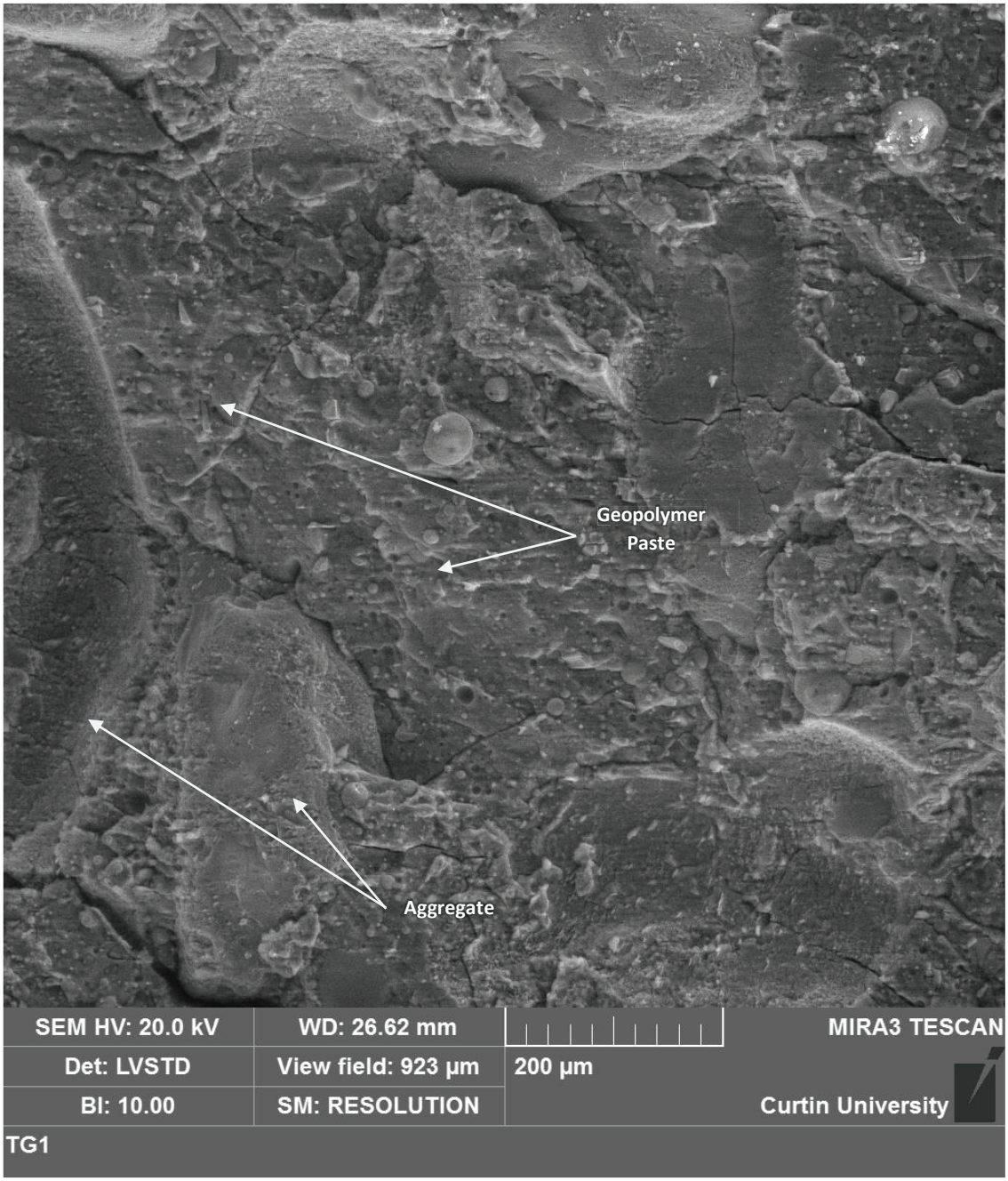

Figure 7-2 - SEM Micrograph of TGE1 at 300x Magnification
(10% Gladstone – 90% Eraring Fly Ash Stock)

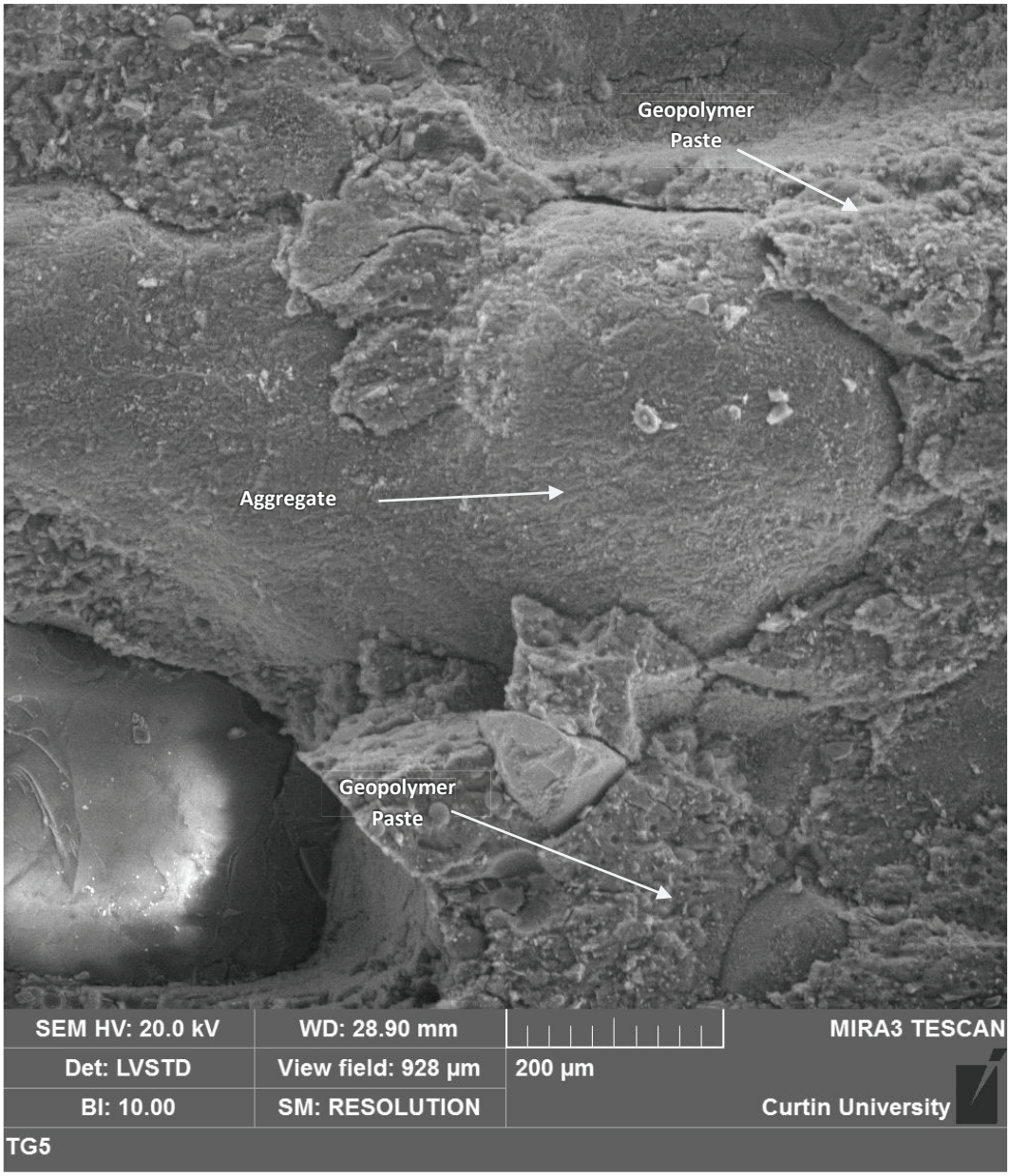

Figure 7-3 - SEM Micrograph of TGE1 at 300x Magnification
(90% Gladstone – 10% Eraring Fly Ash Stock)

The topography of TGE1 shown in Figure 7-2, demonstrates a smoother geopolymer paste compared to TGE5 in Figure 7-3. This observed smoothness is believed to be attributed to mixtures containing higher levels of Eraring fly ash. The increased amorphous content within the Eraring fly ash stock was perceived to produce a more complete geopolymer paste, as typically seen with respect to TGE1 compared to TGE5. The grainy and course nature of the geopolymer paste surface and topography of TGE5 (Figure 7-3), highlights reduced dissolution and less geopolymerisation, potentially due to the reduced amorphous content encapsulated within the Gladstone fly ash stock and increased presence of ferric oxide fillers.

Figure 7-4 and Figure 7-5 further examine TGE1 and TGE5 specifically observing packing, densification and micro-cracking within the Interfacial Transition Zone (ITZ).

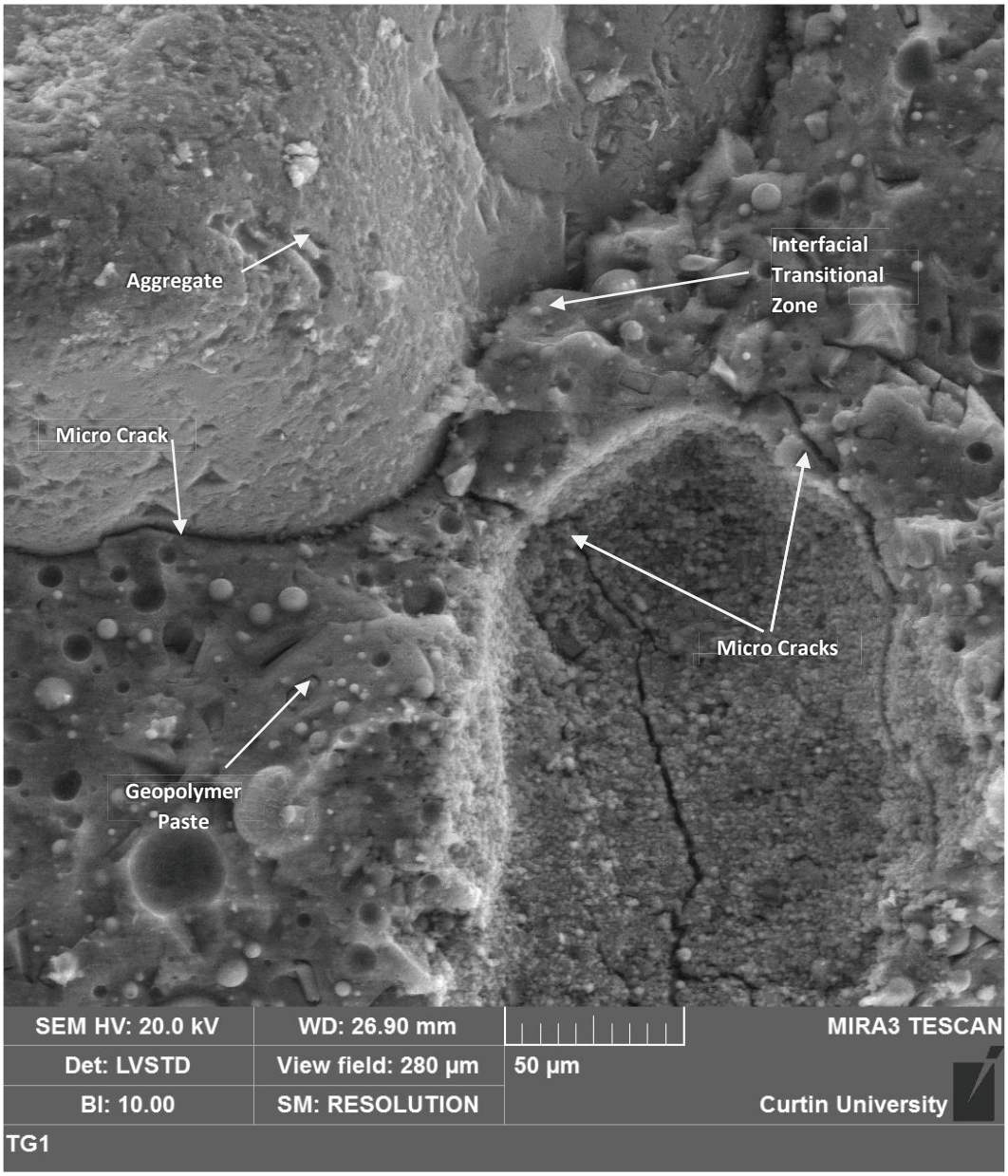

Figure 7-4 - SEM Micrograph of TGE1 at 1000x Magnification
(10% Gladstone – 90% Eraring Fly Ash Stock)

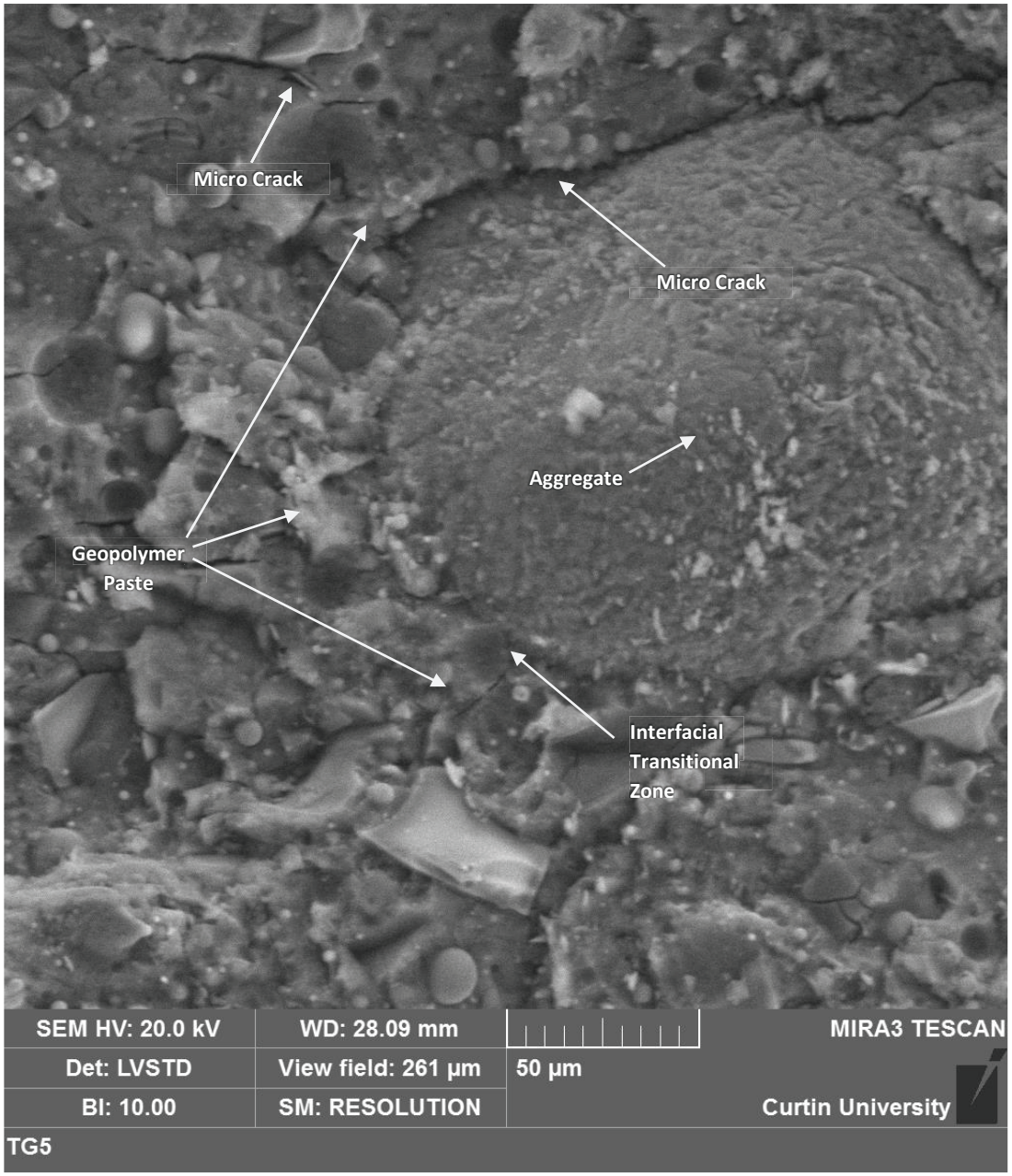

Figure 7-5 - SEM Micrograph of TGE5 at 1000x Magnification
(90% Gladstone – 10% Eraring Fly Ash Stock)

As the ITZ is caused by the disorder of packing of unreacted fly ash microspheres at the transition between geopolymer paste and aggregate, whilst also being deemed the weak link between the two interfaces, it plays an important role in compressive strength. The strength of the ITZ is reflective of extent of micro-cracking and densification of the within the area. As demonstrated in Figure 7-4, the ITZ observed with reference to TGE1 exhibited a continuous micro-crack travelling along the aggregate face and several smaller micro-cracks propagating perpendicular to the ITZ. Inversely, Figure 7-5 and TGE5 demonstrated significantly less micro-cracking and increased discontinuity of micro-cracks along the ITZ. This discontinuity

is believed to be attributed to the higher levels of fine Gladstone fly ash within TGE5 compared to TGE1. The increased fineness of the Gladstone fly ash is believed to result in increased densification and packing of the ITZ, resulting in the reduced presence of micro-cracks and voids. Reduced voids and micro cracking within the ITZ is attributed to higher compressive strengths.

From further qualitative analysis of TGE1 and TGE5 disparity between aspects associated with geopolymer morphology, geopolymerisation and densification were observed, however the extent each of these elements contribute to compressive strength is difficult to ascertain. This is mainly due to the complex bonding mechanisms associated with blended and binary geopolymers, and numerous factors associated with their formation. Overall compressive strength values achieved within this chapter were consistent with minimal variation seen at 28 days. This notion demonstrated that the amorphous framework does have merit in providing a level of consistency when developing and producing geopolymer mortars. Additionally, the framework provides the designer the ability to utilise fly ash blends to design geopolymer mortars. Shortfalls of the frameworks are associated with its inability to consider the effects of fly ash reactivity, fineness and the extent of fillers present in the constituents, specifically fly ash. Williams (2015) paired fly ash reactivity and fineness as these elements were specifically associated with dissolution and the extent of reactive elements available for the geopolymerisation reaction. However, as dissolution is not typically complete, and a significant portion of the reactive content can be locked within the fly ash sphere, quantification of strength contribution is difficult. Additionally, although Chen-Tan (2010) found that ferric oxides act as fillers due to their crystalline nature and extremely slow dissolution rates, there contribution to densification and packing of the macrostructure may be more significant than originally thought, specifically in relation to compressive strength and micro-crack formation.

7.6 Phase Conclusions

Within this phase blended geopolymer mortars were produced using various combinations of Gladstone and Eraring fly ash. This was undertaken to determine if the amorphous framework can be utilised to produce geopolymer mortars of consistent compressive strength, whilst adopt differing and/or blended fly ash stocks. Supplementation of the shortfalls in amorphous content was undertaken inline with the findings of the previous phases to design geopolymer mortar mixtures with the same amorphous mixture ratios.

Statistical analysis determined that there was not any significant difference in the compressive strength of the examined geopolymer mortars at 7 days. Alternatively, statically analysis determined that TG4 was statistically different compared to the other mixtures, by a maximum variance of 4.2 MPa. This difference was deemed marginal. As such, it was deemed that consistent compressive strength were achieved. These results demonstrated that targeting and maintaining specific amorphous ratio could yield consistent compressive strengths, within a limited band of values.

Qualitative disparity was observed between mixtures containing high levels of either type of fly ash via SEM. Mixtures containing higher levels of Eraring fly ash demonstrated smoother surface morphology, typical of geopolymers displaying more complete dissolution and geopolymer bonds. This is believed to be reflective of the higher levels of amorphous content within the Eraring fly ash. Alternatively, those samples containing higher levels of Gladstone fly ash, exhibited less micro-cracks and a more dense ITZ. These observations are believed to be attributed to the finer nature of Gladstone fly ash and higher levels of crystalline iron oxides acting as fillers, therefore promoting increased packing and densification within the ITZ. These notions are not captured within the amorphous framework and are believed to have been “balanced” out through the inclusion of both fly ash materials.

8. CONCLUDING REMARKS

8.1 Conclusions

This thesis was aimed at further developing and understanding the formulation and production of ambient cured geopolymer whilst adopting an amorphous approach. The preparatory phase utilised x-ray techniques to quantify and report the difference in reactive composition of two specific fly ash stocks, as well as served as a platform for the formulation of geopolymer binders for subsequent phases via the amorphous framework. The primary phase investigated the influence amorphous H/Si and water inclusion pre and post activation had on compressive strength and flow. Whereas, the secondary phase investigated the influence amorphous Si/Al and Na/Al had on compressive strength via the implementation of supplementary constituents, such as silica fume and sodium aluminate, as well as variation of activator concentration. Finally, the tertiary phase examined the consistency of geopolymers formulated through the amorphous framework whilst utilising various blend ratios of two fly ash stocks.

In the preparatory phase, it was found that the fly ash stock materials examined varied significantly both mechanically and chemically. The following findings were observed:

- Particle laser sizing analysis found that the Gladstone fly ash of this research was significantly finer that the Eraring fly ash, with d_{50} values of 7.8µm (Gladstone) , and 22.3µm (Eraring) respectively.
- A significant portion of the Gladstone's compositions (40.8%) was locked up within crystalline compounds such as Mullite (aluminium rich compound) and iron oxide compounds. The increase presence of these crystalline compound led to higher levels of inert fillers within the Gladstone fly ash as well as lower levels of available amorphous content. These were believed to have attributed both positively in terms of densifications and packing, as well as negatively in terms of extent of geopolymerisation in subsequent experimental phases.
- The Eraring fly ash contained 77.2wt% amorphous oxide content (specific to Ca, Na, Si, Al) compared to 55.0wt% for Gladstone. This lead to the notion that the Eraring fly ash was more reactive than the Gladstone. Differences in the amorphous Si/Al values of each fly ash were determined with Gladstone = 3.8 and Eraring = 2.9, with Gladstone's higher value attributed to the unavailability of aluminium locked within crystalline mullite.

- Disparity in amorphous Si/Al highlighted that via the amorphous mathematical framework , Si and Al inclusion could be undertaken to target specific Si/Al values from a mixture design perspective.
- Disparity in the mechanical and chemical properties of each fly ash identified with phase highlighted potential influences to compressive strength outcomes observed in the subsequent phases.

In the primary phase, the following findings and conclusions were made:

- Free water inclusion was directly related to amorphous H/Si values and the amorphous framework, however the point at which dosing occurs within the production process has the potential to affect both compressive strength and flow.
- Higher levels of amorphous H/Si yielded increased flow due to the increased presence of free water to lubricated the system.
- Some disparity was observed between the Gladstone mixtures of this phase and the Eraring mixtures of previous works in terms of targeting specific H/Si values to achieve a sufficient level of flow. This was attributed to disparities in fly ash fineness and reactivity, not captured in the amorphous framework.
- Increased flow levels were also observed when H/Si was held constant and levels of free water increased post activation. This further supported the notion that when targeting amorphous H/Si in an effort to control flow values, it should be directed towards pre-activation dosing levels.
- The role amorphous H/Si played mirrored trends of previous work in relation to compressive strength. Increased levels of H/Si resulted in reduced compressive strength, believed to be attributed to dilution of the alkalinity of the system and reduced dissolution of the aluminosilicate materials. This was reflective of the mixtures dosed pre and post activation.
- Disparity in optimum H/Si values were observed between the Gladstone mixtures of this phase and the Eraring mixtures of previous works, believed to be attributed to fly ash reactivity.
- It was identified the commonly prescribed amorphous H/Si values to achieve specific compressive strength and flow values could not be adopted with respect to binary geopolymers of differing fly ash stocks, and that additional factors associated with fineness and reactivity play a concurrent role. These factors are not currently addressed in the amorphous framework.

In the secondary phase, the following findings and conclusions were made:

- Targeting specific amorphous values related to Na/Al and Si/Al could lead to optimum compressive strength at both 7 and 28 days.
- When referencing amorphous Na/Al, optimum compressive strength values at 7 and 28 days were achieved for Na/Al values of 0.54 and 0.74. The values obtained whilst examining Gladstone

ternary geopolymers within this research correlated to those reported in previous works pertaining to Eraring ternary geopolymers.

- With reference to amorphous Si/Al, optimum compressive strength values were achieved at 7 and 28 days, for Si/Al values of 3.5 and 3.1-3.5. These correlated with previous Eraring based works.
- Although matching optimum amorphous Na/Al and Si/Al values were observed with respect to both Gladstone and Eraring fly ash ternary geopolymers, some disparity in optimum compressive strength results were observed. The Eraring samples obtained higher compressive strength values whilst targeting the same amorphous values. This disparity is believed to be attributed to the differing reactivity and availability of amorphous content of the two fly ash materials.
- Through the investigation of Si and Al inclusion, targeting lower bound amorphous Si/Al values (<3.0) through sodium aluminate integration was deemed impracticable as it lead to increased water demand and accelerated/flash setting. Flash setting mitigation through increased water inclusion resulted in a significant reduction in compressive strength. This further supported the notion of sodium aluminate acting as an alkaline accelerator and increased water values (H/Si) diluting the dissolution process.

The tertiary phase utilised the amorphous finding and methodologies of the subsequent phases to develop blended geopolymer mortars which combined various quantities of both Eraring and Gladstone fly ashes, in an effort to test the robustness and consistency of compressive strength outcomes via utilisation of the amorphous framework. As such the following findings and conclusions were made:

- It was determined that at 7 days the compressive strength values of all 5 mixtures were comparable and statically equal. Similarly at 28 days the compressive strength of 4 mixtures were deemed equal, however one blended fly ash was deemed statistically different. The maximum variance observed between this mixture and the lower bound values was 4.2MPa (8%) and deemed marginal as the compressive strengths of the mixtures at 28 days range from 47.1 to 51.2 MPa.
- Although statistically equal, quantitative disparity was observed between mixtures containing high levels of either fly ash. The disparities observed were related to geopolymer morphology and paste formation, as well as densification and the formation of micro-cracks within the ITZ. It was concluded that the complimentary notions associated with the Gladstone's fineness and increased packing; and Eraring's higher levels of amorphous content leading to increased geopolymer bonds, balanced out through the various blend configurations.
- It is hypothsised that targeting specific amorphous ratios can lead to consisted compressive strength values. However, concurrent mechanisms associated with particle size effects, packing and densification, fly ash reactivity and amorphous content play a pivot role in strength outcomes although they are not currently considered in the amorphous framework.

8.2 Future Work

The following recommendations and future work items are believed to further develop the amorphous framework and mixture design approach with respect to ambient cured geopolymer mortars.

Further investigation and reporting on the interaction between elemental ratios, associated with calcium (Ca), sodium (Na), hydrogen (H) and aluminium (Al), whilst utilising fly ashes not referenced in this research. The fly ashes utilised within this research and past research by Spano (2018) focused mainly on Eraring and Gladstone fly ash stocks. Investigation of optimum amorphous ratios whilst utilising alternative fly ash stocks will aid in the development of the amorphous approach beyond the scope of this research project.

Exploration of fly ash reactivity and the extent in which amorphous content is leached from the fly ash stock during dissolution. Establishment of the extent of dissolution and the extent of geopolymerisation due to available amorphous content, could assist in further developing the amorphous framework to consider fly ash reactivity. Fly ash reactivity is believed to influence the extent of geopolymerisation as much of the amorphous content can be locked within the fly ash spheres, therefore being inaccessible dissolution process.

Examine whether or not fly ash fineness/particle size is a significant factor in the formation of geopolymer bonds or densification of geopolymer matrix through packing effects. One of the shortfalls of the amorphous framework is that constituent mechanical properties, such as particle size and fineness are not considered in the formulation of mixture designs. Future work could mill, grind of sieve differing fly ashes to a consistent range of particles sizes and ascertain the influence particles sizes play on dissolution rates, workability, packing and mechanical properties such as compressive strength.

Further assessment of blended fly ash geopolymer mortars and the consistency of compressive strength outcomes whilst targeting specific amorphous ratios. Detailed analysis of blended geopolymers mortars which utilise differing fly ash stocks, outside of Gladstone and Eraring could aid in assessing the robustness of the amorphous framework and mixture design process.

9. REFERENCES

ACI-Committee 116R-00. 2000. "Cement and Concrete Terminology." American Concrete Institute.

ACI-Committee 232. 2018. " ACI PRC-232.2-18: Report on the Use of Fly Ash in Concrete" American Concrete Institute.

Andrew, R. M. 2018: Global CO2 emissions from cement production, Earth Syst. Sci. Data, 10, 195–217, https://doi.org/10.5194/essd-10-195-2018.

ASTM. 2017. " C330/C330M-17a, Standard specification for Lightweight Aggregates for structural concrete." 2017. ASTM International: West Conshohocken, PA.

ASTM. 2019-1. "C192/C192M-19 Standard Practice for Making and Curing Concrete Test Specimens in the Laboratory." 2019. ASTM International: West Conshohocken, PA.

ASTM. 2019-2. "C270-19a, Standard Specification for Mortar for Unit Masonry." 2019. ASTM International: West Conshohocken, PA.

ASTM. 2019-3. "C618-19, Standard Specification for Coal Fly Ash and Raw or Calcined Natural Pozzolan for Use in Concrete." 2019. ASTM International, West Conshohocken, PA.

ASTM. 2020-1. "C1437-20, Standard Test Method for Flow of Hydraulic Cement Mortar." 2020 ASTM International: West Conshohocken, PA.

ASTM. 2020-2. "C109/C109M-20b, Standard test method for compressive strength of hydraulic cement mortars (Using 2-in. or [50-mm] cube specimens)." 2020. ASTM International: West Conshohocken, PA.

Bakharev, T. 2005. "Resistance of geopolymer materials to acid attack." Cement and Concrete Research 35 (4):658-670. doi: https://doi.org/10.1016/j.cemconres.2004.06.005.

Barbosa, Valeria F. F., Kenneth J. D. MacKenzie, and Clelio Thaumaturgo. 2000. "Synthesis and characterisation of materials based on inorganic polymers of alumina and silica: sodium polysialate polymers." International Journal of Inorganic Materials 2 (4):309-317. doi: https://doi.org/10.1016/S1466-6049(00)00041-6.

Bouzoubaa, N, and M Lachemi. 2001. "Self-compacting concrete incorporating high volumes of class F fly ash: Preliminary results." Cement and concrete research 31 (3):413-420.

Brough, A. R., and A. Atkinson. 2002. "Sodium silicate-based, alkali-activated slag mortars: Part I. Strength, hydration and microstructure." Cement and Concrete Research 32 (6):865-879. doi: https://doi.org/10.1016/S0008-8846(02)00717-2.

Cheah Chee Ban, Part Wei Ken, Mahyuddin Ramli. 2017. "Mechanical and Durability Performance of Novel Self-activating Geopolymer Mortars." Procedia Engineering,Volume 171:564-571.doi:https://doi.org/10.1016/j.proeng.2017.01.374.

Chee Keong Lau, Matthew R. Rowles, Glenn N. Parnham, Trevor Htut, Tian Sing Ng. 2019. " Investigation of geopolymers containing fly ash and ground-granulated blast-furnace slag blended by amorphous ratios". Construction and Building Materials Vol. 222:731-737. doi: https://doi.org/10.1016/j.conbuildmat.2019.06.198.

Chee Keong Lau, Trevor Htut, Geoff Thompson, Matthew R. Rowles, Tian Sing Ng. 2020. " The Characteristics of Amorphous Composition of Alkali Activated Ground Granulated Blast Furnace Slag Mortar Mix Design." "Under Submission-In Review"

Chen, Wei, and HJH Brouwers. 2007. "The hydration of slag, part 1: reaction models for alkali-activated slag." Journal of materials science 42 (2):428-443.

Chen-Tan, Nigel. 2010. "Geopolymer from a Western Australian Fly Ash." Doctor of Philosophy, Department of Imaging and Applied Science, Curtin Unviersity of Technology.

Chindaprasirt, P, T Chareerat, and Vute Sirivivatnanon. 2007. "Workability and strength of coarse high calcium fly ash geopolymer." Cement and concrete composites 29 (3):224-229.

Coelho, Alan. 2018. "TOPAS and TOPAS-Academic: an optimization program integrating computer algebra and crystallographic objects written in C++." Journal of Applied Crystallography 51 (1):210-218. doi: doi:10.1107/S1600576718000183.

Davidovits, J. 1976. "Solid phase synthesis of a mineral blockpolymer by low temperature polycondensation of aluminosilicate polymers." IUPAC International Symposium on Macromolecules, Stockholm.

Davidovits, J. 1991. "Geopolymers." Journal of thermal analysis 37 (8):1633-1656. doi: 10.1007/bf01912193.

Davidovits, Joseph. 2002. "30 Years of Successes and Failures in Geopolymer Applications. Market Trends and Potential Breakthroughs." Proceedings of 2002 Geopolymer Conference. Melbourne. Australia.

Davidovits, J., 2020. Geopolymer Chemistry And Applications. 5th ed. Saint-Quentin, France: Institut Géopolymère.

Deb, Partha Sarathi, Pradip Nath, and Prabir Kumar Sarker. 2014. "The effects of ground granulated blast-furnace slag blending with fly ash and activator content on the workability and strength properties of geopolymer concrete cured at ambient temperature." Materials & Design (1980-2015) 62:32-39.

Diamond, Sidney, and Sadananda Sahu. 2006. "Densified silica fume: particle sizes and dispersion in concrete." Materials and Structures 39 (9):849-859.

Dutta, Debabrata, Suresh Thokchom, Partha Ghosh, and Somnath Ghosh. 2010. "Effect of silica fume additions on porosity of fly ash geopolymers." J. Eng. Appl. Sci 5 (10):74-79.

Duxon, P., A. Fernandez-Jiminez, J.L. Provis, G.C. Luckey, A. Palomo, and Van Deventure. 2007. "Geopolymer Technology." Geopolymer Technology: The Current State of The Art (4):2917-2933.

Duxson, Peter, John L. Provis, Grant C. Lukey, and Jannie S. J. van Deventer. 2007. "The role of inorganic polymer technology in the development of 'green concrete'." Cement and Concrete Research 37 (12):1590-1597. doi: https://doi.org/10.1016/j.cemconres.2007.08.018.

Favier, A., Scrivener, K. and Habert, G., 2019. Decarbonizing the cement and concrete sector: integration of the full value chain to reach net zero emissions in Europe. IOP Conference Series: Earth and Environmental Science, 225, p.012009.

Garcia-Lodeiro, I, A Palomo, A Fernández-Jiménez, and DE Macphee. 2011. "Compatibility studies between NASH and CASH gels. Study in the ternary diagram Na2O–CaO–Al2O3–SiO2–H2O." Cement and Concrete Research 41 (9):923-931.

García-Lodeiro, I., A. Fernández-Jiménez, and A. Palomo. 2013. "Variation in hybrid cements over time. Alkaline activation of fly ash–portland cement blends." Cement and Concrete Research 52:112-122. doi: https://doi.org/10.1016/j.cemconres.2013.03.022.

Garcia-Lodeiro, I.; Palomo, A. & Fernández-Jiménez, A. 2015. "An overview of the chemistry of alkali-activated cement-based binders". Handbook of Alkali-Activated Cements, Mortars and Concretes: 19-47. Elsevier. doi:10.1533/9781782422884.1.19.

Gardner, Laura J., Susan A. Bernal, Samuel A. Walling, Claire L. Corkhill, John L. Provis, and Neil C. Hyatt. 2015. "Characterisation of magnesium potassium phosphate cements blended with fly ash and ground granulated blast furnace slag." Cement and Concrete Research 74:78-87. doi: https://doi.org/10.1016/j.cemconres.2015.01.015.

Grubb, Michael, Christiaan Vrolijk, and Duncan Brack. 1997. The Kyoto Protocol: a guide and assessment: Royal Institute of International Affairs Energy and Environmental Programme.

Han J, Wang K, Shi J and Wang Y. 2014. "Influence of sodium aluminate on cement hydration and concrete properties." Constuction and Building Materials (64) 342-349.doi:https://doi.org/ 10.1016/j.conbuildmat.2014.04.089

Hanjitsuwan, Sakonwan, Sitchai Hunpratub, Prasit Thongbai, Santi Maensiri, Vanchai Sata, and Prinya Chindaprasirt. 2014. "Effects of NaOH concentrations on physical and electrical properties of high calcium fly ash geopolymer paste." Cement and Concrete Composites 45:9-14. doi: https://doi.org/10.1016/j.cemconcomp.2013.09.012.

Hardjito, D. 2004. "ACI Materials." Journal:467-472.

Hardjito, D., and S. S. Fung. 2010. "Fly ash-based geopolymer mortar incorporating bottom ash." Mod Appl Sci 4 (1):44-52.

Hardjito, Djwantoro, and B Vijaya Rangan. 2005. "Development and properties of low-calcium fly ash-based geopolymer concrete."

Hill, RJ, and CJ Howard. 1987. "Quantitative phase analysis from neutron powder diffraction data using the Rietveld method." Journal of Applied Crystallography 20 (6):467-474.

Hela, R, and D. Orsáková. 2013. " The Mechanical Activation of Fly Ash" Prcedia Engineering (65):87-93. doi: https://doi.org/10.1016/j.proeng.2013.09.016.

Heo JH, Park JS and Kim H. 2019. "Effect of Sodium Aluminate on Compressive Strength of Geopolymer at Elevated Temperatures." International Journal of Architectural, Civil and Construction Sciences: 12.0 (9): 618-624. doi: https://doi.org/ 10.5281/zenodo.3462105

Khater, Hisham M. 2013. "Effect of silica fume on the characterization of the geopolymer materials." International Journal of Advanced Structural Engineering 5 (1):12.

Khatri, R. P., V. Sirivivatnanon, and W. Gross. 1995. "Effect of different supplementary cementitious materials on mechanical properties of high performance concrete." Cement and Concrete Research 25 (1):209-220. doi: https://doi.org/10.1016/0008-8846(94)00128-L.

Kropyvnytska, Tetiana & Kaminskyy, A & Semeniv, R & Chekaylo, Mykola. (2019). The effect of sodium aluminate on the properties of the composite cements. IOP Conference Series: Materials Science and Engineering. 708. 012091. 10.1088/1757-899X/708/1/012091.

Kumar, Sanjay, Rakesh Kumar, TC Alex, A Bandopadhyay, and SP Mehrotra. 2007. "Influence of reactivity of fly ash on geopolymerisation." Advances in Applied Ceramics 106 (3):120-127.

Langan, BW, K Weng, and MA Ward. 2002. "Effect of silica fume and fly ash on heat of hydration of Portland cement." Cement and Concrete research 32 (7):1045-1051.

Lee, Bokyeong, Gyuyong Kim, Raehwan Kim, Bongsuk Cho, Sujeong Lee, and Chul-Min Chon. 2017. "Strength development properties of geopolymer paste and mortar with respect to amorphous Si/Al ratio of fly ash." Construction and Building Materials 151:512-519.

Lee, WKW, and JSJ Van Deventer. 2002. "Structural reorganisation of class F fly ash in alkaline silicate solutions." Colloids and Surfaces A: Physicochemical and Engineering Aspects 211 (1):49-66.

Malhotra, V.M., A.A. Ramezanianpour, Canada Centre for Mineral, and Energy Technology. 1994. Fly Ash in Concrete: CANMET.

Mostafa, N. Y., S. A. S. El-Hemaly, E. I. Al-Wakeel, S. A. El-Korashy, and P. W. Brown. 2001. "Characterization and evaluation of the pozzolanic activity of Egyptian industrial by-products: I: Silica fume and dealuminated kaolin." Cement and Concrete Research 31 (3):467-474. doi: https://doi.org/10.1016/S0008-8846(00)00485-3.

Ng, Tian Sing, and Stephen J Foster. 2013. "Development of a mix design methodology for high-performance geopolymer mortars." Structural Concrete 14 (2):148-156.

Nugteren, Henk W, Mary B Ogundiran, Geert-Jan Witkamp, and M Kreutzer. 2011. "Coal fly ash activated by waste sodium aluminate solutions as an immobilizer for hazardous waste." 2011 World Coal Ash (WOCA) Conference, Denver, CO, USA.

Nuruddin, F & Demie, S & Memon, F.A. & Shafiq, Nasir. (2011). Effect of Superplasticizer and NaOH Molarity on Workability, Compressive Strength and Microstructure Properties of Self-Compacting Geopolymer Concrete. World Academy of Science, Engineering and Technology. 51.

Okoye, F. N., J. Durgaprasad, and N. B. Singh. 2016. "Effect of silica fume on the mechanical properties of fly ash based-geopolymer concrete." Ceramics International 42 (2, Part B):3000-3006. doi: https://doi.org/10.1016/j.ceramint.2015.10.084.

Olivia, Monita and Nikraz, Hamid. 2009. Durability of Low Calcium Fly Ash Geopolymer Concrete in Chloride Solution, in Peiming Wang and Shiyun Zhong (ed), The 6th Asian Symposium on Polymers in Concrete, Oct 29 2009, pp. 153-161. Shanghai, China: Tongji University Press.

Oualit, M., Jauberthie, R., Rendell, F., Melinge, Y. & Abadlia, M. T. 2012. External corrosion to concrete sewers: a case study. Urban Water Journal, 9, 6, 429-434.10.1080/1573062X.2012.668916

Palamo, A, MW Grutzeck, and MT Blanco. 1999. "Alkali-activated fly ashes." Cement and Concrete Research 29 (8):1323-1329.

Parnham, Glenn N. 2016. "Developing a Unified Approach For Mixture Design of Fly Ash and Ground Granulated Blast Furnace Slag Compostie Geopolymer Mortar." Bachelor of Civil and Constrcution Engineering Honours, Department of Civil Engineering, Curtin University.

Part, Wei Ken, Mahyuddin Ramli, and Chee Ban Cheah. 2015. "An overview on the influence of various factors on the properties of geopolymer concrete derived from industrial by-products." Construction and Building Materials 77:370-395. doi: https://doi.org/10.1016/j.conbuildmat.2014.12.065.

Perera, DS, O Uchida, ER Vance, and KS Finnie. 2007. "Influence of curing schedule on the integrity of geopolymers." Journal of materials science 42 (9):3099-3106.

Phoo-ngernkham, Tanakorn, Sakonwan Hanjitsuwan, Nattapong Damrongwiriyanupap, and Prinya Chindaprasirt. 2017. "Effect of sodium hydroxide and sodium silicate solutions on strengths of alkali activated high calcium fly ash containing Portland cement." KSCE Journal of Civil Engineering 21 (6):2202-2210. doi: 10.1007/s12205-016-0327-6.

Provis, John L, and Jan Stephanus Jakob Van Deventer. 2009. Geopolymers: structures, processing, properties and industrial applications: Elsevier.

Puertas, F., M. Palacios, H. Manzano, J. S. Dolado, A. Rico, and J. Rodríguez. 2011. "A model for the C-A-S-H gel formed in alkali-activated slag cements." Journal of the European Ceramic Society 31 (12):2043-2056. doi: https://doi.org/10.1016/j.jeurceramsoc.2011.04.036.

Rahim, RH Abdul, KA Azizli, Z Man, T Rahmiati, and MF Nuruddin. 2014. "Effect of sodium hydroxide concentration on the mechanical property of non sodium silicate fly ash based geopolymer." Journal of Applied Sciences 14 (23):3381-3384.

Rangan, B Vijaya. 2008. "Fly ash-based geopolymer concrete."

Rietveld, H. 1969. "A profile refinement method for nuclear and magnetic structures." Journal of Applied Crystallography 2 (2):65-71. doi: doi:10.1107/S0021889869006558.

Rogelj, Joeri, Michel Den Elzen, Niklas Höhne, Taryn Fransen, Hanna Fekete, Harald Winkler, Roberto Schaeffer, Fu Sha, Keywan Riahi, and Malte Meinshausen. 2016. "Paris Agreement climate proposals need a boost to keep warming well below 2 C." Nature 534 (7609):631.

Rowles, Matthew, and Brian O'connor. 2003. "Chemical optimisation of the compressive strength of aluminosilicate geopolymers synthesised by sodium silicate activation of metakaolinite." Journal of Materials Chemistry 13 (5):1161-1165.

Saha, Suman, and C. Rajasekaran. 2017. "Enhancement of the properties of fly ash based geopolymer paste by incorporating ground granulated blast furnace slag." Construction and Building Materials 146:615-620. doi: https://doi.org/10.1016/j.conbuildmat.2017.04.139.

Singh, B., G. Ishwarya, M. Gupta, and S. K. Bhattacharyya. 2015. "Geopolymer concrete: A review of some recent developments." Construction and Building Materials 85:78-90. doi: https://doi.org/10.1016/j.conbuildmat.2015.03.036.

K. Somna, C. Jaturapitakkul, P. Kajitvichyanukul, P. Chindaprasirt. 2011."NaOH-activated ground fly ash geopolymer cured at ambient temperature." Fuel, 90 (6) (2011), pp. 2118-2124, 10.1016/j.fuel.2011.01.018

Spano, Julian. 2018. " An amorphous approach to ambient cured geopolymer composite mortars and the contributing factors associated with compressive strength " Bachelor of Civil and Construction Engineering Honours, Department of Civil Engineering, Curtin University.

Spano J, Lau CK, Htut T, Rowles M. 2018. " Preliminary Investigation on the Impact of Water Addition on Geopolymer Mortar by Amorphous Ratio" The Ninth International Conference on Science and Engineering. Yangon, Myanmar.

Spano J, Lau CK, Htut T, Rowles M, Chegenizadeh A. 2020. "Application of Taguchi Method for the Optimisation of Alkali Activated Materials by Amorphous Ratios." Under Submission/In Review.

Standards-Australia. 1974. AS1141-1974 Methods For Sampling and Testing Aggregates, Australian standard AS1141. e1974: Standard Australia.

Standards-Australia. 2000. AS4863.1-2000 Particle Size Analysis–Laser Diffraction Methods, Australian standard AS4863. 1e2000: Standard Australia.

Standards-Australia. 2014. AS1012.9-2014 Methods of Testing Concrete: Compressive Strength Tests of Concrete, Mortar and Grout Specimens, Australian standard AS1012. 9e2014: Standard Australia.

Sweeney J, Htut T, Huen WY, Vimonsatit V, Ng T. 2017. " Investigating Amorphous Composition Mix Design Performance and Properties of Fly Ash-Based Geopolymer." Electronic Journal of Structural Engineering.

Temuujin, J, RP Williams, and Arie Van Riessen. 2009. "Effect of mechanical activation of fly ash on the properties of geopolymer cured at ambient temperature." Journal of materials processing technology 209 (12-13):5276-5280.

Temuujin, J., A. van Riessen, and K. J. D. MacKenzie. 2010. "Preparation and characterisation of fly ash based geopolymer mortars." Construction and Building Materials 24 (10):1906-1910. doi: https://doi.org/10.1016/j.conbuildmat.2010.04.012.

Tennakoon, Chandani & Sagoe-Crentsil, Kwesi & San Nicolas, Rackel & Sanjayan, Jay. (2015). Characteristics of Australian brown coal fly ash blended geopolymers. Construction and Building Materials. 101. 396-409. 10.1016/j.conbuildmat.2015.10.089.

Thompson, Geoffry M. 2016. "Developing a Systematic Mix Design Method to Analytically Produce and Evaluate Alkali Activated Slag Composites." Bachelor of Civil and Construction Engineering Honours, Department of Civil Engineering, Curtin University.

Topark-Ngarm, Pattanapong & Chindaprasirt, Prinya & Sata, Vanchai. (2015). Setting Time, Strength, and Bond of High-Calcium Fly Ash Geopolymer Concrete. Journal of Materials in Civil Engineering. 27. 04014198. 10.1061/(ASCE)MT.1943-5533.0001157.

Turner, Louise K., and Frank G. Collins. 2013. "Carbon dioxide equivalent (CO2-e) emissions: A comparison between geopolymer and OPC cement concrete." Construction and Building Materials 43:125-130. doi: https://doi.org/10.1016/j.conbuildmat.2013.01.023.

UNSTATS. 2010. Greenhouse gas emissions by sector (absolute values). edited by United Nations Statistical Division.

van Deventer, Jannie S. J., John L. Provis, Peter Duxson, and David G. Brice. 2010. "Chemical Research and Climate Change as Drivers in the Commercial Adoption of Alkali Activated Materials." Waste and Biomass Valorization 1 (1):145-155. doi: 10.1007/s12649-010-9015-9.

van Jaarsveld, J. G. S., and J. S. J. van Deventer. 1999. "Effect of the Alkali Metal Activator on the Properties of Fly Ash-Based Geopolymers." Industrial & Engineering Chemistry Research 38 (10):3932-3941. doi: 10.1021/ie980804b.

van Riessen, Arie & Chen-Tan, Nigel. (2013). Beneficiation of Collie fly ash for synthesis of geopolymer Part 2-Geopolymers. Fuel. 106. 569–575. 10.1016/j.fuel.2012.11.070.

Virgalitte, Stanley J, Mark D Luther, Jere H Rose, Bryant Mather, Leonard W Bell, Bryce A Ehmke, Paul Klieger, Della M Roy, Bayard M Call, and R Douglas Hooton. 1995. "Ground granulated blast-furnace slag as a cementitious constituent in concrete." American Concrete Institute ACI Report 233R-95.

Williams, Ross P., and Arie van Riessen. 2010. "Determination of the reactive component of fly ashes for geopolymer production using XRF and XRD." Fuel 89 (12):3683-3692. doi: https://doi.org/10.1016/j.fuel.2010.07.031.

Williams, Ross Peter. 2015. "Optimising geopolymer formation." Curtin University.

Xu, Hua & Van Deventer, Jannie. (2000). The geopolymerisation of alumino-silicate minerals. International Journal of Mineral Processing. 59. 247-266. 10.1016/S0301-7516(99)00074-5

Xu Qi, Stark J and Finger F. 2008. "A model of early cement hydration with an alkaline setting accelerator." Cement Internations (1):67-74.

Ye, Hailong & Radlińska, Aleksandra. (2017). Effect of Alkalis on Cementitious Materials:Understanding the Relationship between Composition, Structure, and Volume Change Mechanism. Journal of Advanced Concrete Technology. 15. 165-177. 10.3151/jact.15.165.

Yip, Ch K, GC Lukey, and JSJ Van Deventer. 2005. "The coexistence of geopolymeric gel and calcium silicate hydrate at the early stage of alkaline activation." Cement and concrete research 35 (9):1688-1697.

Yip, Christina K, Grant C Lukey, John L Provis, and Jannie SJ van Deventer. 2008. "Effect of calcium silicate sources on geopolymerisation." Cement and Concrete Research 38 (4):554-564.

Zuhua, Zhang, Yao Xiao, Zhu Huajun, and Chen Yue. 2009. "Role of water in the synthesis of calcined kaolin-based geopolymer." Applied Clay Science 43 (2):218-223.

Zhang, Peng et al. 2020. "Properties of fresh and hardened fly ash/slag based geopolymer concrete: A review". Journal of Cleaner Production 270: 122389. Elsevier BV. doi:10.1016/j.jclepro.2020.122389.

APPENDIX A – Particle Laser Sizing Results

Eraring Fly Ash

MASTERSIZER 2000

Laser Diffraction Sizing - Result Analysis Report

Sample Name: ERARING FLY ASH 1 OF 3	**SOP Name:** UT-Manual	**Measured:** Wednesday, 9 May 2018 8:54:50 AM	
	Result Source: Measurement	**Sample bulk lot ref:**	**Sample Source & type:**
Particle Name: Pulp	**Accessory Name:** Hydro 2000G (A)	**Analysis model:** General purpose	**Dispersant Name:** Water
Particle RI: 1.700	**Absorption:** 1	**Size range:** 0.020 to 2000.000 um	**Dispersant RI:** 1.330
Specific Surface Area: 0.318 m²/g	**Surface Weighted Mean D[3,2]:** 6.986 um	**Vol. Weighted Mean D[4,3]:** 35.551 um	**Result units:** Volume %
d(0.1): 3.953 um	**d(0.5):** 22.263 um	**d(0.8) or P80:** 54.875 um	**% passing -75um:** 87.79

Note. When multiple distributions appear in the graph, all other data is of the sample name listed.

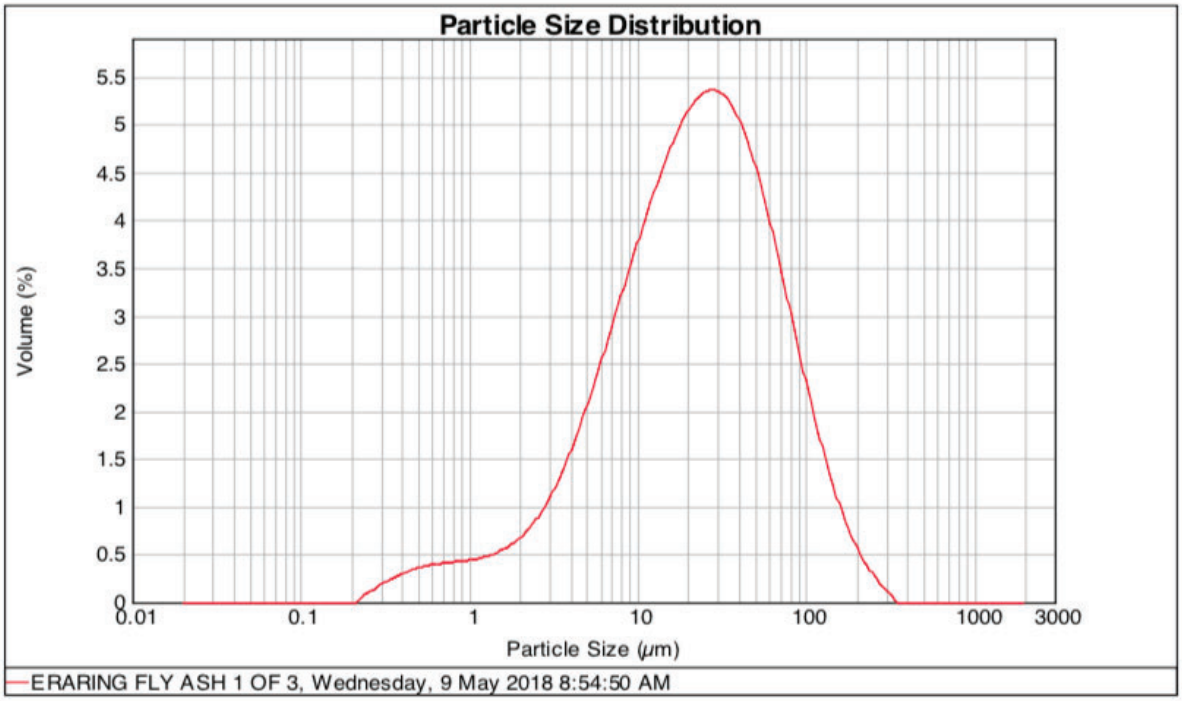

Size (µm)	Vol Under %	Size (µm)	Vol Under %	Size (µm)	Vol Under %	Size (µm)	Vol Under %	Size (µm)	Vol Under %	Size (µm)	Vol Under %
0.100	0.00	8.000	20.81	50.000	77.30	106.000	93.89	200.000	99.09	1200.000	100.00
0.250	0.05	9.000	23.40	55.000	80.06	110.000	94.39	225.000	99.46	1300.000	100.00
0.500	1.16	10.000	25.90	60.000	82.44	115.000	94.95	250.000	99.70	1400.000	100.00
0.600	1.61	12.000	30.63	65.000	84.48	120.000	95.45	300.000	99.94	1500.000	100.00
0.750	2.19	15.000	37.10	70.000	86.25	125.000	95.90	400.000	100.00	1600.000	100.00
1.000	3.00	18.000	42.86	75.000	87.79	130.000	96.29	500.000	100.00	1700.000	100.00
2.000	5.38	20.000	46.35	80.000	89.13	135.000	96.65	600.000	100.00	1800.000	100.00
3.000	7.65	25.000	54.02	85.000	90.31	140.000	96.97	700.000	100.00	1900.000	100.00
4.000	10.12	30.000	60.41	90.000	91.34	150.000	97.52	800.000	100.00	2000.000	100.00
5.000	12.76	35.000	65.75	95.000	92.25	160.000	97.97	900.000	100.00		
6.000	15.46	40.000	70.25	100.000	93.05	170.000	98.34	1000.000	100.00		
7.000	18.16	45.000	74.06	105.000	93.76	175.000	98.49	1100.000	100.00		

The sample has been analysed using a Malvern Mastersizer 2000. Particles are passed through a focused laser beam that scatter light at an angle inversely proportional to their size. The intensity of light is measured and converted to a volume in particle size distribution.

Gladstone Fly Ash

MASTERSIZER 2000

Laser Diffraction Sizing - Result Analysis Report

Sample Name: Gladstone Fly Ash 3.4
SOP Name: UT-Manual
Result Source: Measurement
Measured: Wednesday, 11 September 2019 10:29:35
Sample bulk lot ref:
Sample Source & type:

Particle Name: Pulp
Particle RI: 1.700
Accessory Name: Hydro 2000G (A)
Absorption: 1
Analysis model: General purpose
Size range: 0.020 to 2000.000 um
Dispersant Name: Water
Dispersant RI: 1.330

Specific Surface Area: 0.707 m²/g
Surface Weighted Mean D[3,2]: 3.145 um
Vol. Weighted Mean D[4,3]: 19.448 um
Result units: Volume %

d(0.1): 1.185 um
d(0.5): 7.793 um
d(0.8) or P80: 27.754 um
% passing -75um: 94.39

Note. When multiple distributions appear in the graph, all other data is of the sample name listed.

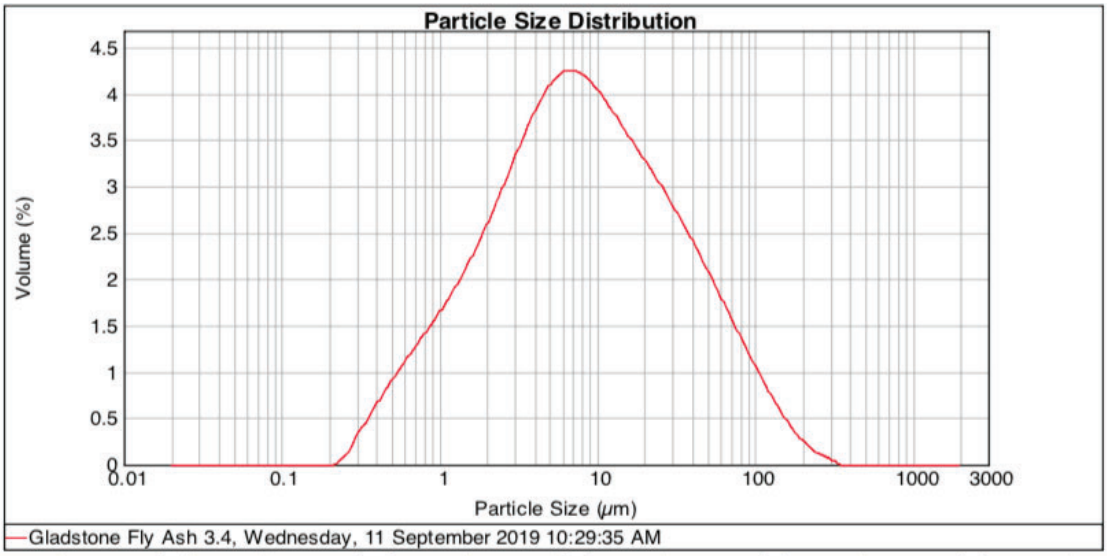

Size (µm)	Vol Under %	Size (µm)	Vol Under %	Size (µm)	Vol Under %	Size (µm)	Vol Under %	Size (µm)	Vol Under %	Size (µm)	Vol Under %
0.010	0.00	0.105	0.00	1.096	9.09	11.482	60.35	120.226	97.92	1258.925	100.00
0.011	0.00	0.120	0.00	1.259	10.74	13.183	63.81	138.038	98.57	1445.440	100.00
0.013	0.00	0.138	0.00	1.445	12.55	15.136	67.12	158.489	99.06	1659.587	100.00
0.015	0.00	0.158	0.00	1.660	14.53	17.378	70.30	181.970	99.43	1905.461	100.00
0.017	0.00	0.182	0.00	1.905	16.69	19.953	73.33	208.930	99.67	2187.762	100.00
0.020	0.00	0.209	0.00	2.188	19.06	22.909	76.22	239.883	99.83	2511.886	100.00
0.023	0.00	0.240	0.02	2.512	21.65	26.303	78.97	275.423	99.93	2884.032	100.00
0.026	0.00	0.275	0.11	2.884	24.46	30.200	81.57	316.228	99.99	3311.311	100.00
0.030	0.00	0.316	0.38	3.311	27.49	34.674	84.01	363.078	100.00	3801.894	100.00
0.035	0.00	0.363	0.78	3.802	30.75	39.811	86.28	416.869	100.00	4365.158	100.00
0.040	0.00	0.417	1.34	4.365	34.21	45.709	88.38	478.630	100.00	5011.872	100.00
0.046	0.00	0.479	2.05	5.012	37.84	52.481	90.30	549.541	100.00	5754.399	100.00
0.052	0.00	0.550	2.89	5.754	41.59	60.256	92.03	630.957	100.00	6606.934	100.00
0.060	0.00	0.631	3.87	6.607	45.42	69.183	93.58	724.436	100.00	7585.776	100.00
0.069	0.00	0.724	4.98	7.586	49.26	79.433	94.93	831.764	100.00	8709.636	100.00
0.079	0.00	0.832	6.22	8.710	53.05	91.201	96.11	954.993	100.00	10000.000	100.00
0.091	0.00	0.955	7.59	10.000	56.76	104.713	97.10	1096.478	100.00		

The sample has been analysed using a Malvern Mastersizer 2000. Particles are passed through a focused laser beam that scatter light at an angle inversely proportional to their size. The intensity of light is measured and converted to a volume in particle size distribution.

WestBuild GGBFS

MASTERSIZER 2000

Laser Diffraction Sizing - Result Analysis Report

Sample Name: Westbuild GGBFS	**SOP Name:** UT-Manual	**Measured:** Wednesday, 11 September 2019 10:35:51	
	Result Source: Measurement	**Sample bulk lot ref:**	**Sample Source & type:**
Particle Name: Pulp	**Accessory Name:** Hydro 2000G (A)	**Analysis model:** General purpose	**Dispersant Name:** Water
Particle RI: 1.700	**Absorption:** 1	**Size range:** 0.020 to 2000.000 um	**Dispersant RI:** 1.330
Specific Surface Area: 0.492 m^2/g	**Surface Weighted Mean D[3,2]:** 4.520 um	**Vol. Weighted Mean D[4,3]:** 44.128 um	**Result units:** Volume %
d(0.1): 1.929 um	**d(0.5):** 14.955 um	**d(0.8) or P80:** 31.055 um	**% passing -75um:** 96.97

Note. When multiple distributions appear in the graph, all other data is of the sample name listed.

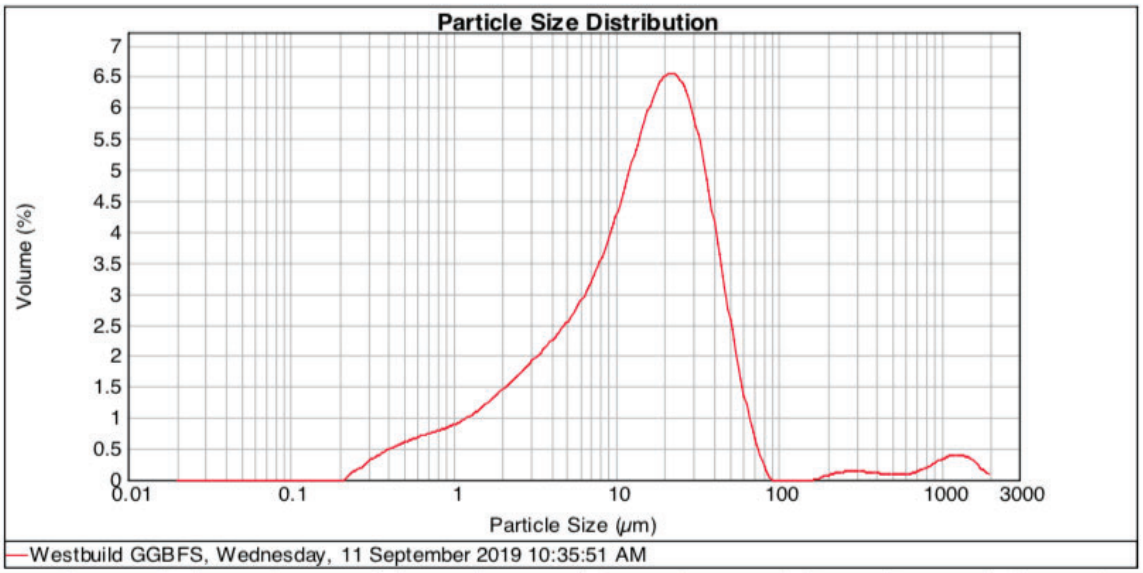

Size (µm)	Vol Under %	Size (µm)	Vol Under %	Size (µm)	Vol Under %	Size (µm)	Vol Under %	Size (µm)	Vol Under %	Size (µm)	Vol Under %
0.010	0.00	0.105	0.00	1.096	5.77	11.482	40.90	120.226	97.19	1258.925	99.17
0.011	0.00	0.120	0.00	1.259	6.65	13.183	45.43	138.038	97.19	1445.440	99.52
0.013	0.00	0.138	0.00	1.445	7.62	15.136	50.46	158.489	97.19	1659.587	99.81
0.015	0.00	0.158	0.00	1.660	8.69	17.378	55.91	181.970	97.20	1905.461	99.96
0.017	0.00	0.182	0.00	1.905	9.89	19.953	61.68	208.930	97.25	2187.762	100.00
0.020	0.00	0.209	0.00	2.188	11.21	22.909	67.60	239.883	97.35	2511.886	100.00
0.023	0.00	0.240	0.03	2.512	12.66	26.303	73.43	275.423	97.47	2884.032	100.00
0.026	0.00	0.275	0.18	2.884	14.25	30.200	78.95	316.228	97.59	3311.311	100.00
0.030	0.00	0.316	0.43	3.311	15.99	34.674	83.90	363.078	97.70	3801.894	100.00
0.035	0.00	0.363	0.77	3.802	17.87	39.811	88.12	416.869	97.80	4365.158	100.00
0.040	0.00	0.417	1.20	4.365	19.91	45.709	91.48	478.630	97.88	5011.872	100.00
0.046	0.00	0.479	1.69	5.012	22.11	52.481	93.97	549.541	97.95	5754.399	100.00
0.052	0.00	0.550	2.25	5.754	24.51	60.256	95.64	630.957	98.02	6606.934	100.00
0.060	0.00	0.631	2.86	6.607	27.13	69.183	96.63	724.436	98.13	7585.776	100.00
0.069	0.00	0.724	3.51	7.586	30.03	79.433	97.12	831.764	98.28	8709.636	100.00
0.079	0.00	0.832	4.21	8.710	33.24	91.201	97.19	954.993	98.51	10000.000	100.00
0.091	0.00	0.955	4.96	10.000	36.85	104.713	97.19	1096.478	98.82		

The sample has been analysed using a Malvern Mastersizer 2000. Particles are passed through a focused laser beam that scatter light at an angle inversely proportional to their size. The intensity of light is measured and converted to a volume in particle size distribution.

APPENDIX B - Complete XRF Analysis Results

XRF RESULTS				
Compound	**West Build GGBFS**	**Gladstone Fly Ash**	**Eraring Fly Ash**	**Silica Fume**
	(%wt)			
Al_2O_3	13.200	26.990	22.750	0.450
As	0.003	<0.001	0.007	<0.001
BaO	0.050	0.121	0.030	<0.001
CaO	40.900	5.450	6.780	0.940
Cl	<0.001	<0.001	<0.001	<0.001
Co	0.003	0.004	0.011	<0.001
Cr_2O_3	0.010	0.007	0.005	0.010
Cu	0.006	0.013	0.009	<0.001
Fe_2O_3	0.940	14.300	3.800	1.160
K_2O	0.297	0.418	0.066	1.750
MgO	5.390	1.440	1.280	1.860
MnO	0.200	0.197	1.290	0.080
Na_2O	0.026	0.420	0.051	0.680
Ni	0.004	0.005	0.008	<0.001
P_2O_5	0.032	1.450	1.061	<0.001
Pb	<0.001	0.010	<0.001	<0.001
SiO_2	33.240	45.260	60.030	89.750
SO_3	4.940	0.248	0.248	0.500
SrO	0.100	0.130	0.050	0.010
TiO_2	0.560	1.447	0.540	0.010
V_2O_5	<0.001	0.028	0.889	<0.001
Zn	0.004	0.008	0.005	0.139
Sub Total	99.905	97.908	98.910	97.339
LOI-1000	-0.290	1.740	1.090	2.770
Total	99.615	99.648	100.000	100.109

APPENDIX C – QXRD Results and Crystalline Composition Calculations

QXRD & CRYSTALLINE ELEMENTS					
Compound	**Element**	**Molecular Weight**	**West Build GGBFS**	**Gladstone Fly Ash**	**Eraring Fly Ash**
		(g/mol)	**(%wt)**	**(%wt)**	**(%wt)**
Quartz					
SiO_2		60.084	1.3	8.435	6.1
	Si	28.086	0.608	3.943	2.851
	O_2	31.999	0.692	4.492	3.249
Mullite					
$Al_{4.5}Si_{1.5}O_{9.74}$		319.379	0	22.505	6.3
	$Al_{4.5}$	121.417	0.000	8.556	2.395
	$Si_{1.5}$	42.128	0.000	2.969	0.831
	$O_{9.74}$	155.7426	0.000	10.974	3.072
Hermatite					
Fe_2O_3		159.688	0	3.149	0.7
	Fe_2	111.69	0.000	2.202	0.490
	O_3	47.998	0.000	0.947	0.210
Magnetite					
Fe_3O_4		231.533	0	6.713	1.5
	Fe_2	167.535	0.000	4.857	1.085
	O_4	63.998	0.000	1.856	0.415
Gypsum					
$CaSO_4$		136.141	4.9	0	0
	Ca	40.078	1.442	0.000	0.000
	S	32.065	1.154	0.000	0.000
	O_4	63.998	2.303	0.000	0.000
Bassanite					
$CaSO_4.0.5(H_2O)$		145.106	2.5	0	0
	Ca	40.078	0.690	0.000	0.000
	S	32.065	0.552	0.000	0.000
	$O_{4.5}$	71.955	1.240	0.000	0.000
	0.5H	0.504	0.009	0.000	0.000
Crystalline Elements					
	Si		0.608	6.911	3.682
	O		4.235	18.269	6.946
	Al		0.000	8.556	2.395
	Fe		0.000	7.060	1.575
	Ca		2.133	0.000	0.000
	S		1.707	0.000	0.000

APPENDIX D – Amorphous Composition Calculations

DETERMINATION OF AMORPHOUS CONTENT						
Compound	**Element**	**Molecular Weight**	**West Build GGBFS**	**Gladstone Fly Ash**	**Eraring Fly Ash**	**Comments**
		(g/mol)	**(%wt)**	**(wt%)**	**(%wt)**	
Al_2O_3		101.961				
	Al_2	53.963	0.000	8.556	2.395	*Crystalline Element %wt From QXRD*
	O_3	47.998				
			0.000	16.166	4.525	*Equivalent Crystaline Oxide %wt*
			13.200	26.990	22.750	*%wt From XRF*
	Amorphous Content		13.200	10.824	18.225	
CaO		56.077				
	Ca	40.078	2.133	0.000	0.000	*Crystalline Element %wt From QXRD*
	O	15.999				
			2.984	0.000	0.000	*Equivalent Crystaline Oxide %wt*
			40.900	5.450	6.780	*%wt From XRF*
	Amorphous Content		37.916	5.450	6.780	
SiO_2		60.084				
	Si	28.086	0.608	6.911	3.682	*Crystalline Element %wt From QXRD*
	O_2	31.999				
			1.300	6.911	7.878	*Equivalent Crystaline Oxide %wt*
			33.240	45.260	60.030	*%wt From XRF*
	Amorphous Content		31.940	38.349	52.152	
Na_2O		61.979				
	Na_2	45.979	0.000	0.000	0.000	*Crystalline Element %wt From QXRD*
	O	15.990				
			0.000	0.000	0.000	*Equivalent Crystaline Oxide %wt*
			0.026	0.420	0.051	*%wt From XRF*
	Amorphous Content		0.026	0.420	0.051	

APPENDIX E – Sample Calculation of Partial F-Matrix

*Below is an example of how the elemental molarities of the **F1 – Constituent (Eraring fly ash)** was determined.*

*From the reactive composition of the Eraring fly ash determined in 4.2 - Determination of the Amorphous Phase, the reactive elemental proportions of Si, Al, Na, H and Ca, were calculated in terms of moles per gram of fly ash. Determination of the reactive element proportions can be seen within the example below. This example refers to the determination of the **F1(Al)** component.*

No. of atoms in Compound (Al) = 2 *(Number of Al in Al_2O_3)*

Amorphous Content (Al_2O_3) = 18.225% = 0.18225 *(Determined in 4.1.5)*

MW(Compound) = 101.961 g/mol

F1 (Al)** = 2 x (0.18225 / 101.961) = **0.00357 (mol/g)

This process was undertaken for all the reactive elements of interest with the Eraring fly ash constituent. Table A-E, summarises the amorphous composition and mol/g of each reactive element within the Eraring fly ash.

Table AE – Summary of the reactive elemental of Eraring fly ash

Compound	Amorphous (%wt)	Element	Total Molecular Weight (g/mol)	(mol/g)
SiO_2	52.152		60.084	
		Si	28.086	**0.00868**
		O	31.999	
Al_2O_3	18.225		101.961	
		Al	53.963	**0.00357**
		O	47.998	
Na_2O	0.051		61.979	
		Na	45.979	**0.00002**
		O	15.990	
H_2O	0		18.015	
		H	2.916	**0**
		O	15.999	
CaO	6.780		56.077	
		Ca	40.078	**0.00121**
		O	15.999	

These values, were then introduced into the F-matrix as seen below.

$$F = \begin{bmatrix} 0.00868 & F2_{Si} & F3_{Si} & F4_{Si} & F5_{Si} & F6_{Si} & F7_{Si} \\ 0.00357 & F2_{Al} & F3_{Al} & F4_{Al} & F5_{Al} & F6_{Al} & F7_{Al} \\ 0.00002 & F2_{Na} & F3_{Na} & F4_{Na} & F5_{Na} & F6_{Na} & F7_{Na} \\ - & F2_{H} & F3_{H} & F4_{H} & F5_{H} & F6_{H} & F7_{H} \\ 0.00121 & F2_{Ca} & F3_{Ca} & F4_{Ca} & F5_{Ca} & F6_{Ca} & F7_{Ca} \end{bmatrix}$$

This was repeated for each constituent for each mixture, eg F2, F3, F4.. etc.

APPENDIX F - F-Matrix of Individual Mixture Constituents and Calculations

ERARING				
Compound	Amorphous (%wt)	Element	Molecular Weight (g/mol)	mol/g
SiO_2	52.152		60.084	0.00868
		Si	28.086	
		O_2	31.999	
Al_2O_3	18.224655		101.961	0.00357
		Al_2	53.963	
		O_3	47.998	
Na_2O	0.051		61.979	0.00002
		Na_2	45.979	
		O	15.990	
CaO	6.78		56.077	0.00121
		Ca	40.078	
		O	15.999	

	ERARING FLY ASH						
	FA	SA	SF	SS	SH	H2O	GGBFS
	F1	F2A	F2B	F3A	F3B	F4	F5
Si	0.00868	-	-	-	-	-	-
Al	0.00357	-	-	-	-	-	-
Na	0.00002	-	-	-	-	-	-
H	-	-	-	-	-	-	-
Ca	0.00121	-	-	-	-	-	-

GLADSTONE				
Compound	Amorphous (%wt)	Element	Molecular Weight (g/mol)	mol/g
SiO_2	38.349		60.084	0.00638
		Si	28.086	
		O_2	31.999	
Al_2O_3	10.8244621		101.961	0.00212
		Al_2	53.963	
		O_3	47.998	
Na_2O	0.42		61.979	0.00014
		Na_2	45.979	
		O	15.990	
CaO	5.45		56.077	0.00097
		Ca	40.078	
		O	15.999	

	GLADSTONE FLY ASH						
	FA	SA	SF	SS	SH	H2O	GGBFS
	F1	F2A	F2B	F3A	F3B	F4	F5
Si	0.00638	-	-	-	-	-	-
Al	0.00212	-	-	-	-	-	-
Na	0.00014	-	-	-	-	-	-
H	-	-	-	-	-	-	-
Ca	0.00097	-	-	-	-	-	-

FLY ASH BLEND G25-E75				
Compound	Amorphous (%wt)	Element	Molecular Weight (g/mol)	mol/g
SiO_2	48.701		60.084	0.00811
		Si	28.086	
		O_2	31.999	
Al_2O_3	16.375		101.961	0.00321
		Al_2	53.963	
		O_3	47.998	
Na_2O	0.143		61.979	0.00005
		Na_2	45.979	
		O	15.990	
CaO	6.448		56.077	0.00115
		Ca	40.078	
		O	15.999	

	FLY ASH BLEND G25-E75						
	FA	SA	SF	SS	SH	H2O	GGBFS
	F1	F2A	F2B	F3A	F3B	F4	F5
Si	0.00811	-	-	-	-	-	-
Al	0.00321	-	-	-	-	-	-
Na	0.00005	-	-	-	-	-	-
H	-	-	-	-	-	-	-
Ca	0.00115	-	-	-	-	-	-

FLY ASH BLEND G50-E50				
Compound	Amorphous (%wt)	Element	Molecular Weight (g/mol)	mol/g
SiO_2	45.250		60.084	0.00753
		Si	28.086	
		O_2	31.999	
Al_2O_3	14.525		101.961	0.00285
		Al_2	53.963	
		O_3	47.998	
Na_2O	0.236		61.979	0.00008
		Na_2	45.979	
		O	15.990	
CaO	6.115		56.077	0.00109
		Ca	40.078	
		O	15.999	

	FLY ASH BLEND G50-E50						
	FA	SA	SF	SS	SH	H2O	GGBFS
	F1	F2A	F2B	F3A	F3B	F4	F5
Si	0.00753	-	-	-	-	-	-
Al	0.00285	-	-	-	-	-	-
Na	0.00008	-	-	-	-	-	-
H	-	-	-	-	-	-	-
Ca	0.00109	-	-	-	-	-	-

FLY ASH BLEND G75-E25				
Compound	Amorphous (%wt)	Element	Molecular Weight (g/mol)	mol/g
SiO_2	41.799		60.084	0.00696
		Si	28.086	
		O_2	31.999	
Al_2O_3	12.675		101.961	0.00249
		Al_2	53.963	
		O_3	47.998	
Na_2O	0.328		61.979	0.00011
		Na_2	45.979	
		O	15.990	
CaO	5.783		56.077	0.00103
		Ca	40.078	
		O	15.999	

	FLY ASH BLEND G75-E25						
	FA	SA	SF	SS	SH	H2O	GGBFS
	F1	F2A	F2B	F3A	F3B	F4	F5
Si	0.00696	-	-	-	-	-	-
Al	0.00249	-	-	-	-	-	-
Na	0.00011	-	-	-	-	-	-
H	-	-	-	-	-	-	-
Ca	0.00103	-	-	-	-	-	-

FLY ASH BLEND G90-E10				
Compound	Amorphous (%wt)	Element	Molecular Weight (g/mol)	mol/g
SiO_2	39.729		60.084	0.00661
		Si	28.086	
		O_2	31.999	
Al_2O_3	11.564		101.961	0.00227
		Al_2	53.963	
		O_3	47.998	
Na_2O	0.383		61.979	0.00012
		Na_2	45.979	
		O	15.990	
CaO	5.583		56.077	0.00100
		Ca	40.078	
		O	15.999	

	FLY ASH BLEND G90-E10						
	FA	SA	SF	SS	SH	H2O	GGBFS
	F1	F2A	F2B	F3A	F3B	F4	F5
Si	0.00661	-	-	-	-	-	-
Al	0.00227	-	-	-	-	-	-
Na	0.00012	-	-	-	-	-	-
H	-	-	-	-	-	-	-
Ca	0.00100	-	-	-	-	-	-

SODIUM ALUMINATE SOLIDS				
Compound	Amorphous (%wt)	Element	Molecular Weight (g/mol)	mol/g
Al_2O_3	56.000		101.961	0.00549
		Al_2	53.963	
		O_3	47.998	
Na_2O	35.000		61.979	0.00565
		Na_2	45.979	
		O	15.990	

	SODIUM ALUMINATE SOLIDS						
	FA	SA	SF	SS	SH	H2O	GGBFS
	F1	F2A	F2B	F3A	F3B	F4	F5
Si	-	-	-	-	-	-	-
Al	-	0.00549	-	-	-	-	-
Na	-	0.00565	-	-	-	-	-
H	-	-	-	-	-	-	-
Ca	-	-	-	-	-	-	-

SILICA FUME				
Compound	Amorphous (%wt)	Element	Molecular Weight (g/mol)	mol/g
SiO_2	89.750		60.084	0.01494
		Si	28.086	
		O_2	31.999	
Al_2O_3	0.45		101.961	0.00009
		Al_2	53.963	
		O_3	47.998	
Na_2O	0.68		61.979	0.00022
		Na_2	45.979	
		O	15.990	
CaO	0.94		56.077	0.00017
		Ca	40.078	
		O	15.999	

	SILICA FUME						
	FA	SA	SF	SS	SH	H2O	GGBFS
	F1	F2A	F2B	F3A	F3B	F4	F5
Si	-	-	0.01494	-	-	-	-
Al	-	-	0.00009	-	-	-	-
Na	-	-	0.00022	-	-	-	-
H	-	-	-	-	-	-	-
Ca	-	-	0.00017	-	-	-	-

SODIUM SILICATE SOLUTION				
Compound	Amorphous (%wt)	Element	Molecular Weight (g/mol)	mol/g
SiO_2	29.400		60.084	0.00489
		Si	28.086	
		O_2	31.999	
Na_2O	14.700		61.979	0.00237
		Na_2	45.979	
		O	15.990	
H_2O	55.900		18.015	0.06206
		H_2	2.016	
		O	15.999	

	SODIUM SILICATE SOLUTION						
	FA	SA	SF	SS	SH	H2O	GGBFS
	F1	F2A	F2B	F3A	F3B	F4	F5
Si	-	-	-	0.00489	-	-	-
Al	-	-	-	-	-	-	-
Na	-	-	-	0.00237	-	-	-
H	-	-	-	0.06206	-	-	-
Ca	-	-	-	-	-	-	-

SODIUM HYDROXIDE SOLUTION (6M)				
Compound	Amorphous (%wt)	Element	Molecular Weight (g/mol)	mol/g
NaOH	24.000		39.996	0.00600
		Na	22.989	
		O	15.999	
		H	1.008	
H_2O	76.000		18.015	0.08437
		H_2	2.916	
		O	15.999	

	SODIUM HYDROXIDE SOLUTION (6M)						
	FA	SA	SF	SS	SH	H2O	GGBFS
	F1	F2A	F2B	F3A	F3B	F4	F5
Si	-	-	-	-	-	-	-
Al	-	-	-	-	-	-	-
Na	-	-	-	-	0.00600	-	-
H	-	-	-	-	0.09037	-	-
Ca	-	-	-	-	-	-	-

SODIUM HYDROXIDE SOLUTION (8M)				
Compound	Amorphous (%wt)	Element	Molecular Weight (g/mol)	mol/g
NaOH	32.000		39.996	0.00800
		Na	22.989	
		O	15.999	
		H	1.008	
H_2O	68.000		18.015	0.07549
		H2	2.916	
		O	15.999	

	SODIUM HYDROXIDE SOLUTION (8M)						
	FA	SA	SF	SS	SH	H2O	GGBFS
	F1	F2A	F2B	F3A	F3B	F4	F5
Si	-	-	-	-	-	-	-
Al	-	-	-	-	-	-	-
Na	-	-	-	-	0.00800	-	-
H	-	-	-	-	0.08349	-	-
Ca	-	-	-	-	-	-	-

SODIUM HYDROXIDE SOLUTION (10M)				
Compound	Amorphous (%wt)	Element	Molecular Weight (g/mol)	mol/g
NaOH	40.000		39.996	0.01000
		Na	22.989	
		O	15.999	
		H	1.008	
H_2O	60.000		18.015	0.06661
		H_2	2.916	
		O	15.999	

	SODIUM HYDROXIDE SOLUTION (10M)						
	FA	SA	SF	SS	SH	H2O	GGBFS
	F1	F2A	F2B	F3A	F3B	F4	F5
Si	-	-	-	-	-	-	-
Al	-	-	-	-	-	-	-
Na	-	-	-	-	0.01000	-	-
H	-	-	-	-	0.07661	-	-
Ca	-	-	-	-	-	-	-

SODIUM HYDROXIDE SOLUTION (12M)				
Compound	Amorphous (%wt)	Element	Molecular Weight (g/mol)	mol/g
NaOH	48.000		39.996	0.01200
		Na	22.989	
		O	15.999	
		H	1.008	
H_2O	52.000		18.015	0.05773
		H_2	2.916	
		O	15.999	

	SODIUM HYDROXIDE SOLUTION (12M)						
	FA	SA	SF	SS	SH	H2O	GGBFS
	F1	F2A	F2B	F3A	F3B	F4	F5
Si	-	-	-	-	-	-	-
Al	-	-	-	-	-	-	-
Na	-	-	-	-	0.01200	-	-
H	-	-	-	-	0.06973	-	-
Ca	-	-	-	-	-	-	-

SODIUM HYDROXIDE SOLUTION (14M)				
Compound	Amorphous (%wt)	Element	Molecular Weight (g/mol)	mol/g
NaOH	56.000		39.996	0.01400
		Na	22.989	
		O	15.999	
		H	1.008	
H_2O	44.000		18.015	0.04885
		H_2	2.916	
		O	15.999	

	SODIUM HYDROXIDE SOLUTION (14M)						
	FA	SA	SF	SS	SH	H2O	GGBFS
	F1	F2A	F2B	F3A	F3B	F4	F5
Si	-	-	-	-	-	-	-
Al	-	-	-	-	-	-	-
Na	-	-	-	-	0.01400	-	-
H	-	-	-	-	0.06285	-	-
Ca	-	-	-	-	-	-	-

WATER				
Compound	Amorphous (%wt)	Element	Molecular Weight (g/mol)	mol/g
H_2O	100.000		18.015	0.11102
		H_2	2.916	
		O	15.999	

	WATER						
	FA	SA	SF	SS	SH	H2O	GGBFS
	F1	F2A	F2B	F3A	F3B	F4	F5
Si	-	-	-	-	-	-	-
Al	-	-	-	-	-	-	-
Na	-	-	-	-	-	-	-
H	-	-	-	-	-	0.11102	-
Ca	-	-	-	-	-	-	-

WESTBUILD GGBFS				
Compound	Amorphous (%wt)	Element	Molecular Weight (g/mol)	mol/g
SiO_2	31.940		60.084	0.00532
		Si	28.086	
		O_2	31.999	
Al_2O_3	13.200		101.961	0.00259
		Al_2	53.963	
		O_3	47.998	
Na_2O	0.026		61.979	0.000008
		Na_2	45.979	
		O	15.990	
CaO	37.916		56.077	0.00676
		Ca	40.078	
		O	15.999	

	WESTBUILD GGBFS						
	FA	SA	SF	SS	SH	H2O	GGBFS
	F1	F2A	F2B	F3A	F3B	F4	F5
Si	-	-	-	-	-	-	0.005316
Al	-	-	-	-	-	-	0.002589
Na	-	-	-	-	-	-	0.000008
H	-	-	-	-	-	-	-
Ca	-	-	-	-	-	-	0.006761

APPENDIX G – Preliminary Phase Mixture Designs

PG1

F MATRIX (mol/g)							
	FA	SA	SF	SS	SH	H2O	GGBFS
	F1	F2A	F2B	F3A	F3B	F4	F5
Si	0.006382		0.014937	0.004893			0.005316
Al	0.002123	0.005492	0.000088				0.002589
Na	0.000136	0.005647	0.000219	0.002372	0.00600		0.000008
H				0.062059	0.09037	0.111019	
Ca	0.000972		0.000168				0.006761

W MATRIX (g)			
FA	W1	841	
SA	W2A	0	
SF	W2B	0	
SS	W3A	392	
SH	W3B	158	6M
H2O	W4	400	
GGBFS	W5	672	

	Mol
Si	10.858
Al	3.526
Na	1.997
H	83.014
Ca	5.361

R MATRIX	
Si/Al	3.08
Al/Al	1.00
Na/Al	0.57
(Si/Al)(H/Si)	23.55
(Ca/Si)(Si/Al)	1.52

RELATIVE ATOMIC RATIOS	
Si/Al	3.080
Al/Al	1.000
Na/Al	0.567
(H/Si)	7.645
(Ca/Si)	0.494

FA	FLY ASH
SA	SODIUM ALUMINATE
SF	SILICA FUME
SS	SODIUM SILICATE
SH	SODIUM HYDROXIDE
H2O	WATER
GGBFS	SLAG

PG2

F MATRIX (mol/g)							
	FA	SA	SF	SS	SH	H2O	GGBFS
	F1	F2A	F2B	F3A	F3B	F4	F5
Si	0.006382		0.014937	0.004893			0.005316
Al	0.002123	0.005492	0.000088				0.002589
Na	0.000136	0.005647	0.000219	0.002372	0.00600		0.000008
H				0.062059	0.09037	0.111019	
Ca	0.000972		0.000168				0.006761

W MATRIX (g)			
FA	W1	841	
SA	W2A	0	
SF	W2B	0	
SS	W3A	392	
SH	W3B	158	6M
H2O	W4	450	
GGBFS	W5	672	

	Mol
Si	10.858
Al	3.526
Na	1.997
H	88.565
Ca	5.361

R MATRIX	
Si/Al	3.08
Al/Al	1.00
Na/Al	0.57
(Si/Al)(H/Si)	25.12
(Ca/Si)(Si/Al)	1.52

RELATIVE ATOMIC RATIOS	
Si/Al	3.080
Al/Al	1.000
Na/Al	0.567
(H/Si)	8.157
(Ca/Si)	0.494

FA	FLY ASH
SA	SODIUM ALUMINATE
SF	SILICA FUME
SS	SODIUM SILICATE
SH	SODIUM HYDROXIDE
H2O	WATER
GGBFS	SLAG

PG3

F MATRIX (mol/g)							
	FA	SA	SF	SS	SH	H2O	GGBFS
	F1	F2A	F2B	F3A	F3B	F4	F5
Si	0.006382		0.014937	0.004893			0.005316
Al	0.002123	0.005492	0.000088				0.002589
Na	0.000136	0.005647	0.000219	0.002372	0.00600		0.000008
H				0.062059	0.09037	0.111019	
Ca	0.000972		0.000168				0.006761

W MATRIX (g)			
FA	W1	841	
SA	W2A	0	
SF	W2B	0	
SS	W3A	392	
SH	W3B	158	6M
H2O	W4	500	
GGBFS	W5	672	

	Mol
Si	10.858
Al	3.526
Na	1.997
H	94.116
Ca	5.361

R MATRIX	
Si/Al	3.08
Al/Al	1.00
Na/Al	0.57
(Si/Al)(H/Si)	26.69
(Ca/Si)(Si/Al)	1.52

RELATIVE ATOMIC RATIOS	
Si/Al	3.080
Al/Al	1.000
Na/Al	0.567
(H/Si)	8.668
(Ca/Si)	0.494

FA	FLY ASH
SA	SODIUM ALUMINATE
SF	SILICA FUME
SS	SODIUM SILICATE
SH	SODIUM HYDROXIDE
H2O	WATER
GGBFS	SLAG

PG4-7

F MATRIX (mol/g)							
	FA	SA	SF	SS	SH	H2O	GGBFS
	F1	F2A	F2B	F3A	F3B	F4	F5
Si	0.006382		0.014937	0.004893			0.005316
Al	0.002123	0.005492	0.000088				0.002589
Na	0.000136	0.005647	0.000219	0.002372	0.00600		0.000008
H				0.062059	0.09037	0.111019	
Ca	0.000972		0.000168				0.006761

W MATRIX (g)			
FA	W1	841	
SA	W2A	0	
SF	W2B	0	
SS	W3A	392	
SH	W3B	158	6M
H2O	W4	600	
GGBFS	W5	672	

	Mol
Si	10.858
Al	3.526
Na	1.997
H	105.218
Ca	5.361

R MATRIX	
Si/Al	3.08
Al/Al	1.00
Na/Al	0.57
(Si/Al)(H/Si)	29.84
(Ca/Si)(Si/Al)	1.52

RELATIVE ATOMIC RATIOS	
Si/Al	3.080
Al/Al	1.000
Na/Al	0.567
(H/Si)	9.690
(Ca/Si)	0.494

FA	FLY ASH
SA	SODIUM ALUMINATE
SF	SILICA FUME
SS	SODIUM SILICATE
SH	SODIUM HYDROXIDE
H2O	WATER
GGBFS	SLAG

APPENDIX H – Preliminary Phase Raw Data

					PRIOR TO CASTING	
MIX ID	**7 DAY**	**AV. 7 DAY**	**28 DAY**	**AV. 28 DAY**	**FLOW MEASUREMENTS**	**FLOW**
	Mpa	**Mpa**	**Mpa**	**Mpa**	**mm**	
PG1	37.558	40.3	56.8334	57.7	140	43%
	37.9135		56.1721		140	
	45.3244		60.2136		145	
					145	
PG2	38.9977	39.0	46.0263	49.0	150	54%
	38.1726		51.9147		160	
	39.8306		49.0026		150	
					155	
PG3	45.5802	44.2	55.7753	55.4	180	81%
	42.1833		55.8499		180	
	44.8768		54.5231		185	
					180	
PG4	31.7332	30.3	51.8852	53.6	250	150%
	31.5541		53.8281		250	
	30.7929		55.206		250	
	28.4193		50.7934		250	
	29.2805		50.7223			
	30.0667		54.083			
PG5	27.4917	28.6	42.4384	44.1	215	119%
	29.1705		43.0544		215	
	29.1096		46.7574		220	
					225	
PG6	32.041	33.3	46.1077	47.4	210	110%
	32.3289		49.414		210	
	35.4541		46.5563		215	
					205	
PG7	33.5566	33.7	48.6643	49.4	250	150%
	33.6232		50.1318		250	
	33.965		49.5388		250	
					250	

APPENDIX I – Secondary Phase Mixture Designs

SG1

F MATRIX (mol/g)							
	FA	SA	SF	SS	SH	H2O	GGBFS
	F1	F2A	F2B	F3A	F3B	F4	F5
Si	0.006382		0.014937	0.004893			0.005316
Al	0.002123	0.005492	0.000088				0.002589
Na	0.000136	0.005647	0.000219	0.002372	0.00600		0.000008
H				0.062059	0.09037	0.111019	
Ca	0.000972		0.000168				0.006761

W MATRIX (g)			
FA	W1	845	
SA	W2A	0	
SF	W2B	15	
SS	W3A	396	
SH	W3B	158	6M
H2O	W4	550	
GGBFS	W5	678	

	Mol
Si	11.157
Al	3.551
Na	2.011
H	99.902
Ca	5.408

R MATRIX	
Si/Al	3.14
Al/Al	1.00
Na/Al	0.57
(Si/Al)(H/Si)	28.13
(Ca/Si)(Si/Al)	1.52

RELATIVE ATOMIC RATIOS	
Si/Al	3.142
Al/Al	1.000
Na/Al	0.566
(H/Si)	8.954
(Ca/Si)	0.485

FA	FLY ASH
SA	SODIUM ALUMINATE
SF	SILICA FUME
SS	SODIUM SILICATE
SH	SODIUM HYDROXIDE
H2O	WATER
GGBFS	SLAG

SG2

F MATRIX (mol/g)							
	FA	SA	SF	SS	SH	H2O	GGBFS
	F1	F2A	F2B	F3A	F3B	F4	F5
Si	0.006382		0.014937	0.004893			0.005316
Al	0.002123	0.005492	0.000088				0.002589
Na	0.000136	0.005647	0.000219	0.002372	0.00800		0.000008
H				0.062059	0.08349	0.111019	
Ca	0.000972		0.000168				0.006761

W MATRIX (g)			
FA	W1	845	
SA	W2A	0	
SF	W2B	15	
SS	W3A	396	
SH	W3B	158	8M
H2O	W4	550	
GGBFS	W5	678	

	Mol
Si	11.157
Al	3.551
Na	2.327
H	98.813
Ca	5.408

R MATRIX	
Si/Al	3.14
Al/Al	1.00
Na/Al	0.66
(Si/Al)(H/Si)	27.83
(Ca/Si)(Si/Al)	1.52

RELATIVE ATOMIC RATIOS	
Si/Al	3.142
Al/Al	1.000
Na/Al	0.655
(H/Si)	8.857
(Ca/Si)	0.485

FA	FLY ASH
SA	SODIUM ALUMINATE
SF	SILICA FUME
SS	SODIUM SILICATE
SH	SODIUM HYDROXIDE
H2O	WATER
GGBFS	SLAG

SG3

F MATRIX (mol/g)							
	FA	SA	SF	SS	SH	H2O	GGBFS
	F1	F2A	F2B	F3A	F3B	F4	F5
Si	0.006382		0.014937	0.004893			0.005316
Al	0.002123	0.005492	0.000088				0.002589
Na	0.000136	0.005647	0.000219	0.002372	0.01000		0.000008
H				0.062059	0.07661	0.111019	
Ca	0.000972		0.000168				0.006761

W MATRIX (g)			
FA	W1	845	
SA	W2A	0	
SF	W2B	15	
SS	W3A	396	
SH	W3B	158	10M
H2O	W4	550	
GGBFS	W5	678	

	Mol
Si	11.157
Al	3.551
Na	2.644
H	97.725
Ca	5.408

R MATRIX	
Si/Al	3.14
Al/Al	1.00
Na/Al	0.74
(Si/Al)(H/Si)	27.52
(Ca/Si)(Si/Al)	1.52

RELATIVE ATOMIC RATIOS	
Si/Al	3.142
Al/Al	1.000
Na/Al	0.744
(H/Si)	8.759
(Ca/Si)	0.485

FA	FLY ASH
SA	SODIUM ALUMINATE
SF	SILICA FUME
SS	SODIUM SILICATE
SH	SODIUM HYDROXIDE
H2O	WATER
GGBFS	SLAG

SG4

F MATRIX (mol/g)							
	FA	SA	SF	SS	SH	H2O	GGBFS
	F1	F2A	F2B	F3A	F3B	F4	F5
Si	0.006382		0.014937	0.004893			0.005316
Al	0.002123	0.005492	0.000088				0.002589
Na	0.000136	0.005647	0.000219	0.002372	0.01200		0.000008
H				0.062059	0.06973	0.111019	
Ca	0.000972		0.000168				0.006761

W MATRIX (g)			
FA	W1	845	
SA	W2A	0	
SF	W2B	15	
SS	W3A	396	
SH	W3B	158	12M
H2O	W4	550	
GGBFS	W5	678	

	Mol
Si	11.157
Al	3.551
Na	2.960
H	96.636
Ca	5.408

R MATRIX	
Si/Al	3.14
Al/Al	1.00
Na/Al	0.83
(Si/Al)(H/Si)	27.21
(Ca/Si)(Si/Al)	1.52

RELATIVE ATOMIC RATIOS	
Si/Al	3.142
Al/Al	1.000
Na/Al	0.834
(H/Si)	8.662
(Ca/Si)	0.485

FA	FLY ASH
SA	SODIUM ALUMINATE
SF	SILICA FUME
SS	SODIUM SILICATE
SH	SODIUM HYDROXIDE
H2O	WATER
GGBFS	SLAG

SG5

F MATRIX (mol/g)							
	FA	SA	SF	SS	SH	H2O	GGBFS
	F1	F2A	F2B	F3A	F3B	F4	F5
Si	0.006382		0.014937	0.004893			0.005316
Al	0.002123	0.005492	0.000088				0.002589
Na	0.000136	0.005647	0.000219	0.002372	0.01000		0.000008
H				0.062059	0.07661	0.111019	
Ca	0.000972		0.000168				0.006761

W MATRIX (g)			
FA	W1	845	
SA	W2A	100	
SF	W2B	0	
SS	W3A	373	
SH	W3B	149	10M
H2O	W4	550	
GGBFS	W5	650	

	Mol
Si	10.673
Al	4.026
Na	3.061
H	95.633
Ca	5.216

R MATRIX	
Si/Al	2.65
Al/Al	1.00
Na/Al	0.76
(Si/Al)(H/Si)	23.75
(Ca/Si)(Si/Al)	1.30

RELATIVE ATOMIC RATIOS	
Si/Al	2.651
Al/Al	1.000
Na/Al	0.760
(H/Si)	8.960
(Ca/Si)	0.489

FA	FLY ASH
SA	SODIUM ALUMINATE
SF	SILICA FUME
SS	SODIUM SILICATE
SH	SODIUM HYDROXIDE
H2O	WATER
GGBFS	SLAG

SG6

F MATRIX (mol/g)							
	FA	SA	SF	SS	SH	H2O	GGBFS
	F1	F2A	F2B	F3A	F3B	F4	F5
Si	0.006382		0.014937	0.004893			0.005316
Al	0.002123	0.005492	0.000088				0.002589
Na	0.000136	0.005647	0.000219	0.002372	0.01000		0.000008
H				0.062059	0.07661	0.111019	
Ca	0.000972		0.000168				0.006761

W MATRIX (g)			
FA	W1	845	
SA	W2A	50	
SF	W2B	0	
SS	W3A	384	
SH	W3B	153	10M
H2O	W4	550	
GGBFS	W5	650	

	Mol
Si	10.728
Al	3.752
Na	2.844
H	96.625
Ca	5.216

R MATRIX	
Si/Al	2.86
Al/Al	1.00
Na/Al	0.76
(Si/Al)(H/Si)	25.75
(Ca/Si)(Si/Al)	1.39

RELATIVE ATOMIC RATIOS	
Si/Al	2.860
Al/Al	1.000
Na/Al	0.758
(H/Si)	9.006
(Ca/Si)	0.486

FA	FLY ASH
SA	SODIUM ALUMINATE
SF	SILICA FUME
SS	SODIUM SILICATE
SH	SODIUM HYDROXIDE
H2O	WATER
GGBFS	SLAG

SG7

F MATRIX (mol/g)							
	FA	SA	SF	SS	SH	H2O	GGBFS
	F1	F2A	F2B	F3A	F3B	F4	F5
Si	0.006382		0.014937	0.004893			0.005316
Al	0.002123	0.005492	0.000088				0.002589
Na	0.000136	0.005647	0.000219	0.002372	0.01000		0.000008
H				0.062059	0.07661	0.111019	
Ca	0.000972		0.000168				0.006761

W MATRIX (g)			
FA	W1	845	
SA	W2A	0	
SF	W2B	0	
SS	W3A	400	
SH	W3B	160	10M
H2O	W4	550	
GGBFS	W5	665	

	Mol
Si	10.886
Al	3.516
Na	2.669
H	98.142
Ca	5.318

R MATRIX	
Si/Al	3.10
Al/Al	1.00
Na/Al	0.76
(Si/Al)(H/Si)	27.91
(Ca/Si)(Si/Al)	1.51

RELATIVE ATOMIC RATIOS	
Si/Al	3.096
Al/Al	1.000
Na/Al	0.759
(H/Si)	9.016
(Ca/Si)	0.488

FA	FLY ASH
SA	SODIUM ALUMINATE
SF	SILICA FUME
SS	SODIUM SILICATE
SH	SODIUM HYDROXIDE
H2O	WATER
GGBFS	SLAG

SG8

F MATRIX (mol/g)							
	FA	SA	SF	SS	SH	H2O	GGBFS
	F1	F2A	F2B	F3A	F3B	F4	F5
Si	0.006382		0.014937	0.004893			0.005316
Al	0.002123	0.005492	0.000088				0.002589
Na	0.000136	0.005647	0.000219	0.002372	0.01000		0.000008
H				0.062059	0.07661	0.111019	
Ca	0.000972		0.000168				0.006761

W MATRIX (g)			
FA	W1	775	
SA	W2A	0	
SF	W2B	75	
SS	W3A	400	
SH	W3B	160	10M
H2O	W4	550	
GGBFS	W5	725	

	Mol
Si	11.878
Al	3.529
Na	2.676
H	98.142
Ca	5.668

R MATRIX	
Si/Al	3.37
Al/Al	1.00
Na/Al	0.76
(Si/Al)(H/Si)	27.81
(Ca/Si)(Si/Al)	1.61

RELATIVE ATOMIC RATIOS	
Si/Al	3.366
Al/Al	1.000
Na/Al	0.758
(H/Si)	8.262
(Ca/Si)	0.477

FA	FLY ASH
SA	SODIUM ALUMINATE
SF	SILICA FUME
SS	SODIUM SILICATE
SH	SODIUM HYDROXIDE
H2O	WATER
GGBFS	SLAG

SG9

F MATRIX (mol/g)							
	FA	SA	SF	SS	SH	H2O	GGBFS
	F1	F2A	F2B	F3A	F3B	F4	F5
Si	0.006382		0.014937	0.004893			0.005316
Al	0.002123	0.005492	0.000088				0.002589
Na	0.000136	0.005647	0.000219	0.002372	0.01000		0.000008
H				0.062059	0.07661	0.111019	
Ca	0.000972		0.000168				0.006761

W MATRIX (g)			
FA	W1	700	
SA	W2A	0	
SF	W2B	125	
SS	W3A	400	
SH	W3B	160	10M
H2O	W4	550	
GGBFS	W5	750	

	Mol
Si	12.279
Al	3.439
Na	2.677
H	98.142
Ca	5.772

R MATRIX	
Si/Al	3.57
Al/Al	1.00
Na/Al	0.78
(Si/Al)(H/Si)	28.54
(Ca/Si)(Si/Al)	1.68

RELATIVE ATOMIC RATIOS	
Si/Al	3.570
Al/Al	1.000
Na/Al	0.779
(H/Si)	7.993
(Ca/Si)	0.470

FA	FLY ASH
SA	SODIUM ALUMINATE
SF	SILICA FUME
SS	SODIUM SILICATE
SH	SODIUM HYDROXIDE
H2O	WATER
GGBFS	SLAG

SE

F MATRIX (mol/g)							
	FA	SA	SF	SS	SH	H2O	GGBFS
	F1	F2A	F2B	F3A	F3B	F4	F5
Si	0.008680		0.014937	0.004893			0.005316
Al	0.003575	0.005492	0.000088				0.002589
Na	0.000016	0.005647	0.000219	0.002372	0.01200		0.000008
H				0.062059	0.06973	0.111019	
Ca	0.001209		0.000168				0.006761

W MATRIX (g)			
FA	W1	676	
SA	W2A	0	
SF	W2B	75	
SS	W3A	429	
SH	W3B	172	12M
H2O	W4	520	
GGBFS	W5	720	

	Mol
Si	12.915
Al	4.287
Na	3.111
H	96.319
Ca	5.698

R MATRIX	
Si/Al	3.01
Al/Al	1.00
Na/Al	0.73
(Si/Al)(H/Si)	22.47
(Ca/Si)(Si/Al)	1.33

RELATIVE ATOMIC RATIOS	
Si/Al	3.012
Al/Al	1.000
Na/Al	0.725
(H/Si)	7.458
(Ca/Si)	0.441

FA	FLY ASH
SA	SODIUM ALUMINATE
SF	SILICA FUME
SS	SODIUM SILICATE
SH	SODIUM HYDROXIDE
H2O	WATER
GGBFS	SLAG

APPENDIX J – Secondary Phase Raw Data

					PRIOR TO CASTING	
MIX ID	**7 DAY**	**AV. 7 DAY**	**28 DAY**	**AV. 28 DAY**	**FLOW MEASUREMENTS**	**FLOW**
	Mpa	**Mpa**	**Mpa**	**Mpa**	**mm**	
SG1	39.8054	38.6	54.6085	53.7	190	90%
	40.0766		56.9391		180	
	35.9751		50.2029		200	
	39.2241		55.2787		190	
	39.1146		55.6896			
	37.4589		49.5995			
SG2	36.658	36.2	56.5915	54.9	200	101%
	36.189		53.9271		200	
	35.6725		56.8392		205	
	37.6164		51.9523		200	
	36.9183		55.7298			
	34.2439		54.2687			
SG3	32.1087	33.6	56.6405	56.4	190	88%
	33.8982		55.3411		190	
	34.7912		57.8999		180	
	33.7749		60.3014		190	
	34.2232		54.0038			
	32.7807		54.4945			
SG4	29.1152	31.3	47.3841	49.8	200	110%
	30.4967		51.2463		215	
	32.6078		49.0829		210	
	31.3778		49.3102		215	
	31.4227		49.1118			
	32.9873		52.5039			
SG5	3.63998	3.6	9.53747	9.6	220	130%
	3.5907		9.34568		230	
	3.58799		10.0839		240	
	3.66535		9.10231		230	
	3.35598		8.5338			
	4.08451		11.1524			
SG6	9.96809	9.7	21.6767	22.6	240	139%
	9.21486		24.4521		240	
	8.84779		20.5418		240	
	9.85914		22.8561		235	
	10.2267		23.6652			
	9.80339		16.407			
SG7	33.6522	32.6	52.0466	52.9	190	90%
	29.5777		56.0852		190	
	31.9613		52.69		185	
	31.7168		54.8245		195	
	33.9088		50.0298			
	34.808		51.7951			
SG8	34.373	32.6	54.9365	52.7	180	79%
	32.6683		51.1245		180	
	32.1509		50.3976		180	
	32.9877		57.2616		175	
	31.543		52.2601			
	31.8068		54.9559			
SG9	40.6197	39.5	53.4785	52.0	190	88%
	40.3926		50.6471		185	
	39.5697		52.6526		180	
	38.6219		52.0395		195	
	38.274		51.4258			
	35.5673		52.1688			
SE	38.2229	37.8	59.7351	59.8	170	70%
	37.2607		60.1723		170	
	37.0341		61.8318		175	
	36.3607		57.8318		165	
	38.4635		59.6064			
	39.3041		61.8293			

* The *highlighted red values* represent outliers defined through the interquartile rule.

APPENDIX K – Tertiary Phase Mixture Designs

TGE1

F MATRIX (mol/g)							
	FA	SA	SF	SS	SH	H2O	GGBFS
	F1	F2A	F2B	F3A	F3B	F4	F5
Si	0.008450		0.014937	0.004893			0.005316
Al	0.003430	0.000000	0.000088				0.002589
Na	0.000028	0.000000	0.000219	0.002372	0.00800		0.000008
H				0.062059	0.08349	0.111019	
Ca	0.001185		0.000168				0.006761

W MATRIX (g)			
FA	W1	625	
SA	W2A	0	
SF	W2B	75	
SS	W3A	450	
SH	W3B	180	8M
H2O	W4	600	
GGBFS	W5	800	

	Mol
Si	12.856
Al	4.222
Na	2.548
H	109.567
Ca	6.162

R MATRIX	
Si/Al	3.05
Al/Al	1.00
Na/Al	0.60
(Si/Al)(H/Si)	25.95
(Ca/Si)(Si/Al)	1.46

RELATIVE ATOMIC RATIOS	
Si/Al	3.045
Al/Al	1.000
Na/Al	0.604
(H/Si)	8.522
(Ca/Si)	0.479

FA	FLY ASH
SA	SODIUM ALUMINATE
SF	SILICA FUME
SS	SODIUM SILICATE
SH	SODIUM HYDROXIDE
H2O	WATER
GGBFS	SLAG

TGE2

F MATRIX (mol/g)							
	FA	SA	SF	SS	SH	H2O	GGBFS
	F1	F2A	F2B	F3A	F3B	F4	F5
Si	0.008106		0.014937	0.004893			0.005316
Al	0.003212	0.000000	0.000088				0.002589
Na	0.000046	0.000000	0.000219	0.002372	0.00800		0.000008
H				0.062059	0.08349	0.111019	
Ca	0.001150		0.000168				0.006761

W MATRIX (g)			
FA	W1	710	
SA	W2A	0	
SF	W2B	60	
SS	W3A	440	
SH	W3B	170	8M
H2O	W4	600	
GGBFS	W5	740	

	Mol
Si	12.738
Al	4.202
Na	2.456
H	108.111
Ca	5.830

R MATRIX	
Si/Al	3.03
Al/Al	1.00
Na/Al	0.58
(Si/Al)(H/Si)	25.73
(Ca/Si)(Si/Al)	1.39

RELATIVE ATOMIC RATIOS	
Si/Al	3.032
Al/Al	1.000
Na/Al	0.584
(H/Si)	8.487
(Ca/Si)	0.458

FA	FLY ASH
SA	SODIUM ALUMINATE
SF	SILICA FUME
SS	SODIUM SILICATE
SH	SODIUM HYDROXIDE
H2O	WATER
GGBFS	SLAG

TGE3

F MATRIX (mol/g)							
	FA	SA	SF	SS	SH	H2O	GGBFS
	F1	F2A	F2B	F3A	F3B	F4	F5
Si	0.007531		0.014937	0.004893			0.005316
Al	0.002849	0.000000	0.000088				0.002589
Na	0.000076	0.000000	0.000219	0.002372	0.00800		0.000008
H				0.062059	0.08349	0.111019	
Ca	0.001090		0.000168				0.006761

W MATRIX (g)			
FA	W1	750	
SA	W2A	0	
SF	W2B	40	
SS	W3A	410	
SH	W3B	170	8M
H2O	W4	550	
GGBFS	W5	700	

	Mol
Si	11.973
Al	3.953
Na	2.404
H	100.698
Ca	5.557

R MATRIX	
Si/Al	3.03
Al/Al	1.00
Na/Al	0.61
(Si/Al)(H/Si)	25.48
(Ca/Si)(Si/Al)	1.41

RELATIVE ATOMIC RATIOS	
Si/Al	3.029
Al/Al	1.000
Na/Al	0.608
(H/Si)	8.410
(Ca/Si)	0.464

FA	FLY ASH
SA	SODIUM ALUMINATE
SF	SILICA FUME
SS	SODIUM SILICATE
SH	SODIUM HYDROXIDE
H2O	WATER
GGBFS	SLAG

TGE4

F MATRIX (mol/g)							
	FA	SA	SF	SS	SH	H2O	GGBFS
	F1	F2A	F2B	F3A	F3B	F4	F5
Si	0.006957		0.014937	0.004893			0.005316
Al	0.002486	0.000000	0.000088				0.002589
Na	0.000106	0.000000	0.000219	0.002372	0.00800		0.000008
H				0.062059	0.08349	0.111019	
Ca	0.001031		0.000168				0.006761

W MATRIX (g)			
FA	W1	825	
SA	W2A	0	
SF	W2B	20	
SS	W3A	400	
SH	W3B	160	8M
H2O	W4	550	
GGBFS	W5	675	

	Mol
Si	11.584
Al	3.801
Na	2.326
H	99.243
Ca	5.418

R MATRIX	
Si/Al	3.05
Al/Al	1.00
Na/Al	0.61
(Si/Al)(H/Si)	26.11
(Ca/Si)(Si/Al)	1.43

RELATIVE ATOMIC RATIOS	
Si/Al	3.048
Al/Al	1.000
Na/Al	0.612
(H/Si)	8.568
(Ca/Si)	0.468

FA	FLY ASH
SA	SODIUM ALUMINATE
SF	SILICA FUME
SS	SODIUM SILICATE
SH	SODIUM HYDROXIDE
H2O	WATER
GGBFS	SLAG

TGE5

F MATRIX (mol/g)							
	FA	SA	SF	SS	SH	H2O	GGBFS
	F1	F2A	F2B	F3A	F3B	F4	F5
Si	0.006612		0.014937	0.004893			0.005316
Al	0.002268	0.000000	0.000088				0.002589
Na	0.000124	0.000000	0.000219	0.002372	0.00800		0.000008
H				0.062059	0.08349	0.111019	
Ca	0.000996		0.000168				0.006761

W MATRIX (g)			
FA	W1	860	
SA	W2A	0	
SF	W2B	0	
SS	W3A	400	
SH	W3B	150	8M
H2O	W4	550	
GGBFS	W5	650	

	Mol
Si	11.099
Al	3.634
Na	2.261
H	98.408
Ca	5.251

R MATRIX	
Si/Al	3.05
Al/Al	1.00
Na/Al	0.62
(Si/Al)(H/Si)	27.08
(Ca/Si)(Si/Al)	1.45

RELATIVE ATOMIC RATIOS	
Si/Al	3.054
Al/Al	1.000
Na/Al	0.622
(H/Si)	8.866
(Ca/Si)	0.473

FA	FLY ASH
SA	SODIUM ALUMINATE
SF	SILICA FUME
SS	SODIUM SILICATE
SH	SODIUM HYDROXIDE
H2O	WATER
GGBFS	SLAG

APPENDIX L – Tertiary Phase Raw Data

					PRIOR TO CASTING	
MIX ID	**7 DAY**	**AV. 7 DAY**	**28 DAY**	**AV. 28 DAY**	**FLOW MEASUREMENTS**	**FLOW**
	Mpa	**Mpa**	**Mpa**	**Mpa**	**mm**	
TGE1	32.1315	32.0	49.1652	47.1	200	103%
	28.61		45.2628		205	
	32.8082		46.0317		205	
	31.6358		50.0836		200	
	33.8941		44.6122			
	32.7726		47.407			
TGE2	30.4545	31.4	50.5779	48.1	195	91%
	31.9478		47.9198		185	
	31.2451		47.2833		190	
	31.2823		48.7047		195	
	31.9807		49.5259			
	31.4805		44.7113			
TGE3	31.4887	33.6	51.0758	49.0	230	131%
	32.8867		48.7035		230	
	37.2091		51.1769		230	
	35.8595		47.7394		235	
	32.7772		49.1862			
	31.4432		46.3034			
TGE4	32.3825	31.9	51.6277	51.2	240	140%
	31.3826		49.7789		240	
	31.8006		51.7652		240	
	32.0669		50.3678		240	
	31.6813		51.449			
	32.2873		52.3553			
TGE5	32.3103	31.5	51.92	49.8	210	115%
	30.7612		48.6055		210	
	31.4318		51.0467		220	
	31.3725		49.425		220	
	28.5927		49.2474			
	34.1455		48.4871			

* The *highlighted red values* represent outliers defined through the interquartile rule.

APPENDIX M – THIRD PARTY COPY RIGHT PERMISSION

ELSEVIER LICENSE
TERMS AND CONDITIONS

Feb 10, 2021

This Agreement between Curtin University of Technology -- Spano Julian ("You") and Elsevier ("Elsevier") consists of your license details and the terms and conditions provided by Elsevier and Copyright Clearance Center.

License Number	5005310173668
License date	Feb 10, 2021
Licensed Content Publisher	Elsevier
Licensed Content Publication	Construction and Building Materials
Licensed Content Title	Strength development properties of geopolymer paste and mortar with respect to amorphous Si/Al ratio of fly ash
Licensed Content Author	Bokyeong Lee,Gyuyong Kim,Raehwan Kim,Bongsuk Cho,Sujeong Lee,Chul-Min Chon
Licensed Content Date	Oct 1, 2017
Licensed Content Volume	151
Licensed Content Issue	n/a
Licensed Content Pages	8
Start Page	512
End Page	519
Type of Use	reuse in a thesis/dissertation
Portion	figures/tables/illustrations
Number of figures/tables/illustrations	3
Format	electronic
Are you the author of this Elsevier article?	No
Will you be translating?	No
Title	The Development of An Amorphous Approach to Ambient Cured Geopolymer Mortar Mixture Design
Institution name	Curtin University of Technology
Expected presentation date	Feb 2021
Portions	Table 2.4, Figure 2.4, Figure 2.9
	Curtin University of Technology
Requestor Location	Australia Attn: Curtin University of Technology
Publisher Tax ID	GB 494 6272 12
Total	0.00 USD

ELSEVIER LICENSE
TERMS AND CONDITIONS

Feb 10, 2021

This Agreement between Curtin University of Technology – Spano Julian ("You") and Elsevier ("Elsevier") consists of your license details and the terms and conditions provided by Elsevier and Copyright Clearance Center.

License Number	5005301023398
License date	Feb 10, 2021
Licensed Content Publisher	Elsevier
Licensed Content Publication	Fuel
Licensed Content Title	Determination of the reactive component of fly ashes for geopolymer production using XRF and XRD
Licensed Content Author	Ross P. Williams,Arie van Riessen
Licensed Content Date	Dec 1, 2010
Licensed Content Volume	89
Licensed Content Issue	12
Licensed Content Pages	10
Start Page	3683
End Page	3692
Type of Use	reuse in a thesis/dissertation
Portion	figures/tables/illustrations
Number of figures/tables/illustrations	3
Format	electronic
Are you the author of this Elsevier article?	No
Will you be translating?	No
Title	The Development of An Amorphous Approach to Ambient Cured Geopolymer Mortar Mixture Design
Institution name	Curtin University of Technology
Expected presentation date	Feb 2021
Portions	Table 2.4, Figure 2.4, Figure 2.9
Requestor Location	Curtin University of Technology Australia Attn: Curtin University of Technology
Publisher Tax ID	GB 494 6272 12
Total	0.00 USD

ELSEVIER LICENSE
TERMS AND CONDITIONS

Feb 10, 2021

This Agreement between Curtin University of Technology -- Spano Julian ("You") and Elsevier ("Elsevier") consists of your license details and the terms and conditions provided by Elsevier and Copyright Clearance Center.

License Number	5005341074174
License date	Feb 10, 2021
Licensed Content Publisher	Elsevier
Licensed Content Publication	Elsevier Books
Licensed Content Title	Handbook of Alkali-Activated Cements, Mortars and Concretes
Licensed Content Author	I. Garcia-Lodeiro,A. Palomo,A. Fernández-Jiménez
Licensed Content Date	Jan 1, 2015
Licensed Content Pages	29
Start Page	19
End Page	47
Type of Use	reuse in a thesis/dissertation
Portion	figures/tables/illustrations
Number of figures/tables/illustrations	1
Format	both print and electronic
Are you the author of this Elsevier chapter?	No
Will you be translating?	No
Title	The Development of An Amorphous Approach to Ambient Cured Geopolymer Mortar Mixture Design
Institution name	Curtin University of Technology
Expected presentation date	Feb 2021
Portions	Figure 2-3
	Curtin University of Technology
Requestor Location	Australia Attn: Curtin University of Technology
Publisher Tax ID	GB 494 6272 12
Total	0.00 USD

ELSEVIER LICENSE
TERMS AND CONDITIONS

Feb 10, 2021

This Agreement between Curtin University of Technology – Spano Julian ("You") and Elsevier ("Elsevier") consists of your license details and the terms and conditions provided by Elsevier and Copyright Clearance Center.

License Number	5005331271201
License date	Feb 10, 2021
Licensed Content Publisher	Elsevier
Licensed Content Publication	Journal of Cleaner Production
Licensed Content Title	Properties of fresh and hardened fly ash/slag based geopolymer concrete: A review
Licensed Content Author	Peng Zhang,Zhen Gao,Juan Wang,Jinjun Guo,Shaowei Hu,Yifeng Ling
Licensed Content Date	Oct 10, 2020
Licensed Content Volume	270
Licensed Content Issue	n/a
Licensed Content Pages	1
Start Page	122389
End Page	0
Type of Use	reuse in a thesis/dissertation
Portion	figures/tables/illustrations
Number of figures/tables/illustrations	1
Format	both print and electronic
Are you the author of this Elsevier article?	No
Will you be translating?	No
Title	The Development of An Amorphous Approach to Ambient Cured Geopolymer Mortar Mixture Design
Institution name	Curtin University of Technology
Expected presentation date	Feb 2021
Portions	Figure 2-2
Requestor Location	Curtin University of Technology 202/60 Riversdale Rd Rivervale, 6103 Australia Attn: Curtin University of Technology
Publisher Tax ID	GB 494 6272 12
Total	0.00 USD
Terms and Conditions	

INTRODUCTION

1. The publisher for this copyrighted material is Elsevier. By clicking "accept" in connection with completing this licensing transaction, you agree that the following terms and conditions apply to this transaction (along with the Billing and Payment terms and conditions established by Copyright Clearance Center, Inc. ("CCC"), at the time that you opened your Rightslink account and that are available at any time at http://myaccount.copyright.com).

GENERAL TERMS

2. Elsevier hereby grants you permission to reproduce the aforementioned material subject to the terms and conditions indicated.

3. Acknowledgement: If any part of the material to be used (for example, figures) has appeared in our publication with credit or acknowledgement to another source, permission must also be sought from that source. If such permission is not obtained then that material may not be included in your publication/copies. Suitable acknowledgement to the source must be made, either as a footnote or in a reference list at the end of your publication, as follows:

"Reprinted from Publication title, Vol /edition number, Author(s), Title of article / title of chapter, Pages No., Copyright (Year), with permission from Elsevier [OR APPLICABLE SOCIETY COPYRIGHT OWNER]." Also Lancet special credit - "Reprinted from The Lancet, Vol. number, Author(s), Title of article, Pages No., Copyright (Year), with permission from Elsevier."

4. Reproduction of this material is confined to the purpose and/or media for which permission is hereby given.

5. Altering/Modifying Material: Not Permitted. However figures and illustrations may be altered/adapted minimally to serve your work. Any other abbreviations, additions, deletions and/or any other alterations shall be made only with prior written authorization of Elsevier Ltd. (Please contact Elsevier's permissions helpdesk here). No modifications can be made to any Lancet figures/tables and they must be reproduced in full.

6. If the permission fee for the requested use of our material is waived in this instance, please be advised that your future requests for Elsevier materials may attract a fee.

7. Reservation of Rights: Publisher reserves all rights not specifically granted in the combination of (i) the license details provided by you and accepted in the course of this licensing transaction, (ii) these terms and conditions and (iii) CCC's Billing and Payment terms and conditions.

8. License Contingent Upon Payment: While you may exercise the rights licensed immediately upon issuance of the license at the end of the licensing process for the transaction, provided that you have disclosed complete and accurate details of your proposed use, no license is finally effective unless and until full payment is received from you (either by publisher or by CCC) as provided in CCC's Billing and Payment terms and conditions. If full payment is not received on a timely basis, then any license preliminarily granted shall be deemed automatically revoked and shall be void as if never granted. Further, in the event that you breach any of these terms and conditions or any of CCC's Billing and Payment terms and conditions, the license is automatically revoked and shall be void as if never granted. Use of materials as described in a revoked license, as well as any use of the materials beyond the scope of an unrevoked license, may constitute copyright infringement and publisher reserves the right to take any and all action to protect its copyright in the materials.

9. Warranties: Publisher makes no representations or warranties with respect to the licensed material.

10. Indemnity: You hereby indemnify and agree to hold harmless publisher and CCC, and their respective officers, directors, employees and agents, from and against any and all claims arising out of your use of the licensed material other than as specifically authorized pursuant to this license.

11. No Transfer of License: This license is personal to you and may not be sublicensed, assigned, or transferred by you to any other person without publisher's written permission.

12. No Amendment Except in Writing: This license may not be amended except in a writing signed by both parties (or, in the case of publisher, by CCC on publisher's behalf).

13. Objection to Contrary Terms: Publisher hereby objects to any terms contained in any purchase order, acknowledgment, check endorsement or other writing prepared by you, which terms are inconsistent with these terms and conditions or CCC's Billing and Payment terms and conditions. These terms and conditions, together with CCC's Billing and Payment terms and conditions (which are incorporated herein), comprise the entire agreement between you and publisher (and CCC) concerning this licensing transaction. In the event of any conflict between your obligations established by these terms and conditions and those established by CCC's Billing and Payment terms and conditions, these terms and conditions shall control.

14. Revocation: Elsevier or Copyright Clearance Center may deny the permissions described in this License at their sole discretion, for any reason or no reason, with a full refund payable to you. Notice of such denial will be made using the contact information provided by you. Failure to receive such notice will not alter or invalidate the denial. In no event will Elsevier or Copyright Clearance Center be responsible or liable for any costs, expenses or damage incurred by you as a result of a denial of your permission request, other than a refund of the amount(s) paid by you to Elsevier and/or Copyright Clearance Center for denied permissions.

LIMITED LICENSE

The following terms and conditions apply only to specific license types:

15. **Translation**: This permission is granted for non-exclusive world **English** rights only unless your license was granted for translation rights. If you licensed translation rights you may only translate this content into the languages you requested. A professional translator must perform all translations and reproduce the content word for word preserving the integrity of the article.

16. **Posting licensed content on any Website**: The following terms and conditions apply as follows: Licensing material from an Elsevier journal: All content posted to the web site must maintain the copyright information line on the bottom of each image; A hyper-text must be included to the Homepage of the journal from which you are licensing at http://www.sciencedirect.com/science/journal/xxxxx or the Elsevier homepage for books at http://www.elsevier.com; Central Storage: This license does not include permission for a scanned version of the material to be stored in a central repository such as that provided by Heron/XanEdu.

Licensing material from an Elsevier book: A hyper-text link must be included to the Elsevier homepage at http://www.elsevier.com . All content posted to the web site must maintain the copyright information line on the bottom of each image.

Posting licensed content on Electronic reserve: In addition to the above the following clauses are applicable: The web site must be password-protected and made available only to bona fide students registered on a relevant course. This permission is granted for 1 year only. You may obtain a new license for future website posting.

17. **For journal authors:** the following clauses are applicable in addition to the above:

Preprints:

A preprint is an author's own write-up of research results and analysis, it has not been peer-reviewed, nor has it had any other value added to it by a publisher (such as formatting, copyright, technical enhancement etc.).

Authors can share their preprints anywhere at any time. Preprints should not be added to or enhanced in any way in order to appear more like, or to substitute for, the final versions of articles however authors can update their preprints on arXiv or RePEc with their Accepted Author Manuscript (see below).

If accepted for publication, we encourage authors to link from the preprint to their formal publication via its DOI. Millions of researchers have access to the formal publications on ScienceDirect, and so links will help users to find, access, cite and use the best available version. Please note that Cell Press, The Lancet and some society-owned have different preprint policies. Information on these policies is available on the journal homepage.

Accepted Author Manuscripts: An accepted author manuscript is the manuscript of an article that has been accepted for publication and which typically includes author-incorporated changes suggested during submission, peer review and editor-author communications.

Authors can share their accepted author manuscript:

- immediately
  - via their non-commercial person homepage or blog
  - by updating a preprint in arXiv or RePEc with the accepted manuscript
  - via their research institute or institutional repository for internal institutional uses or as part of an invitation-only research collaboration work-group
  - directly by providing copies to their students or to research collaborators for their personal use
  - for private scholarly sharing as part of an invitation-only work group on commercial sites with which Elsevier has an agreement
- After the embargo period
  - via non-commercial hosting platforms such as their institutional repository
  - via commercial sites with which Elsevier has an agreement

In all cases accepted manuscripts should:

- link to the formal publication via its DOI
- bear a CC-BY-NC-ND license - this is easy to do
- if aggregated with other manuscripts, for example in a repository or other site, be shared in alignment with our hosting policy not be added to or enhanced in any way to appear more like, or to substitute for, the published journal article.

Published journal article (JPA): A published journal article (PJA) is the definitive final record of published research that appears or will appear in the journal and embodies all value-adding publishing activities including peer review co-ordination, copy-editing, formatting, (if relevant) pagination and online enrichment.

Policies for sharing publishing journal articles differ for subscription and gold open access articles:

Subscription Articles: If you are an author, please share a link to your article rather than the full-text. Millions of researchers have access to the formal publications on ScienceDirect, and so links will help your users to find, access, cite, and use the best available version.

Theses and dissertations which contain embedded PJAs as part of the formal submission can be posted publicly by the awarding institution with DOI links back to the formal publications on ScienceDirect.

If you are affiliated with a library that subscribes to ScienceDirect you have additional private sharing rights for others' research accessed under that agreement. This includes use for classroom teaching and internal training at the institution (including use in course packs and courseware programs), and inclusion of the article for grant funding purposes.

Gold Open Access Articles: May be shared according to the author-selected end-user license and should contain a CrossMark logo, the end user license, and a DOI link to the formal publication on ScienceDirect.

Please refer to Elsevier's posting policy for further information.

18. **For book authors** the following clauses are applicable in addition to the above: Authors are permitted to place a brief summary of their work online only. You are not allowed to download and post the published electronic version of your chapter, nor may you scan the printed edition to create an electronic version. **Posting to a repository:** Authors are permitted to post a summary of their chapter only in their institution's repository.

19. **Thesis/Dissertation**: If your license is for use in a thesis/dissertation your thesis may be submitted to your institution in either print or electronic form. Should your thesis be published commercially, please reapply for permission. These requirements include permission for the Library and Archives of Canada to supply single copies, on demand, of the complete thesis and include permission for Proquest/UMI to supply single copies, on demand, of the complete thesis. Should your thesis be published commercially, please reapply for permission. Theses and dissertations which contain embedded PJAs as part of the formal submission can be posted publicly by the awarding institution with DOI links back to the formal publications on ScienceDirect.

Elsevier Open Access Terms and Conditions

You can publish open access with Elsevier in hundreds of open access journals or in nearly 2000 established subscription journals that support open access publishing. Permitted third party re-use of these open access articles is defined by the author's choice of Creative Commons user license. See our open access license policy for more information.

Terms & Conditions applicable to all Open Access articles published with Elsevier:

Any reuse of the article must not represent the author as endorsing the adaptation of the article nor should the article be modified in such a way as to damage the author's honour or reputation. If any changes have been made, such changes must be clearly indicated.

The author(s) must be appropriately credited and we ask that you include the end user license and a DOI link to the formal publication on ScienceDirect.

If any part of the material to be used (for example, figures) has appeared in our publication with credit or acknowledgement to another source it is the responsibility of the user to ensure their reuse complies with the terms and conditions determined by the rights holder.

Additional Terms & Conditions applicable to each Creative Commons user license:

CC BY: The CC-BY license allows users to copy, to create extracts, abstracts and new works from the Article, to alter and revise the Article and to make commercial use of the Article (including reuse and/or resale of the Article by commercial entities), provided the user gives appropriate credit (with a link to the formal publication through the relevant DOI), provides a link to the license, indicates if changes were made and the licensor is not represented as endorsing the use made of the work. The full details of the license are available at http://creativecommons.org/licenses/by/4.0.

CC BY NC SA: The CC BY-NC-SA license allows users to copy, to create extracts, abstracts and new works from the Article, to alter and revise the Article, provided this is not done for commercial purposes, and that the user gives appropriate credit (with a link to the formal publication through the relevant DOI), provides a link to the license, indicates if changes were made and the licensor is not represented as endorsing the use made of the